2008

Novel devices and protocols enabling isolation and enumeration of low abundant biological cells from complex matrices

Andre Antonio Adams
Louisiana State University and Agricultural and Mechanical College, aadam14@lsu.edu

NOVEL DEVICES AND PROTOCOLS ENABLING ISOLATION AND ENUMERATION OF LOW ABUNDANT BIOLOGICAL CELLS FROM COMPLEX MATRICES

A Dissertation

Submitted to the Graduate Faculty of the
Louisiana State University and
Agricultural and Mechanical College
in partial fulfillment of the
requirements for the degree of
Doctor of Philosophy

in

The Department of Chemistry

by
André A. Adams
B.S., Grambling State University, 2000
August, 2008

DEDICATION

This dissertation is dedicated to many very special people that I have encountered during my lifetime. These people have instilled in me an unquenchable thirst for knowledge, undying zest for success, and an unparalleled determination. To my loving parents, Robert T. and Charlotte C. Adams, thanks for allowing your inquisitive and exuberant son many opportunities to explore the world as I matured in your care. To my paternal grandparents, Samuel and Beatrice Adams, and my maternal grandparents, Monroe and Elzora Smith, the many thought provoking interactions we shared have served to shape my character resulting in my developing into the person I am today. Last, but certainly not least, my wife, Stephanie L. J. Adams, without you beside me I am certain this would not have been possible. Thank you all greatly from the deepest crevices of my being for inspiring, motivating, and stimulating me.

ACKNOWLEDGEMENTS

I would like to begin by thanking my advisor, Prof. Steven A. Soper, for his continuous support and commitment to my successes during my dissertation research here at Louisiana State University's Department of Chemistry. You, sir, have been much more than a mentor and you will certainly have a lasting impression on me as I continue to develop. I thank my committee members: Dr. Robert Cook, Dr. David Spivak, Dr. Steven Watkins, and Dr. Mark Benfield.

To all my colleagues within the department of chemistry, sprinkled in various research groups, a special thanks to you for your "attention to" and many "critiques of" my work. To the Soper Research Group, thanks for listening to me as I perpetually hammered home many points related to circulating tumor cells. Without you my success would not have been possible. Jason, Rondedrick, and Matt have served as sounding boards for many of my ideas, and I would like to include a specific thanks to you for assisting me in weeding through those ideas to find the ones that actually worked. A very special thanks to Maggie, contrary to your belief, the members of this group have come to revere your insights, and if I could (not that it would ever happen), I would not change one single thing about you. Thanks for your enormous efforts in our early cell analysis work. Thanks for always being there to discuss research and/or whatever needed discussing at the time.

Finally, I would like to thank God and these United States of America for affording me every opportunity to achieve. May God bless America and each of you!

TABLE OF CONTENTS

LIST OF TABLES

LIST OF SCHEMES

LIST OF FIGURES

ABBREVIATIONS AND ACRONYMS

A..... Adenine

C..... Cytosine

G .....Guanine

T .....Thymine

DNA..... Deoxyribonucleic Acid

FACS.....Fluorescence Assisted Cell Sorting

MACS.....Magnetic Assisted Cell Sorting

BioMEMS ..... Biological Micro Electro Mechanical Systems

μTAS .....Miniaturized Total Analysis System

GFP..... Green Fluorescent Protein

PDMS.....Poly (dimethylsiloxane)

EOF..... Electroosmotic Flow

ζ..... Zeta Potential

δ .....Double Layer Thickness

e ..... Charge per Unit Surface Area

Є..... Dielectric Constant

HARMs..... High Aspect Ratio Microstructures

T_g .....Glass Transition Temperature

UV ..... Ultraviolet

LiGA ..... Lithography, Electroplating, Embossing

PMMA .....Poly (methylmethacrylate)

PC ..... Polycarbonate

CTC.....Circulating Tumor Cell

DRIE..... Deep reactive Ion Etching

PCR.....Polymerase Chain Reaction

mRNA..... Messenger Ribonucleic Acid

CV ..... Coefficient of Variance

CD .....Cluster of Differentiation

PBS .....Phosphate Buffered Saline

DI..... Deionized

v_{app} ..... Apparent Linear Velocity

μ_{EOF} .....Electroosmotic Mobility

μ_{EP} ..... Electrophoretic Mobility

E..... Electric Field Strength

TEM..... Tunneling Electron Microscope

FITC .....Fluorescein Isothiocyanate

AFM..... Atomic Force Microscopy

MSU .....Microsampling Unit

HTMSU ..... High Throughput Microsampling Unit

EpCAM..... Epithelial Cell Adhesion Molecule

mAB ..... Monoclonal Antibody

U..... Translational Linear Velocity

k_f .....Forward Reaction Rate

C_∞ .....Cell Surface Density of EpCAM

N_r .....Number of Receptors Available for Binding

k_o ..... Encounter Rate

P.....Probability

k_{ads} ..... Rate of Adsorption

k_{in} ..... Forward Rate Constant

F_A ..... Adhesion Force

f_c ..... Single Bond Force

v_c ..... Critical Linear Velocity

F_S ..... Stoke's Force

η ..... Intrinsic Viscosity

r ..... Radius

K ..... Cell Constant

C_p ..... Parasitic Capacitance

C_d ..... Double Layer Capacitance

G_s ..... Solution Conductance

L ..... Synthetic Inductance

f ..... Resonance Frequency

ΔP ..... Pressure Drop

Q ..... Flow Rate

CFU ..... Colony Forming Unit

Ab ..... Antibody

Ag ..... Antigen

Ag* ..... Antigen Analogue

CCD ..... Charge Coupled Device

ABSTRACT

The dimensions of microfluidic devices closely parallel those of biological cells; thusly, they are excellent platforms for the speciation, transport, manipulation, and analysis of cells. Electrokinetic transport of *Escherichia coli* and *Saccharomyces cerevisiae* was evaluated in microfluidic devices fabricated in pristine and UV-modified poly(methylmethacrylate) and polycarbonate. The magnitude and direction of transport of the cells was dictated by the buffer composition, conduit surface chemistry, and intrinsic cellular electrical properties. Baker's yeast in all devices migrated toward the cathode, because of their smaller electrophoretic mobility compared to the electroosmotic flow of the polymer. *E. coli* cells suspended in 20 mM PBS migrated toward the anode, which indicated that the apparent mobility of the *E. coli* cells changed direction at higher ionic strengths. The observed differential migrations were exploited to sort cells, whereby judicious choice of the buffer concentration and the polymeric material in which the cell sorting was performed was controlled, allowed for cell enumeration via laser-based backscatter signals.

A novel microfluidic device that selectively and specifically isolated the exceedingly small numbers of circulating tumor cells (CTCs) from whole blood through a monoclonal antibody (mAB) mediated process by sampling large input volumes (≥1 mL) of whole blood directly in short time periods (<37 min) was designed, manufactured and implemented. Upon processing, the CTCs were concentrated into small volumes (190 nL) and the number of cells captured were read without the need for labeling by using an integrated conductivity sensor following an enzyme mediated release of the captured CTCs from the microchannel surface. The microchannel walls were covalently decorated with mABs directed toward breast cancer cells that over-express epithelial

cell adhesion molecules. The released CTCs were then enumerated on-device using conductivity detection with 100% detection efficiency and exquisite specificity for CTCs. The CTC capture efficiency was made highly quantitative (>97%) by designing capture channels with the appropriate widths and heights. Extension of the technique to environmental samples was performed using analogously patterned polyclonal anti-*E. coli* O157:H7 antibodies directed towards the virolent bacterial strain were used to isolate the enterohemorrhagic bacteria while *E. coli* K12 were not adsorbed to the antibody containing surface.

Introduction

I.1 Origins of Life

The biological cell is the most fundamental of organisms that embody life processes. Individually these small wonders can be considered the manufacturing facilities from which all biological processes find their origins.[1] On a grandiose scale the full gambit of all known biological cells can be classified as one of two major classes: (i) prokaryotic or (ii) eukaryotic. The root, *Karyotic* refers to the nucleus or control center of the cell. The nucleus is enclosed by a sub-membrane within the primary cellular envelope yet separated from it by the cytoplasm. "*Eu*", from the Greek, means true and from this one can surmise that the eukaryotic cell possesses a nucleus and conversely the prokaryotic cell does not.

I.2 Cell Biology: Prokaryotes and Eukaryotes

In this dissertation, I focus on cells originating from the *Monera* and *Anamalia* Kingdoms, primarily owing to the clinical, environmental, and medical information that can be ascertained from the cellular contents. Clinicians are actively pursuing means of isolating, quantitating, and subsequently examining these cells due in part to toxic, virulent, and pathogenic potentials possessed by the various cell types.[2-4] Morphologically, prokaryotes are smaller and less complicated cells typically 5 μm in diameter or smaller with an outer membrane that is composed of a phospholipid bilayer that encompasses a cytoplasm and nucleoid rather than a nucleus.[5,6] In this cell type there exists a high probability of finding genetic materials in the nucleoid.[6] It is widely held in the scientific community that the initial prokaryotes through a series of symbiotic processes took up residence within the early eukaryotic cells significantly increasing their complexity during the evolutionary cycle.[6,7] Specifically, plastids[8] and

mitochondria[9] are cited as originating as free-living prokaryotes that found shelter within primitive eukaryotic cells.[6] As evidenced by the present form of eukaryotes, these moieties eventually became stabilized as permanent symbiotic elements within eukaryotes cellular envelope making eukaryotes larger and more complicated than their counterparts.[7]

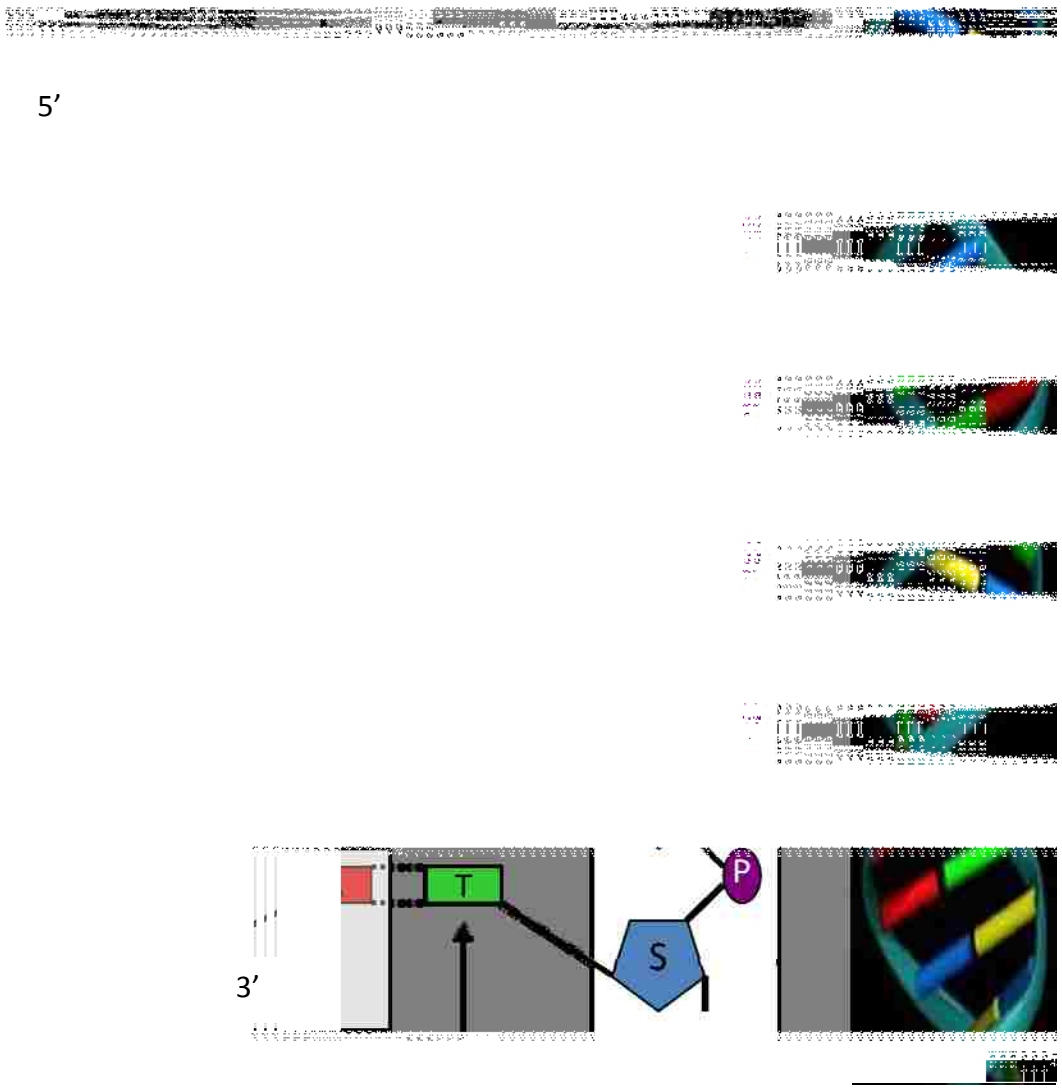

Figure I.1 Illustration of the DNA forming a double helical structure with an expansion of the sugar phosphate backbone. Adapted with permission from www.cnx.org 7/11/2008.

I.3 Molecular Biology

I.3.1 Nucleic Acids. A molecule of deoxyribonucleic acid is composed of a series of smaller subunits. DNA primarily consists of two polymer chains of deoxyribonucleotides that are bound by a hydrogen bonding between each pair of complementary bases. Each nucleotide base exists as a separate unit having its own deoxyribose residue and a phosphate group. Figure I.1 illustrates the deoxyribose sugar unit and the four nucleosides. The four nucleic acids (nucleosides) are grouped into two classes of molecules, pyrimidines and purines. Adenine and guanine are purines that have an imidazole ring fused to the pyrimidine ring. Cytosine and thymine are pyrimidines having a basic six member ring structure with two nitrogens at the 1 and 3 positions.[1]

The nucleosides along with a deoxyribose sugar unit through a B-*N*-glycoside bond between the first carbon C_1 of the sugar unit and either the first nitrogen group N_1 of the pyrimidines or the N_9 group of purines in conjunction with the hydroxyl group at the C_5 (5'-carbon) position can be converted to a phosphate ester, at which point the three units together form a deoxyribonucleotide (nucleotides). Analogous units then link to form a polymer chain via phosphodiester linkages between the C_5 phosphate ester and the C_3 group (3'- carbon) of the next deoxyribonucleotide unit. In this manner, the molecule forms through a backbone or a continuous linkage of C_5 – C_3 (5'$\rightarrow$3') phosphodiester linkages. The end of the linear polymer having no nucleotide linked to the 5'-carbon is said to be the 5'-end while the opposite end, which has no residue at the 3'-carbon, is said to be the 3'-end. This labeling lends itself to some directionality in reading the chain from one terminus to the other, with the forward direction always denoted as 5'$\rightarrow$3'.[1]

DNA acquires its double helical shape from the bonding of the nucleotide bases from one chain with those of the other. In a molecule of DNA, the two linear polynucleotide chains are oriented anti-parallel to each other as demonstrated in Figure I.1, with one chain oriented in the 5'→3' direction, and the anti-parallel chain in the 3'→5' (reverse direction). The ordering of the nucleotide bases from the 5'-chain is complementary to the order of the bases in the 3'-chain. If a planar structure of the molecule is imagined, it would be similar to a ladder, with the nucleotide bases forming the steps, and the sugar-phosphate backbone holding the steps together. The helical formation is partly the result of the simple hydrogen bonding between the nucleotide bases. Based on their structures and the specific binding affinity of each, it is noticed that guanine and cytosine are bound through three hydrogen bonds, while adenine and thymine are bonded through two hydrogen bonds; the double helix is achieved specifically from this purine:pyrimidine pairing. Other pairing possibilities are strictly forbidden. Guanine-thymine and adenine-cytosine bonds would result in mismatches because the pattern of hydrogen acceptors and donors do not correspond. The close proximity of guanine-adenine (purine) molecules bound together is energetically unfavorable, while thymine-cytosine (pyrimidine) bonds are energetically unfavorable since the molecules would be too far apart for hydrogen bonding.[1]

I.3.2 Genetic Link to Tumor Development. Within the DNA are regions (~1%) responsible for coding proteins.[10] Some genes can be correlated to physical traits such as eye or hair color while other genes with specific combinations of errors are correlated with proliferative unregulated cell growth that can result in the development of a genetic disorder termed cancer. In particular, this type of gene is referred to as an oncogene. During early developmental stages of a neoplasm cells with an inherent resistance to

apoptosis, programmed cell death, have the potential to multiply at alarming rates. These cells typically have many cell adhesion molecules decorating their periphery and as a result these cells tend to aggregate forming the tissue that is ultimately referred to as a tumor. In order for tumorigenesis to occur tumors require vascularization to thrive, because oxygen and other blood borne necessities such as divalent cations are necessary components for tumor survival.

I.4 Circulating Tumor Cells

Circulating tumor cells (CTCs) occur with exceedingly low frequency within the peripheral blood matrix, as a result these cells are rare comprising as few as one cell per 10^9 haematologic cells in the blood of a patient with metastatic disease; thereby, indicating the tremendous technical challenges of attempts to isolate and enumerate CTCs. Microfluidic cell handling devices provide seemingly ideal platforms for speciating these events and moderate successes have been yielded in microfluidic flow cytometry,[11,12] continuous size based separation,[13-15] and even chromatographic separations.[16] The essential parameters that determine efficiency of cell capture on a microfluidic platform are: 1) flow velocity, because it dictates residence times;[17] 2) throughput, because rare events require processing large samples;[18] and 3) collision probability, because the cells must interact with the walls in order for a binding event to occur.[18]

CTCs originate from primary neoplastic sites and are subsequently disseminated into the circulatory system and transported by the peripheral blood through a multivariate process termed the “metastatic cascade”. The metastatic cascade is referred to as a series of well defined interdependent events leading to a clinically relevant overt lesion.[19] The single most relevant prognostic factor in epithelial derived

tumors is the metastatic infiltration of distant organs. For example, in International Union against Cancer (UICC) stage II colon cancer patients with locally limited tumor progression have survival rates of 75% contrasted with only 13% for UICC stage IV patients who have evidenced distant organ metastasis.[20] In an analogous manner, in the much more heterogeneous breast cancer diseases the metastatic spread has the most important impact on the patient's outcome.[21] Further, metastatic evidence in the blood and/or bone marrow is also indicative of prognostic impact.[22] Triggering the cascade is a process called the epithelial-mesenchymal transition (EMT). This phenomenon enables otherwise stationary epithelial cells to migrate causing invasion into surrounding tissues eventually resulting in the detachment of neighboring cells and release into in the microenvironment. The scheme for this process is not completely understood; however, several integral components have been identified such as the receptor tyrosine kinase, growth factors, GTPases, and integrins that are closely associated with cell adhesion and migration.[23-25]

I.4.1 Natural Defense from Proliferation Metastasis. The process of hematogenous transport of the disseminated cells is an inherently destructive process that's considered the first line of defense against metastatic disease.[26] From the onset of tumorigenesis CTCs can be released from the very small micrometer scale tumors. Upon being shed, the CTCs are fragile and lack interactions with blood borne fibrin and platelets, and as a result the membrane can be easily destroyed by sheer stress imparted by blood flow.[26] In addition, natural killer cells termed Pit cells[27] and Kupffer cells[28] attack the neoplastic cells immediately upon release.[29] Presence of the CTC in the peripheral blood triggers as much as an 80% increase in the number of natural killer cells within the peripheral blood in a matter of minutes. Most tumor cells subject to hematogenous transport are

either mechanically destroyed from the sheer stress of blood flow rupturing the cells membrane or the CTC undergoes a process called anoikis, a special form of cell death resulting from an adhesion deficiency. The vast majority of the carcinoma cells are killed within a few hours of dissemination through the natural defense systems, thereby demonstrating the relatively low efficiency of metastatic events.[30]

I.4.2 Metastatic Tumor Progression. Cancers that originate in organs such as the mammary glands, colon, and/or prostate are forms of adenocarcinomas. Most often, tumors develop in the organs proximal to capillary beds, owing in part to the metastatic CTC surviving the natural protections provided by the circulatory system. This survival is further supported by the CTC developing a protective barrier consisting of fibrin and platelets sufficient to prevent lysis from blood flow related sheer stress by providing stabilizing reinforcement, and barrier like protective coating from natural killer cells. Subsequently, the surviving CTCs are arrested in capillary beds in which adhesion molecules of the distant organ act on receptors in the CTC membrane forming complexes. Aiding this process is the relatively narrow bore of the capillaries resulting in increasing the probability of adhesion, based on the CTCs and receptors being proximally within binding range of the adhesive molecules on the surface for extended periods due to decreased mobility. Subsequently, extravasation results when the tumor cells migrate across the capillary wall. The morphology of cancer cells is distinct, these cells are often larger (15 – 40 μm dia.) than normal haematopoetic cells and they harbor above average sized nuclei.[31]

I.5 Human Concerns

Cumulatively, cancer is the leading cause of death among the world population and the causes of cancer are generally considered to be some combination of

environmental, occupational, and/or hereditary factors.[32] Though no point source can be cited in most cancer cases, all cancers stem from specific sets of combinations of defects in the genetic code.[1,26] In many cases even this is obscure and not well understood. These defects can be caused by insertion, deletion, or substitution of bases in the genes resulting in producing proteins that have markedly different behaviors.[1,26] As a result, CTCs are of interest to researchers, because they can provide insight into disease states, and when quantified they can provide both valuable prognostic and diagnostic information about patients.[33]

I.6 Environmental Concerns

Some prokaryotes, though indigenous to humans and animals that humans consume can be toxic and potentially lethal.[34] The number of cells required for such an outcome varies, but is contingent upon the nature of cell at issue. As an example as few as 10 Escherichia coli 0157:H7, an enterohemorrhagic bacterium, can proliferate in the digestive system causing *Shigella dysentery,* a potentially fatal disease if not treated.[35,36] Conversely, a benign strain (K12) of bacteria of similar origin that of the 0157:H7 variety is harmless.[37] Morphologically these two strains are identical, but they express markedly different proteins due to differences in their DNA. The toxic strain produces *shiga*-like toxins referred to as SLT-I and SLT-II.[38] These bacteria are indigenous to the gut of bovine animals, and can be isolated from pastures containing feces from the animals. Through precipitation and subsequent runoff these dangerous cells work their way into the water table impacting ground water and aquifers.[39] Maintaining safe recreational areas, fisheries, and drinking water is contingent upon being able to readily identify and quantitate the contaminants on site.

I.7 Research Focus: Need for Greater Selectivity, Sensitivity, and Portability

In this dissertation, I investigate the use of surface modification chemistries and electrokinetic pumping in polymer-based microfluidic devices as a means of controlling the rate and direction of movement of cells in suspension. I also present data from the hydrodynamic manipulation of cells in analogous devices. The need for sensitive selective methods to isolate, enumerate, and phenotype low abundant biological cells is apparent whether the need arises as a result of United States of America Environmental Protection Agency USEPA mandates on water quality or if the need is in the clinical setting at the point of care there exists a need for rapid approaches to selectively speciate and evaluate particular cells from often complex matrices i.e. peripheral blood. Nagrath *et al.* recently presented a device capable of selecting rare cancer cells, but to date, no methodologies presented completely satisfies clinical need.[17] I present a novel approaches toward real solutions to these problems.

I.8 References

(1) Stryer, L. *Biochemistry*; 4th ed.; W. H. Freeman and Company: New York, 2000.

(2) Fidler, I. J.; Yano, S.; Zhang, R. D.; Fujimaki, T.; Bucana, C. D. *Lancet Oncology* **2002**, *3*, 53-57.

(3) McClain, M. A.; Culbertson, C. T.; Jacobson, S. C.; Ramsey, J. M. *Anal. Chem.* **2001**, *73*, 5334-5338.

(4) Wood, D. P.; Banerjee, M. *J. Clin. Oncol.* **1997**, *15*, 3451-3457.

(5) Mader, S. S. *Biology*; 4th ed.; William C. Brown Communications: Dubuque, 1993.

(6) King, G. A. *BioSyst.* **1977**, *9*, 35-42.

(7) Chen, L.-L.; Wang, G.-Z.; Zhang, H.-Y. *Biochem. Biophys. Res. Commun.* **2007**, *363*, 885-888.

(8) Kirk, J. T. O. *Photosyn., Two Centuries Its Discovery Joseph Priestley, Proc. Int. Congr. Photosyn. Res., 2nd* **1972**, *3*, 2333-47.

(9) Schatz, G.; Mason, T. L. *Annu. Rev. Biochem.* **1974**, *43*, 51-87.

(10) Lewin, R. *Science* **1986**, *232*, 577-8.

(11) Simonnet, C.; Groisman, A. *Anal. Chem.* **2006**, *78*, 5653-5663.

(12) Fu, A. Y.; Spence, C.; Scherer, A.; Arnold, F. H.; Quake, S. R. *Nat. Biotechnol.* **1999**, *17*, 1109-1111.

(13) Davis, J. A.; Inglis, D. W.; Morton, K. J.; Lawrence, D. A.; Huang, L. R.; Chou, S. Y.; Sturm, J. C.; Austin, R. H. *Proc. Natl. Acad. Sci. U. S. A.* **2006**, *103*, 14779-14784.

(14) Mohamed, H.; McCurdy, L. D.; Szarowski, D. H.; Duva, S.; Turner, J. N.; Caggana, M. *IEEE Trans. NanoBiosci.* **2004**, *3*, 251-256.

(15) Mohamed, H.; Murray, M.; Turner, J. N.; Caggana, M. *NSTI Nanotech 2005, NSTI Nanotechnology Conference and Trade Show, Anaheim, CA, United States, May 8-12, 2005* **2005**, *1*, 1-4.

(16) Chang, W. C.; Lee, L. P.; Liepmann, D. *Lab Chip* **2005**, *5*, 64-73.

(17) Nagrath, S.; Sequist, L. V.; Maheswaran, S.; Bell, D. W.; Irimia, D.; Ulkus, L.; Smith, M. R.; Kwak, E. L.; Digumarthy, S.; Muzikansky, A.; Ryan, P.; Balis, U. J.; Tompkins, R. G.; Haber, D. A.; Toner, M. *Nature* **2007**, *450*, 1235-U10.

(18) Adams, A. A., Okagbare, P. I. and Soper, S. A. *J. Am. Chem. Soc.* **2008**, *(in press)*.

(19) Fidler, I. J. *Nature Reviews Cancer* **2003**, *3*, 453-458.

(20) Platell, C.; Morris, M.; Lacopetta, B. *Med. J. Aust.* **2007**, *187*, 251-251.

(21) Garcia-Closas, M.; Brinton, L. A.; Lissowska, J.; Chatterjee, N.; Peplonska, B.; Anderson, W. F.; Szeszenia-Dabrowska, N.; Bardin-Mikolajczak, A.; Zatonski, W.; Blair, A.; Kalaylioglu, Z.; Rymkiewicz, G.; Mazepa-Sikora, D.; Kordek, R.; Lukaszek, S.; Sherman, M. E. *Br. J. Cancer* **2006**, *95*, 123-129.

(22) Zitt, M.; Zitt, M.; Muller, H. M.; Dinnewitzer, A. J.; Schwendinger, V.; Goebel, G.; De Vries, A.; Amberger, A.; Weiss, H.; Margreiter, R.; Ofner, D.; Oberwalder, M. *Dis. Colon Rectum* **2006**, *49*, 1484-1491.

(23) Grunert, S.; Jechlinger, M.; Beug, H. *Nature Reviews Molecular Cell Biology* **2003**, *4*, 657-665.

(24) Guarino, M.; Rubino, B.; Ballabio, G. *Pathology* **2007**, *39*, 305-318.

(25) Tse, J. C.; Kalluri, R. *J. Cell. Biochem.* **2007**, *101*, 816-829.

(26) Gassmann, P.; Haier, J. *Clin. Exp. Metastasis* **2008**, *25*, 171-181.

(27) Wisse, E.; Vantnoordende, J. M.; Vandermeulen, J.; Daems, W. T. *Cell Tissue Res.* **1976**, *173*, 423-435.

(28) Wiltrout, R. H. *Immunol. Rev.* **2000**, *174*, 63-76.

(29) Grundy, M. A.; Zhang, T.; Sentman, C. L. *Cancer Immunology Immunotherapy* **2007**, *56*, 1153-1161.

(30) Timmers, M.; Vekemans, K.; Vermijlen, D.; Asosingh, K.; Kuppen, P.; Bouwens, L.; Wisse, E.; Braet, F. *Int. J. Cancer* **2004**, *112*, 793-802.

(31) Fehm, T.; Solomayer, E. F.; Meng, S.; Tucker, T.; Lane, N.; Wang, J.; Gebauer, G. *Cytotherapy* **2005**, *7*, 171-85.

(32) Jemal, A.; Siegel, R.; Ward, E.; Hao, Y.; Xu, J.; Murray, T.; Thun, M. J. *CA. Cancer J. Clin.* **2008**, *58*, 71-96.

(33) Singletary, S. E.; Connolly, J. L. *CA. Cancer J. Clin.* **2006**, *56*, 37-47.

(34) Wang, N.; He, M.; Shi, H. C. *Anal. Chim. Acta* **2007**, *590*, 224-231.

(35) DeCory, T. R.; Durst, R. A.; Zimmerman, S. J.; Garringer, L. A.; Paluca, G.; DeCory, H. H.; Montagna, R. A. *Appl. Environ. Microbiol.* **2005**, *71*, 1856-1864.

(36) Togo, C. A.; Wutor, V. C.; Limson, J. L.; Pletschke, B. I. *Biotechnol. Lett.* **2007**, *29*, 531-537.

(37) Brenner, K. P.; Rankin, C. C.; Roybal, Y. R.; Stelma, G. N.; Scarpino, P. V.; Dufour, A. P. *Appl. Environ. Microbiol.* **1993**, *59*, 3534-3544.

(38) Boyaci, I. H.; Aguilar, Z. P.; Hossain, M.; Halsall, H. B.; Seliskar, C. J.; Heineman, W. R. *Anal. Bioanal. Chem.* **2005**, *382*, 1234-1241.

(39) Ibekwe, A. M.; Watt, P. M.; Grieve, C. M.; Sharma, V. K.; Lyons, S. R. *Appl. Environ. Microbiol.* **2002**, *68*, 4853-4862.

Chapter 1 Recent Microfluidic Approaches toward Cellular Analyses: A Literature Review

1.1 Introduction

Biological cells have been of interest to researchers performing bioassays since the imaging of the first cell by Anton von Leeuwenhoek in 1674.[1] About two centuries later, Ashworth observed an atypical cell type in the peripheral blood that morphologically appeared to be of epithelial origin and was designated as a tumor cell.[2] Since then, isolating and enumerating circulating tumor cells based on phenotype has been of interest in many basic, clinical, and medical research settings. The challenge with using circulating tumor cells present in peripheral blood, or other clinical samples, as a cancer diagnostic marker is the extremely low frequency in which these cells appear in relative to other cell types. For example, it is not uncommon to find 5 – 10 tumor cells in 1 mL of whole blood that also contains 10^7 red blood cells (erythrocytes, RBCs) and 10^3 white blood cells (leukocytes, WBCs). Therefore, enrichment factors exceeding 10^7 must be obtainable by the equipment used to select and subsequently enumerate these cells.

Unfortunately, cancer cells will proliferate due to the cells' lack of appropriate cues for apoptotic or programmed cell death resulting from a combination of genetic defects, which inevitably provides their ability to survive circulation and adhere to secondary sites giving rise to metastatic disease.[3] As a matter of definition, neoplastic cells originating from a primary site are often referred to as tumor cells.[4] The term "tumor cell" can be applied to both benign and malignant varieties of neoplastic cells; however, only malignant cells are aptly termed "cancer cells". As such, circulating tumor cells (CTCs) can or will not spawn metastatic disease depending upon their genetic makeup.

Morphologically, tumor cells are typically smaller than normal epithelial cells and they possess larger nuclei with small cytoplasmic regions (see Figure 1.1). These

morphological differences make them easy to differentiate with respect to normal epithelial cells, which typically do not appear in peripheral blood.[5] The characteristic features of cancer cells' morphology has been linked in part to the pentose phosphate pathway (PPP) generating an increase in glucose metabolism of cancer cells during proliferation.[3]

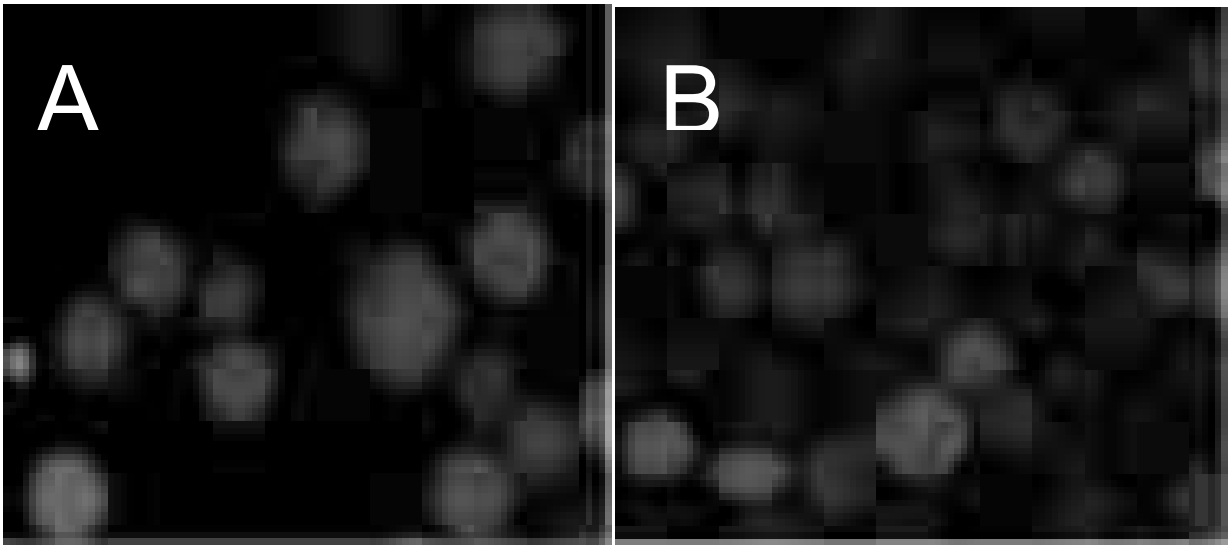

Figure 1.1 Micrographs of (A) normal epithelial cells and (B) malignant epithelial tumor cells. Note the larger size of the normal epithelial cells compared to the tumor cells. Reprinted with permission.[6]

Besides morphological differences, the molecular composition of tumor or cancer cells substantially differs from that of normal epithelial cells as well. Many cancers are characterized by mutations within the genome of tumor/cancer cells that can give rise to gene silencing or gene hyperactivity resulting in the over-expression of various molecular entities, such as integral membrane proteins. For example, many adenomacarinomas over-express the epithelial cell adhesion molecule (EpCAM),[7] or in the case of prostate cancer, the prostate specific membrane antigen (PSMA).[8]

Metastasized epithelial cells undergoing hematogenous transport are atypical in healthy human blood.[9] However, many adenocarcinomas are characterized by tumor cells shed from the primary tumor site into the peripheral blood. As noted above, the number of these cells in the peripheral blood is extremely low compared to the RBC and WBC count. For example, the number of tumor cells from breast cancer patients can be in the range of 5 per mL of whole blood.[10]

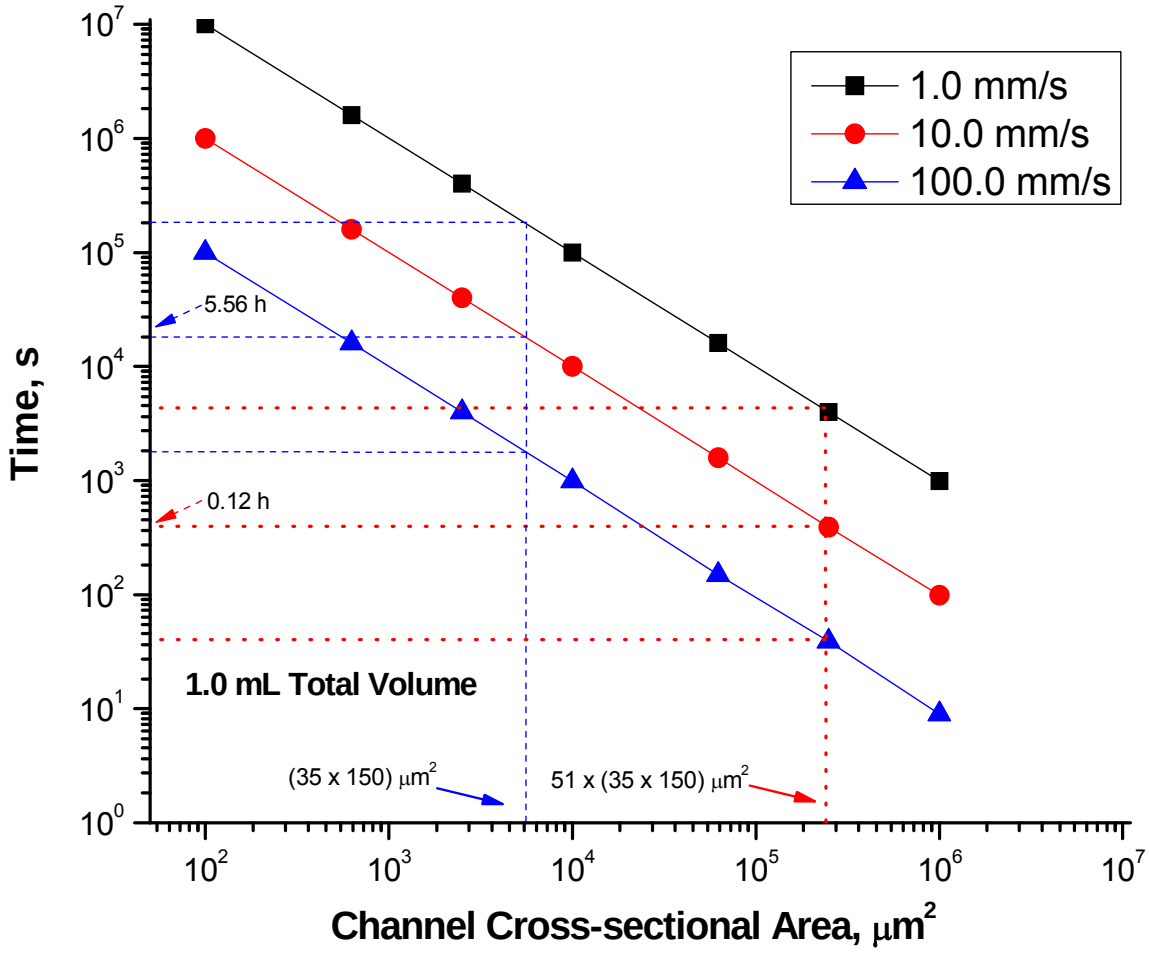

Figure 1.2 Processing time as a function of the fluidic cross-section using microfluidics at three different linear velocities. The total volume sampled is 1.0 mL. Note the 35 × 150 μm^2 cross-section indicated in the figure for a single or 51 parallel channels. These dimensions were used in the device described in Chapter 3 of this dissertation.

The predominate techniques used to select rare tumor cells from peripheral blood or other biological/clinical samples has been carried out using fluorescence assisted cell sorting (FACS) or magnetic assisted cell sorting (MACS);[11,12] the complexity of FACS/MACS instrumentation and the required operator expertise makes these techniques prohibitive toward their widespread adoption for screening applications, which has facilitated a strong interest in producing simpler and more efficient methods for sorting and the subsequent enumeration of these rare cells.[13]

For sampling rare events, four important metrics must be assessed: i) throughput, the number of cell identification or sorting steps per unit time; ii) recovery, an indicator of the fraction of target cells collected from the input sample; iii) purity, which depends on the number of "interfering" cells excluded from the analysis; and iv) analysis time, which is the time it takes to process a specified volume of sample exhaustively.[14] In addition to these metrics, highly efficient quantification of the number of enriched cells must be provided as well.

Throughput is directly proportional to the cross-sectional area of the conduit through which the sample is delivered and the sample volume required for interrogation (see Figure 1.2). The input sample volume required for the assay is determined by the frequency of cell appearance in the sample. At 5 cells mL^{-1}, a sampling volume of 1 μL would produce a probability of finding the cell in that volume of only 0.5%. Because CTCs are of low frequency (1 – 10 cells mL^{-1}), high volume sampling (≥1 mL) is required to increase the probability of isolating these rare events. If the cross-sectional dimensions of 35 x 35 μm are employed to exhaustively search for rare cellular events when the transport rate is 10 mm s^{-1}, and an input volume of 1.0 mL is required, the sampling time would be approximately 278 h. For cell sorters consisting of a single

rectangular via with dimensions of 150 × 35 μm under similar conditions the sampling time would reduced to approximately 5.6 h. However, if the 150 × 35 μm conduit were highly parallelized by incorporating 51 vias, the processing time drops to 0.12 h as shown in Figure 1.2. The time it takes to process 1.0 mL of fluid at varying linear velocities for channels with different cross sectional areas are also shown in Figure 1.2. As can be seen, increases in the linear transport rate does affect the processing time, with higher transport rates reducing the processing time.

The purity of the enriched targets is also critical, because impurities can result in the generation of false positives. For molecular recognition used for cell selection, the level of purity is predicated on the specificity of the recognition element used for its binding partner. For size-based selection, cells with sizes similar to the target cells can provide potential interferences. For example, recovery rates using size selection can typically be on the order of 60%, but are often marred by interferences resulting in low purity enrichments caused by contaminating leukocytes due to the similarity in sizes of the WBCs and tumor cells.[15-19] Attempts to further pre-concentrate the targets and remove potential WBC interferences introduce a significant risk of target loss.[15,20]

There exist two extremes pertaining to the habitat of the target cell. One extreme is that of a relatively simple sample matrix containing few cell-like constituents that would potentially interfere. At the other extreme is whole blood; 40 – 57 (w/w)% of normal peripheral blood from a healthy person consists of suspended solids in the form of leukocytes and erythrocytes.[21] For this reason, analyzing blood directly has presented several distinct challenges requiring in most cases, various types of sample pretreatment prior to the cell sorting. These pre-treatments range from serial dilution (up to 10-fold)[22] to density gradient centrifugation,[23] whereby particles with distinct mass-to-

volume ratios are separated into layers of varying density [40 – 70%(w/w)] in a cushioning medium via centrifugal force.[24] Initially, layers of varying concentrations of sucrose are added to a vessel with the least dense layer being added first with subsequent layers with increasing densities being added above the seed layer. The last layer added to the vessel contains the sample suspension with the target cells. Depending on particle density, a centrifugal force of as much as 150,000×g is applied to the sample using ultracentrifugation resulting in all constituents originating in the sample residing in the layer of solution that matches the density of the respective particles. Layers containing the targets are harvested by recovery with a pipette. These techniques typically provide 70 – 90% target cell recovery.[25] In terms of whole blood, density gradient centrifugation is used to remove the RBC fraction of whole blood, leaving only the mononucleated fraction for cell selection of the targets.

There are fundamentally two different device formats that can be used for selecting rare cells from mixed populations, macro-scale systems and micro-scale systems. Macro-scale systems are attractive for selecting rare cells due to their ability to process large input volumes easily while conventional microsystems do not possess the ability to process large input volumes as easily (see Figure 1.1), which is required to generate a high statistical confidence for successfully securing the rare cells from the processed sample.

1.2 Transport Phenomena

Blood is a uniquely complex fluid composed of deformable cells suspended in an aqueous liquid that contains many proteins, lipids, and other colloids. Blood averages 48% blood cells by weight with greater than 95% of the cells being erythrocytes. Blood exhibits non-Newtonian rheological characteristics unrelated to coagulation or clotting

as the apparent viscosity decreases with increasing shear rate; as blood flows more quickly the apparent viscosity decreases, an effect known as shear thinning.[26] Manipulating viscous samples containing cellular targets in fluidic vias, most commonly microfluidic vias, can be accomplished by establishing a pressure differential or by initiating an electrokinetic flow characterized by either a parabolic or flat profile, respectively.

1.2.1 Electrokinetic Pumping. Glass and fused silica-based substrates have been used extensively in microfluidics for performing bioassays due to its well defined surface chemistry.[27] The presence of these surface silanols in glass and fused silica generates a movement of the bulk solution when an electric field is applied to the fluidic conduit that moves from the anode to the cathode.[28-32] This transport phenomenon is due to the electroosmotic flow (EOF). EOF is brought about when the negatively charged surface that results from the deprotonation of silanols attracts cations forming both a fixed and diffuse mobile layer. The immobile layer is closest to the wall, and adjacent to positive ions separated by a plane of shear. The potential difference across this plane is termed the zeta potential. The zeta potential (ζ) is given by:

$$\zeta = 4\pi\delta e/\epsilon \quad (1)$$

where δ is the double layer thickness, e is the charge per unit surface area, and ϵ is the dielectric constant of the buffer. The mobile layer is carried towards the cathode under applied electric fields dragging the bulk solution along with it. The magnitude of the EOF in glass is typically greater than the electrophoretic mobility of most analytes. The EOF ultimately leads to migration of all positive, neutral, and negative charged components towards the cathode in that respective order. This type of pumping is typically not ideal

for high fluid throughput fluid processing due to its potential for developing voids within the buffer resulting from O_2 and H_2 evolution at the electrodes.[33,34]

While glass and fused silica have relatively large EOF values at high pH values, the situation for polymer-based materials is ill-defined. Different polymeric material as well as the treatment imposed on those materials can dramatically affect the surface chemistry and therefore, produce significant variations in the EOF. In addition, decreases in the number density of ionizable surface groups results in significantly lower EOFs in polymers relative to glass-like materials.[24,35]

Our research group has successfully overcome this obstacle by applying chemistries for surface modification of poly(methyl methacrylate), PMMA, and polycarbonate, PC.[35-38] The potential exists to photo-oxidize polymer surfaces by UV exposure, which result in increased EOFs due to increases in the surface charge density, while not disturbing the integrity of the bulk polymer.[36,37,39] The formation of phenyl salicylates and hydroxybenzophenones as well as other hydroxyl and keto containing groups result on the surface of UV irradiated PC. UV irradiation induces photo-oxidation at the surface of PMMA forming hydroxyl functional groups.[37]

Witek *et al.* reported on the use of polymeric microfluidics for the electrokinetic transport of *E. coli* and *S. cerevisiae* to examine the effects of surface chemistry on the apparent mobility for pristine and UV modified poly(methylmethacrylate) and polycarbonate microdevices at varying ionic strengths.[33] The electrokinetic transport of differing cell types was presented in which the potential for separating cells based on their intrinsic electrical properties was discussed. The magnitude and direction of the apparent mobilities were determined. The fastest electromigration was exhibited by *S. cerevisiae* in a 0.5 mM PBS buffer in a UV-modified microchannel with an apparent

mobility reported to be 4.83 ± 0.80 × 10^4 cm^2 V^{-1} s^{-1}, and a velocity of *E. coli* in pristine PMMA equal to -1.04 ± 0.04 × 10^4 cm^2 V^{-1} s^{-1}.

1.2.2 Hydrodynamic Pumping. Hydrodynamic pumping results from a pressure differential and is characterized by a parabolic profile and this type of pumping is prevalent in high throughput applications owing in part to the ability of mechanical pumps to deliver fluids at well regulated flow rates into high head pressure conduits. In addition, all material move in one direction irrespective of their chemical composition. Another problem avoided by hydrodynamic pumping is Joule heating, which results from resistive heating of the buffer due to current flow and poor heat dissipation. However, hydrodynamic transport generates large pressure drops for long conduits with small inner diameters. The pressure drop is directly proportional to the length of the conduit, flow rate of the solution, and the kinematic viscosity of the solution. The pressure drop (ΔP) across any conduit can be determined using Poiseuille's Law:

$$\Delta P = 8LQ\eta/\pi R^4 \quad (2)$$

where L is the length of the conduit, Q is the flow rate of the fluid, η is the kinematic viscosity of the fluid, and R is the conduit radius. From Poiseuille's equation, it can be seen that the radius has an inverse exponential effect on ΔP. As an example of the throughput potential afforded by hydrodynamic pumping, Adams *et al.* demonstrated the ability to hydrodynamically process solutions through a micro-conduit at velocities as high as 100 mm s^{-1} with no device failure due to the high pressure drop generated under these conditions.[24]

1.3 Composition of Microfluidic Devices

In the production of microdevices for any particular application, the fabrication technique required by the material and the associated cost of the material has to be

considered. For example, when considering clinical assays, sterile materials are required for each assay and the ability to use the same device for multiple samples is not possible due to carryover artifacts. Therefore, low-cost and easy manufacturable devices are ideal. As a result, polymers are attractive substrates because replication-based processes can be used to mass produce devices at low-cost.

Various applications require alternative substrate material. In choosing materials for microfluidic devices, the following should be considered; (i) thermal and electrical properties, (ii) analyte and matrix chemical compatibility, (iii) availability in pure form at an affordable cost, (iv) excellent optical properties in the measurement range, (v) amenable to surface functionalization, (vi) applicable to mass-production using simple fabrication techniques and (vii) the fabrication technique can produce the requisite structures for the intended application.

There exist significant cost advantages associated with polymeric microfluidics using currently available techniques that involve the production of a metal mould with positive relief structures that can be used to produce structures within a polymeric material. Commonly used techniques for producing parts from metal moulds include casting, hot-embossing, and injection moulding.

1.3.1 Polymeric Substrates. Hot embossing and injection moulding are common modalities for producing polymeric micro-parts and can produce fluidic layouts with high aspect ratio microstructures (HARMS).[39] Details of hot embossing and injection moulding are discussed in detail elsewhere.[40-42] Briefly, hot embossing involves the transfer of a positive structure, termed a mould insert/master, to a substrate under precisely controlled temperature and pressure. The substrate is typically heated to above the glass transition (T_g) temperature of the polymer, and an applied force in the

range of several thousand Newtons. The T_g of a polymer indicates the temperature at which the polymer begins to flow due to the thermally initiated breaking of non-covalent bonds between the polymer chains. The application of significant force ensures that the polymer fills the mould cavity completely facilitating the high fidelity of reproducing microstructures.[39,43]

Conventional mold inserts are prepared via lithographic techniques that require radiation sources such as x-rays or UV light and electroplating to produce the mould master. For example, UV and/or x-ray LiGA can produce structures in the submicrometer regime with aspect ratios exceeding 20 or more, but involves 10 – 14 steps to go from concept to final product (see Table 1.1).[42] Alternatives, such as high precision micromilling, has fewer processing steps but can only produce structures with lateral dimensions on the order of 20 μm and aspect ratios of 5. However, mould fabrication only requires a few processing steps.

Table 1.1 Comparisons of Manufacturing Techniques for Microfabrication.

Characteristics	**LiGA – X-ray**	**LiGA – UV**	**Micromilling**
Minimum size	20 nm	500 nm	20 μm
Multilevel	1	3 or less	5 or less
Aspect ratio	100 or more	20 or less	5 or less
Side-wall roughness	1-10 nm	20-50 nm	>150 nm
Production cost	$$$	$$	$
Processing steps	14 steps	10 steps	4 steps
Turnaround time	2 weeks	1 week	< day

In contrast to glass-based microdevices, polymeric microdevices have relatively low EOF resulting from a reduction in the number density of ionizable surface groups. Additionally, polymers have lower occurrences of cell adhesion on pristine surfaces due to the low surface charge density of polymers.[38] The decrease in ionizable surface groups results in significantly lower EOFs in polymers relative to glass-like materials.[24,35] The apparent mobility (μ_{app}) consists of two components:

$$\mu_{app} = \mu_{EOF} + \mu_{EP} \quad (3)$$

where μ_{EOF} is the mobility arising from the EOF and μ_{EP} is the mobility component arising from the electrophoretic mobility of the analyte. According to equation 3, the apparent mobility is the sum of the electrophoretic and electroosmotic mobilities. The EOF component is contingent upon buffer conditions and the microchannel surface chemistry. Our research group has generated novel surface modification chemistries of poly(methylmethacrylate), PMMA, and polycarbonate, PC, to increase the number density of ionizable groups.[35-38] The application of said surface modification chemistries is effective at increasing the number of ionizable surface groups, while not disturbing the integrity of the bulk polymer.[36,37,39]

1.4 Macro-Scale Techniques for Analyzing CTCs

Macro-scale CTC techniques possess the ability to process input volumes exceeding ~5 mL, which is attractive due to the extremely low abundances of these cell types in clinical samples, The commonly used macro-scale formats for enriching CTCs from clinical samples include: (i) Magnetic capture using micrometer-scaled ferromagnetic beads coated with molecular recognition elements in macro-scale vessels;[20,44,45] (ii) size-based separations using tracked membranes;[19,46,47] (iii) flow-assisted cell sorting;[9,46,48] and (iv) reverse-transcription of mRNAs that are used as

chemical surrogates for tumor cell identification.[49,50] Macro-scale techniques for cell processing and selection are typically performed using samples with volumes >1 mL. In the following sections, these macro-scale processing techniques for identifying the presence of tumor cells in clinical samples will be discussed as well as variants of these basic cell selection processes.

1.4.1 Immunomagnetic Affinity Capture (IMAC). Balic *et al*. evaluated two commercially available immunomagnetic isolation kits for selecting CTCs from peripheral blood samples of metastatic patients.[15] Both kits employed anti-epithelial cell adhesion molecules (EpCAM) antibodies for selecting the cancer cells. Twenty-two and one half mL aliquots of blood were taken from each patient with a 15 mL aliquot used for the OncoQuick® system and the remaining 7.5 mL used for the CellSearch® procedure. Both procedures employed density gradient centrifugation followed by a series of washes in order to remove the RBC fraction from the whole blood sample prior to magnetic isolation of the CTCs. Centrifugation of the RBC depleted sample was next performed at 800×g for 10 min to remove the blood plasma. The resulting cellular pellets were resuspended in 10 mL of buffer, and incubated with carboxylate-functionalized ferromagnetic particles that were coated with anti-EpCAM. Immunomagnetically-labeled cells were concentrated using an external magnetic field. Following magnetic isolation, the processed sample was incubated with leukocyte specific anti-cytokeratin antibodies labeled with Alexa Fluor 555, nuclear specific 4',6-diamidino-2-phenylindole (DAPI), and a CTC specific anti-EpCAM antibody conjugated to a fluorescein derivative. Under these conditions, white blood cells and tumor cells harbor blue fluorescing nuclei; however, the fluorescent signatures of the FITC derivative selectively placed a green "halo effect" about the blue nuclei of the CTCs.

The orange fluorescent halo from the Alexa Fluor 555 about the nuclei of the leukocytes was used for exclusion.

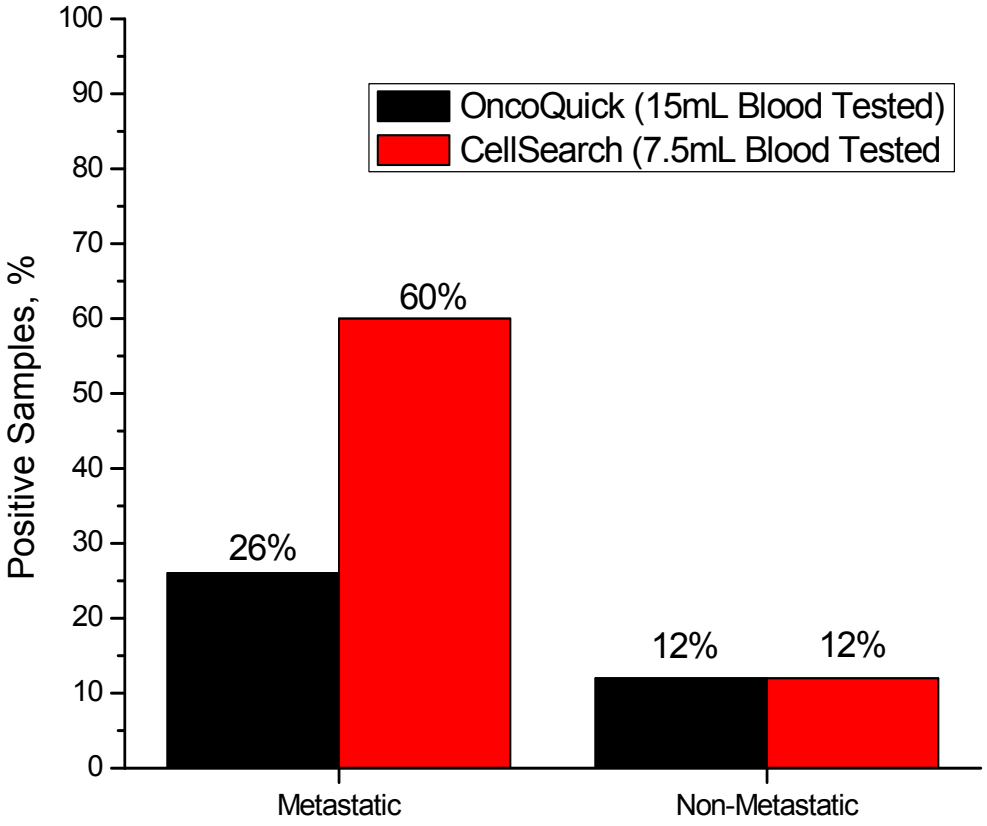

Figure 1.3 CTC recovery results from commercially available immunomagnetic cell isolation strategies from 61 metastatic cancer patients and 8 controls samples that were absent of any form of disease. Reprinted with permission.[15]

The CTC recovery rates using both kits from cancer patients with metastatic disease and healthy donors are shown in Figure 1.3. Data from 53 cancer positive samples (Metastatic, see Figure 1.3) are shown on the left as evaluated by CellSearch and OncoQuick. The data indicated that the recovery of the CTCs was significantly better using the CellSearch system (60% recovery) compared to the OncoQuick system (26%

recovery). In addition, the CellSearch system required a smaller input volume compared to the OncoQuick system. The data for non-metastatic samples (see Figure 1.3) with both kits showed the detection of at least one CTC in the blood of healthy individuals in 12% of these samples analyzed. For the confirmed metastatic cancer cases, CellSearch was capable of producing positive responses in 54% of these samples resulting in a relatively high rate of false negatives.[48] The OncoQuick system demonstrated poorer detection accuracy as only 23% of the samples were reported positive for metastatic disease. In 5 of the 6 varieties of cancer studied, CellSearch was twice as effective as OncoQuick at detecting metastatic disease and CellSearch was also found to be more sensitive in common positive tests often identifying more CTCs within similar amounts of peripheral blood.

1.4.2 Sized-Based Separations. Tracked polycarbonate membranes with varying pore sizes (8 – 14 μm) have also been employed to filter large (9.0 – 18 mL) blood samples spiked with known quantities of CTCs.[51] Prior to filtration using the membrane, the samples were diluted at a 1:1 (v/v) ratio of spiked blood:PBS containing an anticoagulant (ethylene diamine tetra acetic acid). Simple gravimetric filtration through these polycarbonate membranes is sufficient to reduce the erythrocyte content by $>10^5$ cells mL^{-1}. After the initial filtration using the polycarbonate filter, the isolated cells are washed and incubated for 1 h with anti-pan-cytokeratin directed against cytokeratin 5, 6, 8, 17 and 19)-FITC. After a wash to remove the unbound anti-cytokeratin antibodies, nuclei-specific propidium iodide is added, and an additional incubation of 30 min performed. The cells retained by the polycarbonate membrane are analyzed using a combination of laser scanning cytometry (LSC) and microscopy. After analysis, all the cytokeratin positive cells are relocated and examined “by eye” to exclude any false-

positive events. Only positive cells with the appropriate nuclear:cytoplasmic ratio were counted as positive events. False positives were evident in the case of MCF-7 cells, and the authors attributed this to the presence of adhesion molecules on the cells' periphery. The most prominent reduction in leukocyte frequency was demonstrated for 9 mL blood samples that originally contained 50,000,000 leukocytes, which was reduced to 7,000 leukocytes after the filtration step. These membranes were demonstrated to isolate nearly 85 – 100% of the CTCs, but significant numbers of white blood cells were also retained due to their similar size with respect to the CTCs complicating the enumeration process. Also, the process requires pre or post treatment of retained cells with a variety of fluorescent stains before the LSC could be utilized.

Microarrays have also been used in the isolation of target cells. Various "cluster of differentiation" (CD) antigens are affinity-captured onto the arrays containing immobilized antibodies.[52] The arrays contain several surface-immobilized antibodies directed toward target antigenic species, which are used to spatially isolate cells. These methods are limited by slow mass transport but are promising for multiplexed analyses; the array elements are not individually addressable making collecting isolated cells from a multiplexed analysis difficult due to the single chamber of the arrays. Most often in order to isolate a particular phenotype, subsequent processing is required. Belov *et al*. presented an array technique based on cluster of differentiation in leukemia.[52] The CD antigens could be used to phenotype leukocytes based on characteristic abnormal patterns of antigen expression. Microarray technology has also been used to screen HIV positive blood against normal as well as blood from those undergoing therapy and those deemed long term non-progressors.[12]

1.4.3 Fluorescence Activated Cell Sorting (FACS). Gross *et al.* employed FACS to sort spiked breast cancer cells from a BT-20 cell line that were seeded into peripheral blood mononucleated cells (PBMC or WBC) at frequencies of 10^{-5}, 10^{-6}, and 10^{-7}.[9] The PBMCs were suspended in PBS buffer with 20% fetal calf serum. To the PBMC (cell count = 4×10^8) suspensions were added 10, 100, and 1,000 BT-20 cells. The flow cytometer employed three excitation sources; 325 nm, 488 nm, and 633 nm allowing for discrimination between the PBMCs and BT-20 cells via immunoaffinity staining. A panel of fluorescently-labeled antibodies specific for the PBMCs produced a green color for these cell types. Another panel of immunofluorescent markers were used for the BT-20 cells, that produced a yellow color and 2 shades of red, but no green color for these cells.

The extensive cell staining procedure is briefly listed here. The BT-20 cells were stained with a blue fluorescing dye, 7-amino-4-chloromethylcoumarin (CMAC) before seeding these cells into a PBMC suspension. BT-20 breast cancer cells were also characterized by a cocktail containing three anti-cytokeratin antibodies, each tagged with a different colored dye. Leukocytes were identified with monoclonal antibodies labeled with a fourth dye. All cells were incubated for 1 h in 150 µL of an exclusion staining cocktail containing 20% normal mouse serum. The following fluorescein isothiocyanate (FITC) conjugated antibodies were added to the suspension: 14.9 µg of anti-CD45 HLe1-FITC per mL; 54 µg of anti-platelet glycoprotein (gpIX) (CD42a)-FITC per mL; 56.6 µg of anti-pan-platelet (CD61)- FITC per mL; 2.2 µg of anti-CD34 HPCA-2-FITC per mL; and 0.7 µg of anti-glycophorin-FITC per mL. Subsequently, a staining cocktail containing 25% normal mouse serum and the following anti-cytokeratin antibodies conjugated to peridinin chlorophyll protein (PerCP), phycoerythrin (PE) or

allophycocyanin (APC): 2.6 μg of NCL-5D3 anti-cytokeratin components 8 and 18 conjugated to PerCP per mL were used; 1.8 μg of NCL-LP34 anti-cytokeratin components 5, 6, and 18 conjugated to PerCP per mL; 0.27 μg of CAM 5.2 anti-cytokeratin components 8 and 18 conjugated to PE per mL; and 1.43 μg of AE1 anti-cytokeratin components 10, 14, 15, 16, and 19 conjugated to APC per mL. The data were prefiltered, eliminating events negative for FITC but positive for PE, PerCP, and APC. In all instances the goal was to locate events characterized by fluorescence from FITC, PE, PerCP, and APC, which were used as positive signals for the BT-20 cells.

Using a color discrimination algorithm, the authors were successful at detecting rare BT-20 cells with 20% recovery with cancer cell frequencies of 10^{-5} and 10^{-6}. However, the authors indicated that ~200 mL blood sample volumes would be needed to reliably assess rare CTCs in the presence of 10^{8} PBMC cells at frequencies of 10^{-7}. The challenges associated with this assay format is the extensive amount of time required for the immunofluorescent staining (~20 h), the need for removing the RBCs from the blood sample prior to processing and the equipment required for the measurements.

1.4.4 Reverse Transcription Polymerase Chain Reaction (RT-PCR). Another approach for the analysis of CTC presence in peripheral blood is the use of reverse-transcription polymerase chain reaction (RT-PCR), in which mRNAs are used as surrogates to report on the presence of CTCs. This gene expression based assay has high sensitivity, but poor selectivity which leads to false positives. Often nested PCR is performed in which multiple rounds of the PCR amplification are performed in order to generate signal. Reports have documented the ability to detect low numbers of CTCs in 10^{6} PBMCs using an appropriate marker panel set.[50] When expression profiles of healthy females were compared to breast cancer patients, elevated median levels of

three of the markers comprising this panel (p1B, PS2, CK19, and EGP2) were found (see Figure 1.4).

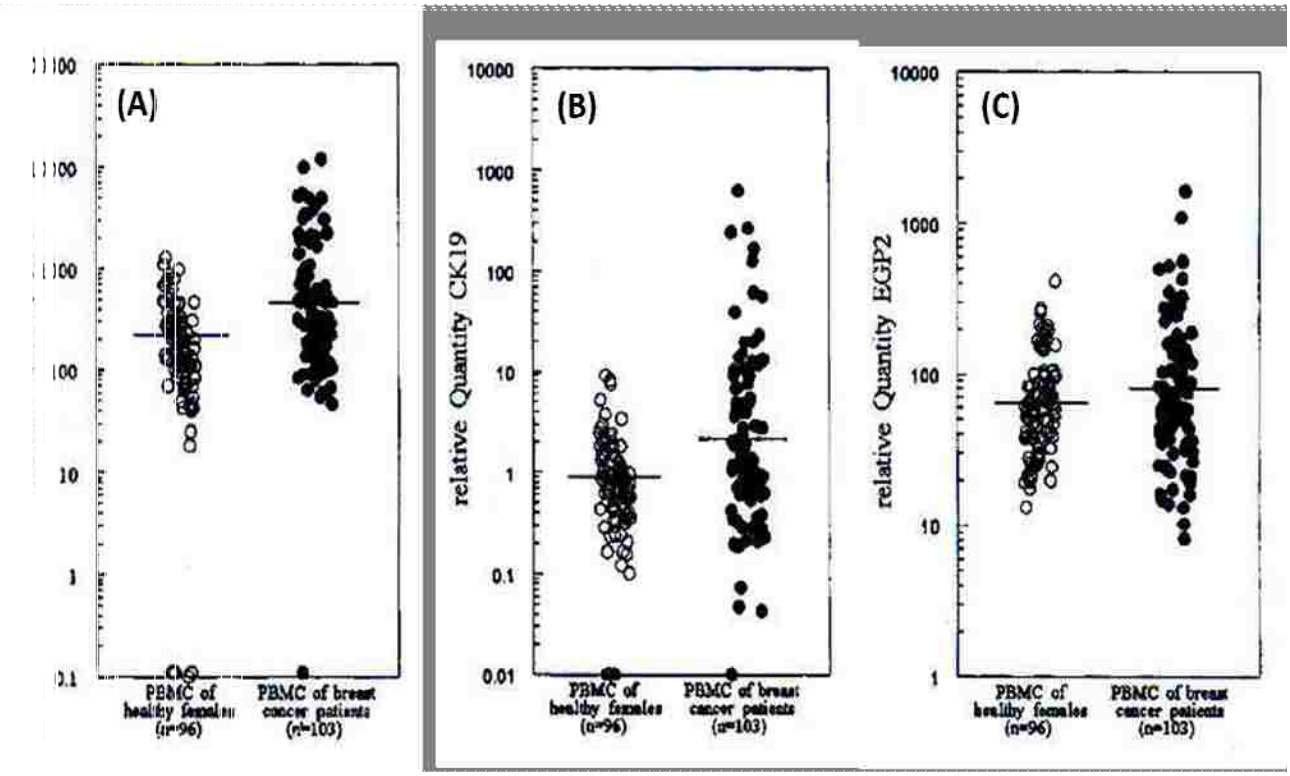

Figure 1.4 RT-PCR expression profiling results for three genetic markers over-expressed in tumor cells p1B (A), CK19 (B) and EGP2 (C). In this study, 103 breast cancer and 96 normal patients were evaluated. The horizontal line presents the median expression level for each group. In all cases, only the PBMC fraction was analyzed using RT-PCR. The number of PCR cycles performed depended upon the expression level of each marker, but ranged from 0-50 cycles. Reprinted with permission.[50]

Though RT-PCR is highly sensitive and specific when employing multiple markers in the expression profiling, securing morphological data on the CTCs is not possible because the cells are sacrificed to obtain the mRNA markers used in the assay. As with many CTC-based assays, the RBC fraction of the blood sample must be removed using for example, Ficoll-Hypaque density gradient centrifugation. In addition, the expression level of the marker genes cannot be related to the absolute number of tumor cells within

the sample. Finally, it has also been noted that these assays are prone to high inter-laboratory variability.

1.5 BioMEMS and μTAS Devices for Sorting CTCs

Near the turn of the 21st century the concepts of biological microelectromechanical systems (BioMEMS) or miniaturized total analysis systems (μTAS) were introduced as a means of processing many biological samples, such as on-chip cell sorting.[27] BioMEMS typically consists of several subcomponents incorporated into a single device that can sample, pretreat, analyze, and detect the material of interest ideally from a raw sample. To some extent, experiments in microdevice electrophoresis using planar substrates by Manz and Harrison in glass devices in the early 1990's set forth the cascade of events that have resulted in advancements in the application of BioMEMS devices in the analysis of cells.[34]

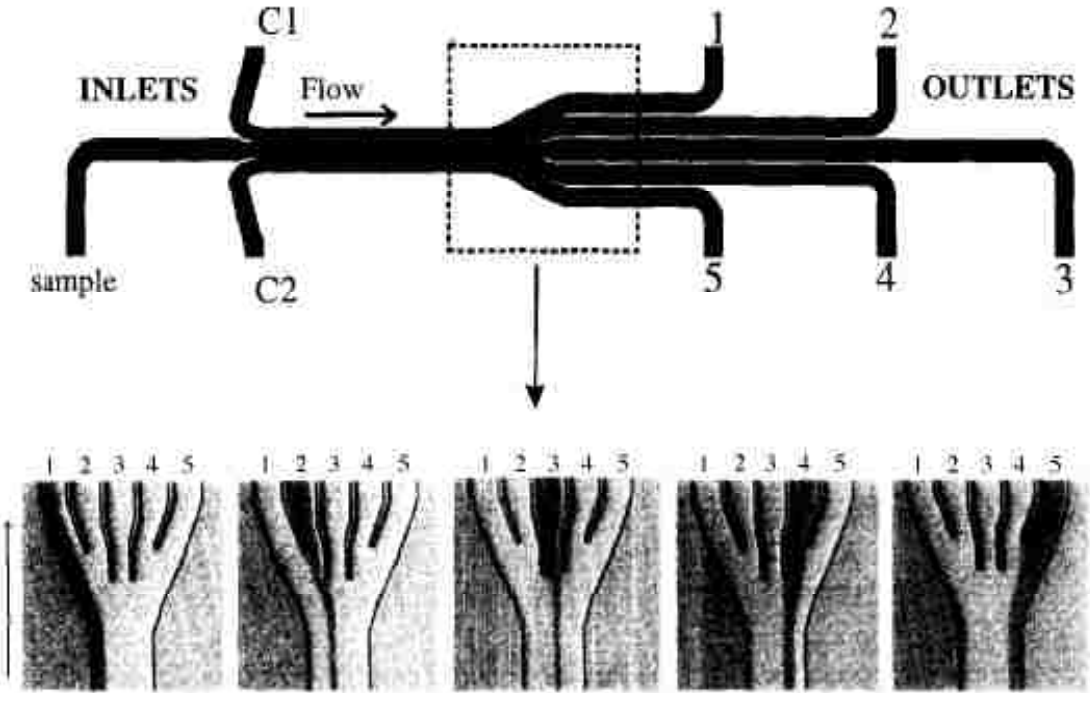

Figure 1.5 Microfabricated flow chip demonstrating directed pressure-induced cell manipulation. Reprinted with permission.[53]

As mentioned previously, glass and polymers have been used extensively as the substrate materials for BioMEMS devices; manufacturing strategies for glass or polymers vary greatly. Early microfluidic devices were dominated by the use of glass substrates, primarily because the surface chemistry of the material was well studied.[35]

For BioMEMS devices, hydrodynamic,[53,54] electroosmotic,[55,56] and dielectrophoretic[57,58] forces have been employed to manipulate and manage biological cells. Blankenstein *et al.* demonstrated the use of differential pressures to manipulate fluids into any one of five channels as shown in Figure 1.5.[53] At the inlet, the sample was introduced into the device and conduits C1 and C2 were used to guide the sample to outlets 1 – 5. This work illustrated a couple interesting points: (i) directed flow could be achieved with simple instrumentation and (ii) fluid mixing on the micrometer scale was not a rapid process.

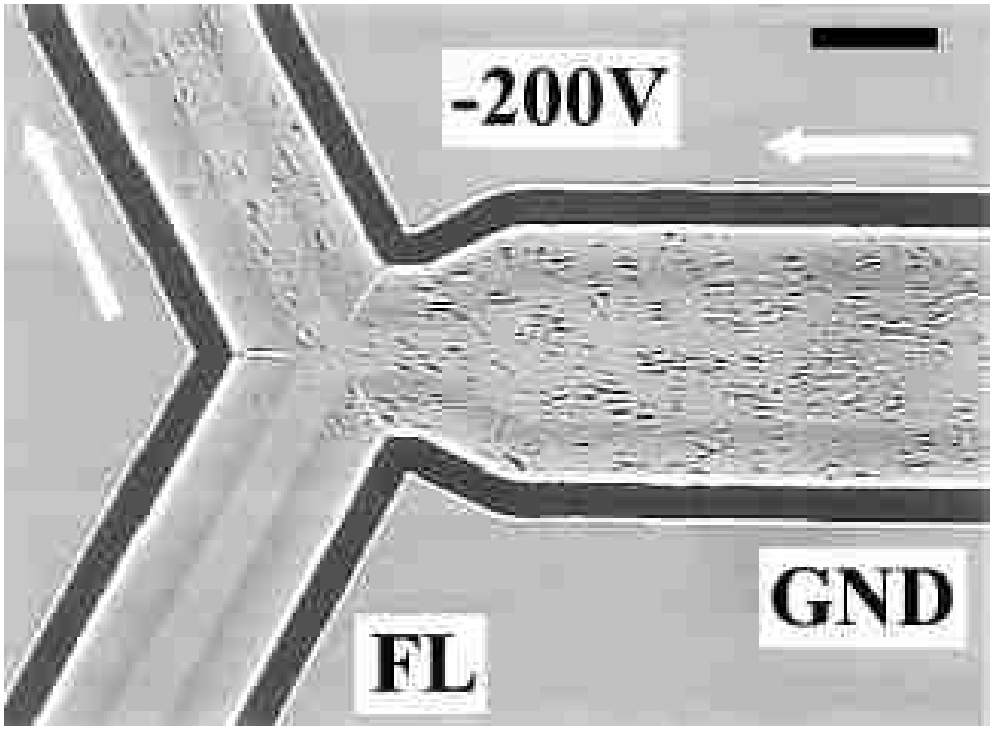

Figure 1.6 Baker's yeast cells are electrokinetically manipulated through a glass microdevice. Reprinted with permission.[59]

Electrokinetic transport was demonstrated in glass microchips by Li *et al*.[59] In these experiments, Li was able to alternate the electro-migratory path of the cells by switching the path of current flow resulting in a directional gate dictating the track followed by the cells through the glass microchips as shown in Figure 1.6. Velocities of 0.054 ± 0.005 mm s^{-1} and 0.28 ± 0.05 mm s^{-1} were achieved at field strengths of 35 V cm^{-1} and 140 V cm^{-1}, respectively, through a 15 × 55 μm^2 cross sectional area. Referring to Figure 1.1, a channel with a cross section of 825 μm^2 and a velocity of 1 mm s^{-1} with a sampling volume of 1 mL would require ~1600 h to complete the analysis.

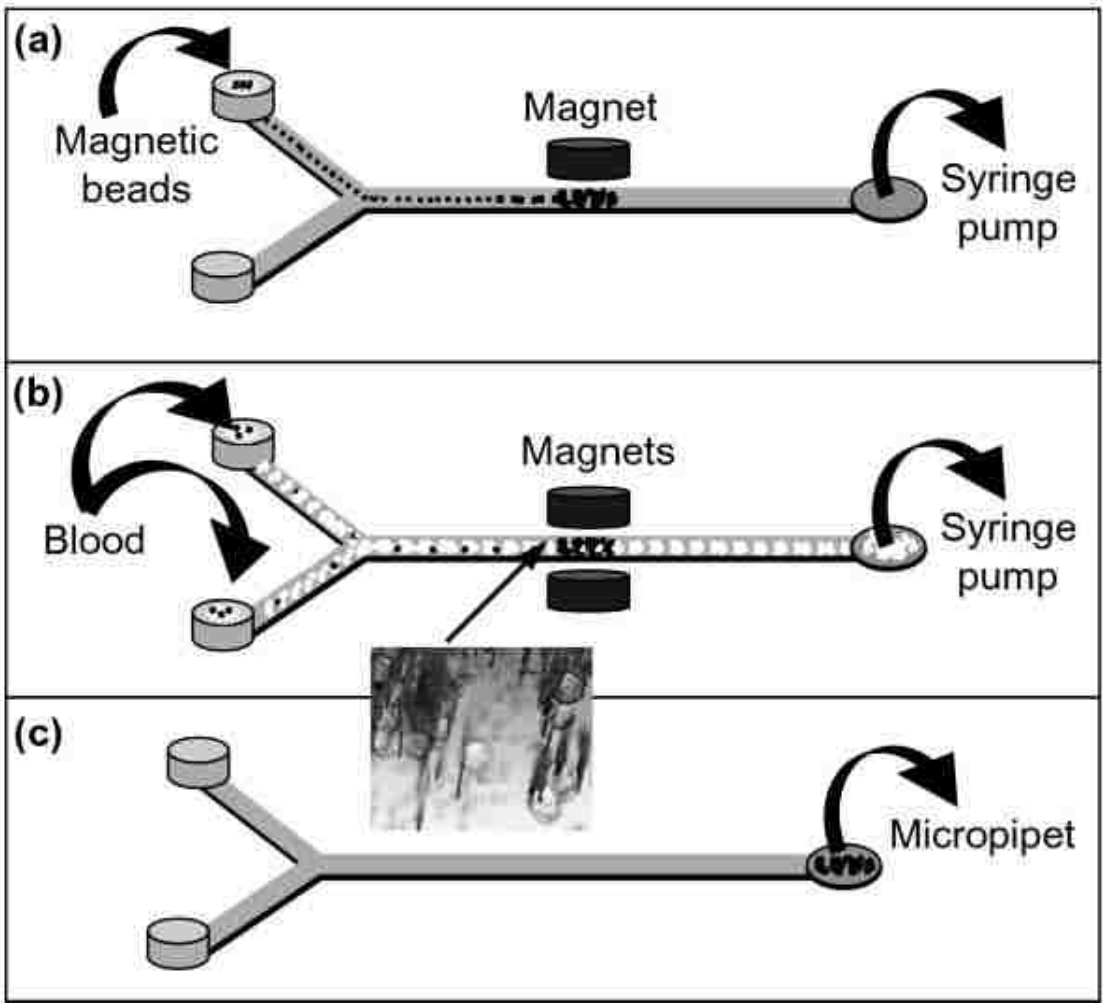

Figure 1.7 Furdui *et al.* presented a magnetic cell isolation strategy adapted to microfluidic platforms. A syringe pump was used to transport suspensions through a magnetic zone where immunomagnetic isolation occurred. Reprinted with permission.[20]

Furdui and Harrison adopted immunomagnetic techniques onto microfluidic platforms in order to enrich Jurkat cells (T cell leukemia) from blood, and their apparatus is shown in Figure 1.7.[20] The model samples used Jurkat cell:erythrocyte cell ratios of 1:10,000 with a total of 1-2 × 10^{10} RBCs mL^{-1} with a Jurkat cell frequency of 1 x 10^6 per mL. The authors removed the leukocytes from the blood prior to the microfluidic analysis. The magnetic beads were initially functionalized with protein A prior to incubating with anti-human CD43. The results of the incubation yielded antibody-functionalized beads, where the antibodies were bound to protein A via their F_c domain. A magnetic zone was used to selectively isolate the magnetic particles bound to the target cells in the microfluidic device. Subsequent to a rinsing step, the captured cells were eluted after removal of the magnetism and initiation of hydrodynamic pumping. Following optimization, the authors were able to isolate 37% of the spiked T-cells with a throughput that corresponded to 3 μL min^{-1} from a 2 μL sample that consisted of 1,070 Jurkat cells.

Becker *et al.* extended dielectrophoresis to mixtures of MDA231 breast cancer cells (1 × 10^7 mL^{-1}) and normal blood cells (3 × 10^7 mL^{-1}).[60] In their work, 30 μL aliquots of the suspensions were applied to a dielectrophoresis chamber. The total number of cells analyzed was 1.2 × 10^6 with a ratio of 1:3 tumor cells to normal hematopoietic cells. Upon 3 analyses of each sample, they were able to increase the ratio of cancer cells to normal cells from 1:3 to 1:1 for 10,000 cells analyzed. Analyte loss was prevalent in their work, in that of the cancer cells originally introduced into the device, only a small percentage (3.33%) of the targets were successfully isolated. It is important to note that typically cancer cells appear at a much lower ratios than those used in these model studies; ratios of 1:10^8 cancer cells to normal blood cells are typical.

Mohamed *et al.* demonstrated the potential for size-based by developing a microfluidic incorporating staggered microposts with incrementally decreasing spacing between the posts as shown in Figure 1.8.[19,22] The size-based isolation of cancer cells was carried out using diluted blood (1:10 blood:buffer) containing neuroblastoma cells. The authors demonstrated the ability to isolate neuroblastoma cells however, the authors did not state the capture efficiencies of the cancer cells using this device. In addition, the enriched cells obtained from the device had low purity with residual erythrocytes and leukocytes also collected within the cancer cell sample.

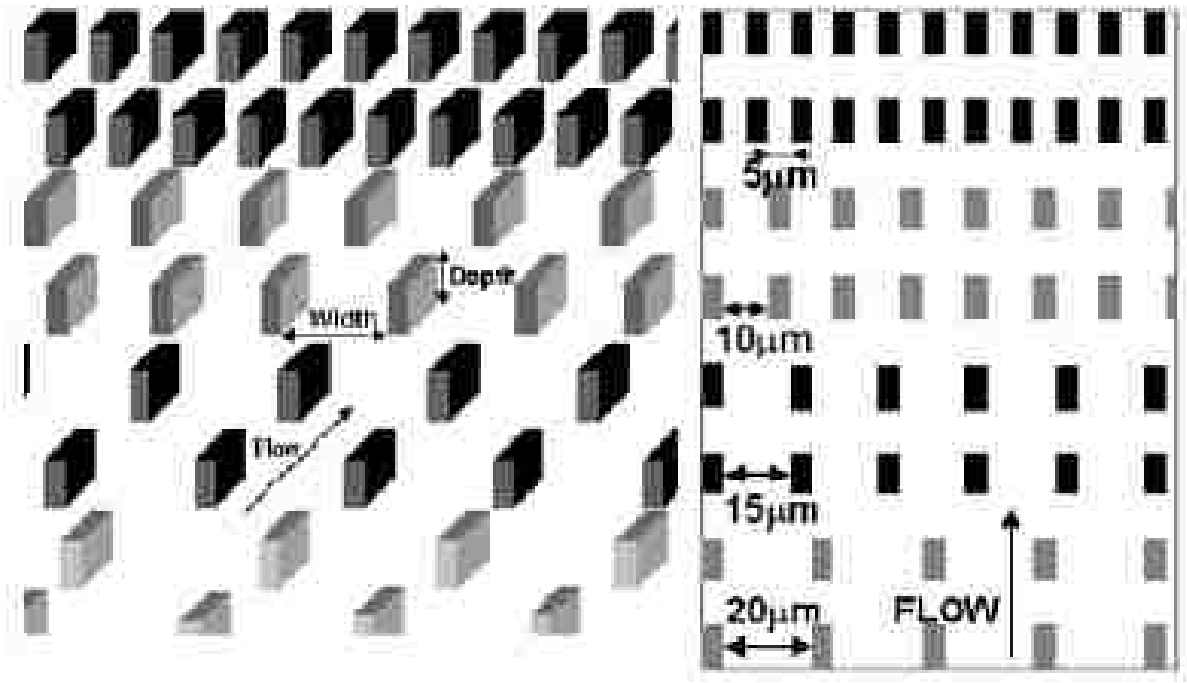

Figure 1.8 Scheme of size based cell separation device presented by Mohamed *et al.* Reprinted with permission.[22]

Chang *et al*. presented a device produced in glass using deep reactive ion etching (DRIE) that incorporated a microchannel that was 10 mm long, 500 μm wide and 40 μm deep with an array of square or offset posts that were 25 × 25 μm^2 or 35 × 10 μm^2,

respectively.[17] The device structures were coated with E-selectin IgG chimera antibodies. Pure suspensions of two myeloid cell lines, HL-60 and U-937, were used to evaluate the ability of the microfluidic platforms to isolate cancer cells using this biomemetic approach. The suspensions reportedly used in this study were on the order of 10^6 cancer cells mL^{-1}, well above a cell density typically associated with clinical samples harboring CTCs. The authors reported a volume throughput of 1 μL min^{-1}, which would require 16.7 hrs to process 1 mL that may be necessary if the cell frequency is more in lines with actual clinical samples. Also, the authors indicated that favorable cell capture efficiencies were achieved when the device surfaces were coated with immobilized cells. Adams *et al.* demonstrated that throughput suffers when maximizing capture efficiency; however, it is unrealistic to process 1 mL sample sizes for 16.7 hrs. Chang and coworkers acheived capture efficiencies of 64% even though the duration of the experiment was lengthy.

Dielectrophoresis is a phenomenon, first detailed in the early 1950s, which involves the translational motion of uncharged dielectric particles by non-uniform electric fields.[61] Depending on the electrode configuration and geometry used to produce the AC electric field, as well as the magnitude and phase variations of this field, cell-based separations can be affected using dielectrophoresis. Gravimetric field flow fractionation is the process by which particles are allowed to settle while under the influence of an axial flow based on their inherent interaction with gravity.[62] Yang et al. combined the two techniques to separate cells based on the balance between the composite electrophoretic mobility and the gravimetric attraction of the cells to settle on the device floor.[63] A schematic of the apparatus used in the work by Yang *et al.* is shown in Figure

1.9. Results suggested that a breast cancer cell line (MDA-435) could be separated from erythrocytes in a 10 µL sample containing ~50,000 cells total.

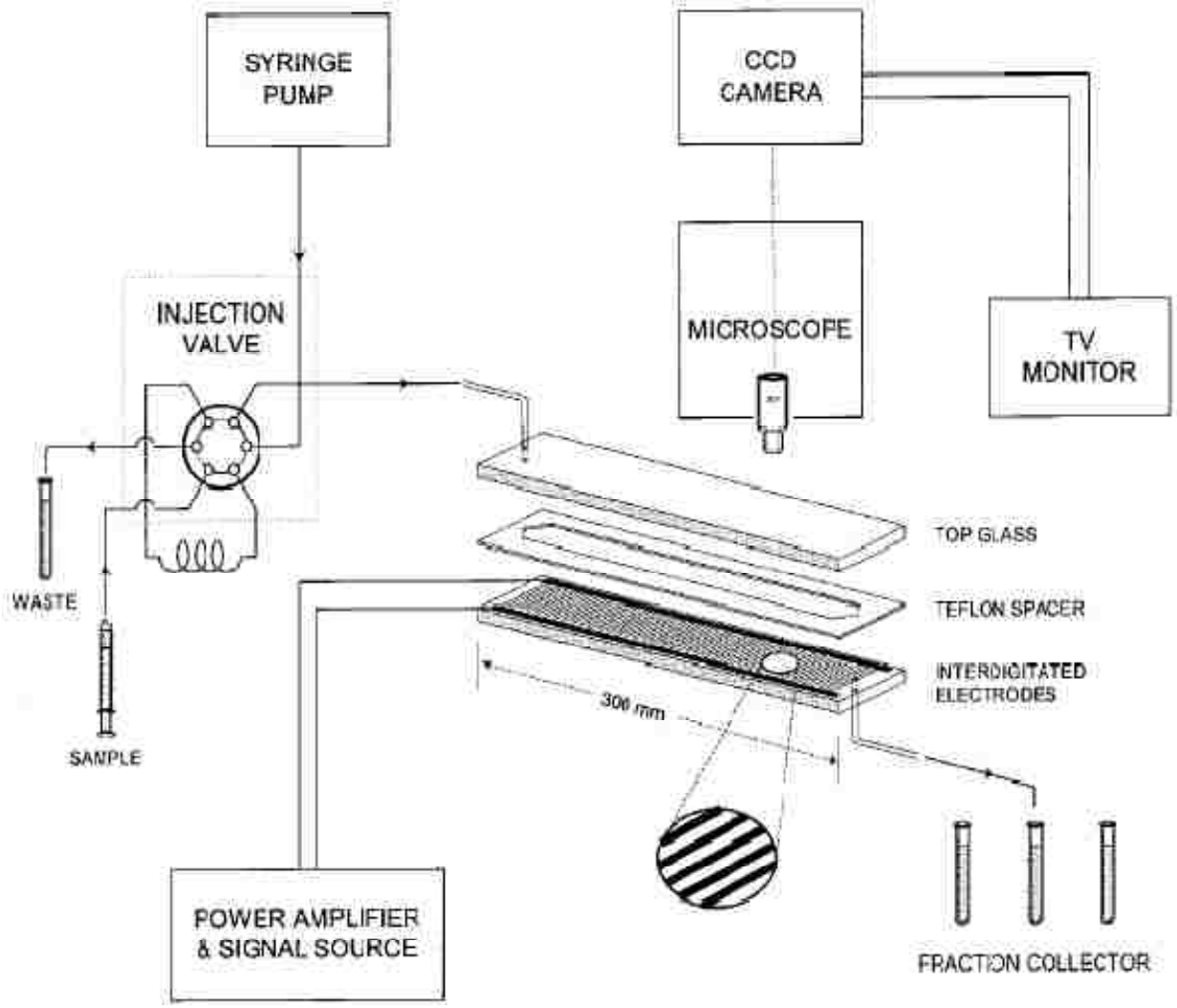

Figure 1.9 Field flow fractionating device was presented by Yang *et al.* in 1999. Reprinted with permission.[63]

The enriched fractions of the MDA-435 cells and erythrocytes were reported to be >98% and >99%, respectively, from 15 fractions collected over a 30 min elution time. The final concentration of MDA-435 cells in the buffer processed was reported to be 5×10^6 cells

mL^{-1} at a nominal ratio of 2:3 of cancer cells:erythrocytes. The authors noted a 20 min distinction between elution times of the erythrocytes and cancer cells, but the model sample in this experiment did not harbor leukocytes. Leukocytes are significantly larger than erythrocytes and thus, could impart interference in the measurements.

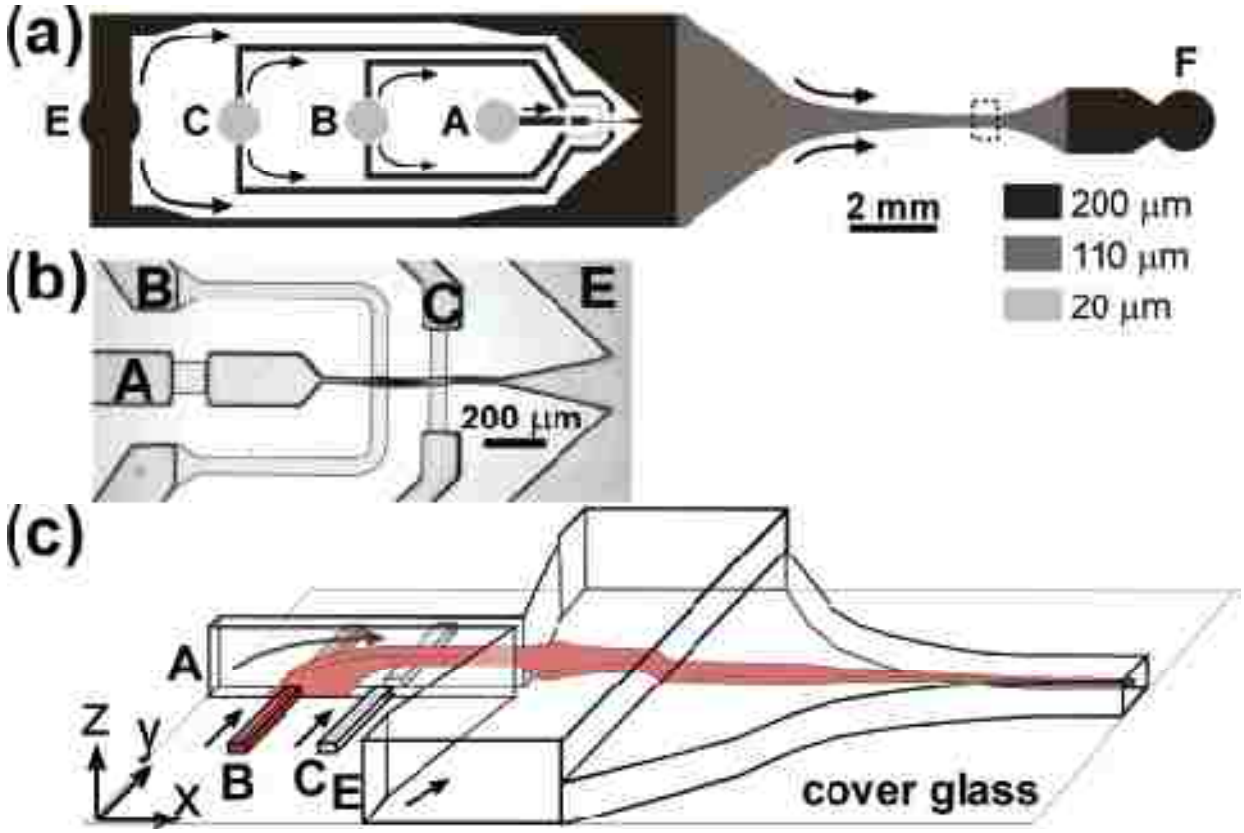

Figure 1.10 Diagram of Simonnet's flow cytometry device and the proposed focused region of high-probability density of analyte location. Reprinted with permission.[64]

Simonnet *et al.* attempted to port conventional high throughput, high resolution cell sorting using flow cytometry to a poly dimethylsiloxane microfluidic platform.[64] Conventional flow cytometry is characterized by typical flow rates of ~10 m s^{-1} corresponding to sampling rates of 1,000 – 50,000 cells s^{-1}. In order for a microfluidic to be considered suitable replacement for flow cytometer, it would have to approach this

threshold in terms of the linear velocity. A diagram of Simonnet's device is shown in Figure 1.10. Briefly, flow was from left-to-right in the diagram and a cross flow was used to hydrodynamically focus both opposing sides of the region labeled E in Figure 1.10C. Using this platform the authors were able to count cells consistently at 1,200, 9,000, and 17,000 particles s^{-1}. As the flow rate was increased the particle number increased and so did the coefficient of variance (CV) in their measurements. At 1,200, 9,000, and 17,000 particles s^{-1} the CVs were 3, 7.6, and 11%, respectively. Remarkably, the CV values for the microfluidic device rivaled those of the commercial instrument for the same sample set. As with the macro-scale version of the flow cytometer, to sort and enumerate the low abundant CTCs, specific staining protocols will need to be invoked as well as some sample pre-processing prior to flow assisted cell sorting.[9]

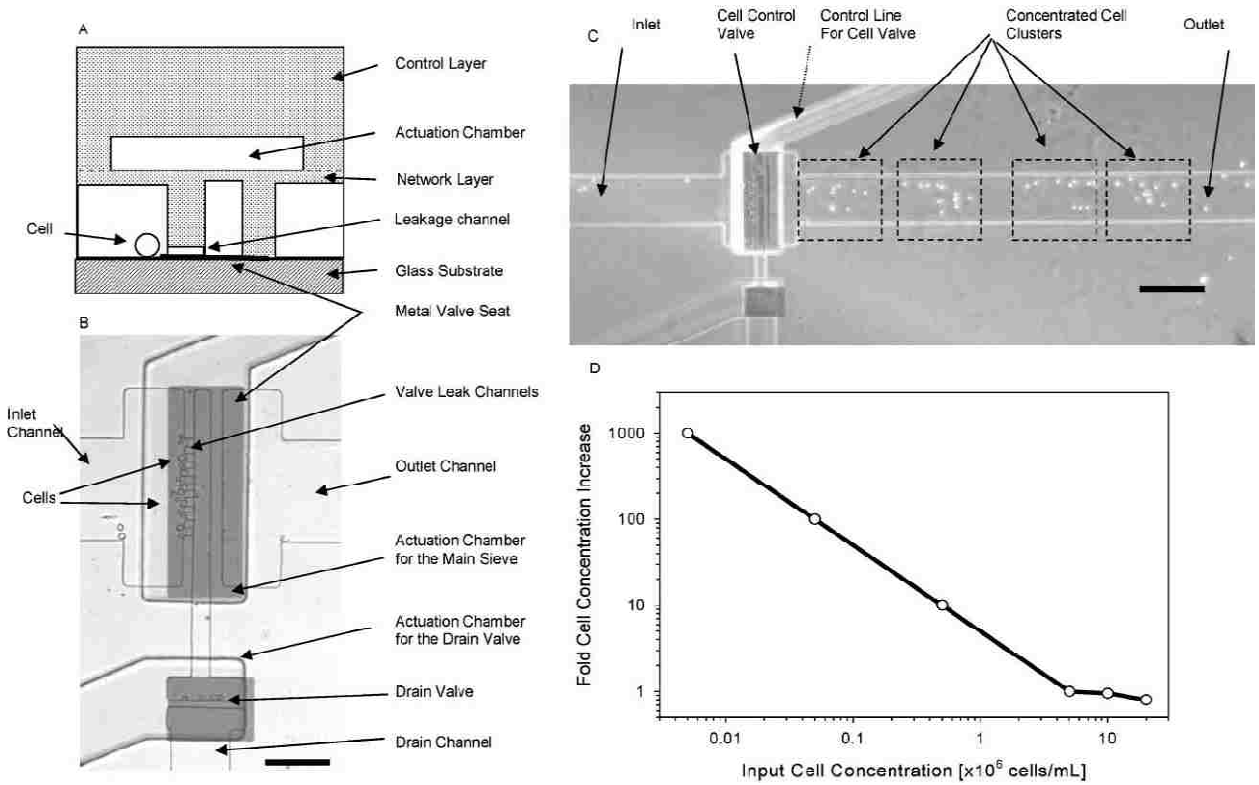

Figure 1.11 Poly dimethylsiloxane microstructures with valves for used for cell isolation. Reprinted with permission.[25]

Valves, actuators, and mechanical trapping of cells using moving parts within a closed microfluidic network is possible when casting elastomers, like poly-dimethylsiloxane, against positive reliefs.[25] Pressure from fluids or air are commonly used to open and close valves within microfluidic networks resulting in temporarily trapping or redirecting the flow path of cells and or fluids within the device. Irimia and Toner produced a device with features designed to accomplish the manipulation of human monocytic leukemia cells in a microfluidic device.[25] In this work, 30 nL aliquots of human monocytic leukemia cells were use to prepare suspensions with densities ranging from 1×10^3 to 1×10^7 cells mL^{-1}. The enrichment was reported to be ~1,000-fold. Figure 1.11A shows a diagram of an actuated valve and subsequently trapped cell and Figure 1.11B and C show actual cells being temporarily isolated on a membrane and transported to a membrane, respectively. Figure 1.11D shows the effectiveness of the cell isolation technique by demonstrating the enrichment potential as a function of the input cell density.

Nagrath *et al.* isolated rare CTCs from blood samples using microfluidic devices that contained 78,000 microposts that were 100 μm tall and 100 μm wide in a total area of 970 mm^2.[5] At flow rates of 1 mL hr^{-1}, 65% of CTCs were isolated from spiked PBS, and as the processing flow rate was increased to 3 mL hr^{-1} the recovery rate was reduced to 25% as shown in Figure 1.12. In whole blood measurements, approximately 2.7 mL of blood was used and the CTC recovery rates were typically 61%. Enrichments from whole blood samples were ~50% pure after analysis and as a result, CTCs had to be differentiated from leukocytes, the main interferent, using fluorescently-labeled cytokeratin and CD45 (see Figure 1.12). Twenty healthy subjects served as controls and those samples evaluated negative for CTCs.

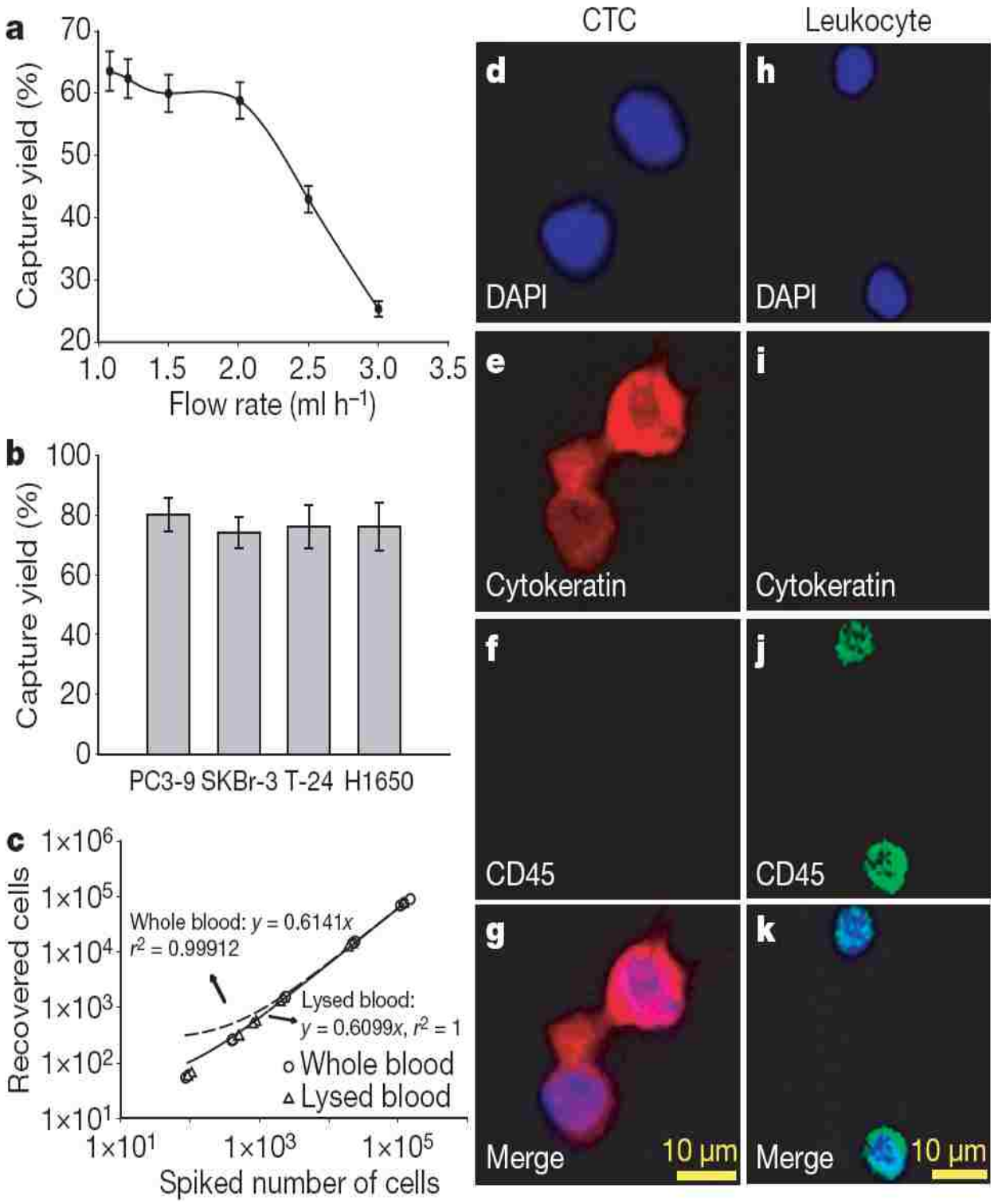

Figure 1.12 Capture efficiency as a function of (A) flow rate, (B) cell line, and (C) spiked cells are shown along with typical micrographs of the stained cells where (D – G) show an event that is positive for cytokeratin and DAPI attributed to a CTC and (H – K) show a cell positive for DAPI and CD45, which is indicative of a leukocyte. Reprinted with permission.[5]

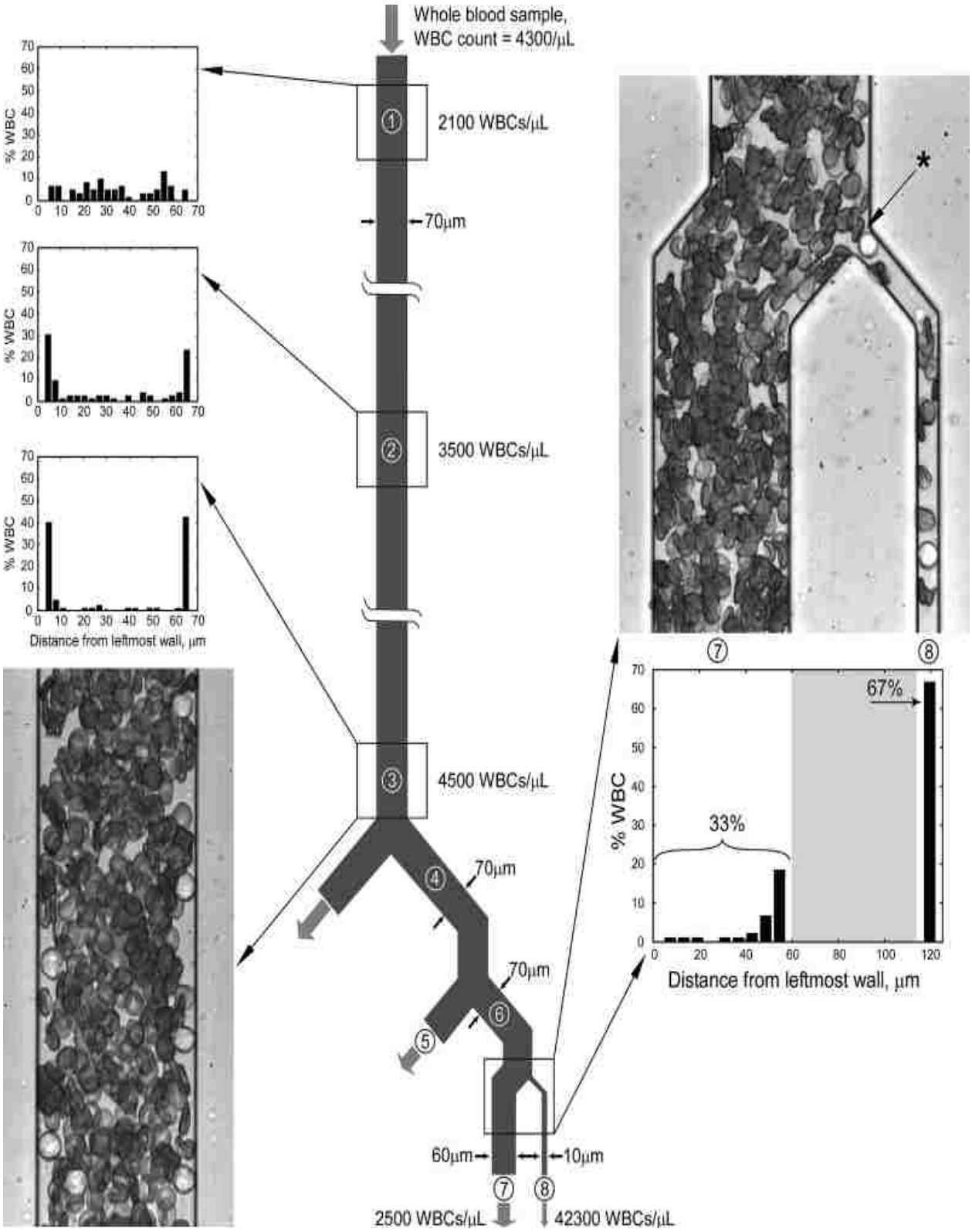

Figure 1.13 Shevkoplyas *et al.* presented a micro-separation device capable of significant leukocyte enrichment. Reprinted with permission.[65]

Shevkoplyas and coworkers presented a microfluidic that was capable of a 34-fold enrichment of white blood cells from samples that contained cell densities of 2,100 cells μL^{-1} to 42,300 cells μL^{-1} using a 10 µL whole blood sample (see Figure 1.13).[65] Whole blood enters the device through a 70 µm supply channel. The histograms in Figure 1.13 show that initially the cells are evenly distributed throughout the channel, but as smaller, more deformable erythrocytes seek the faster flow region in the center of the channel, the lumen of the erythrocytes collide with leukocytes forcing them to migrate toward the walls. The branching nature of the device provided selectivity for large cells, such as leukocytes, that migrate through the device at the walls, while erythrocytes migrate through the center of the device. Ultimately, the effluent shown in zone 8 of Figure 1.13 has a 20-fold increase in leukocyte density from the original input. Unfortunately, the process was marred by significant numbers of contaminating erythrocytes, and the potential for handling large input volumes required for scoring the presence of low-abundant cells was not possible due to the constricted flow after the third bifurcation in the analyte channel.

Adams *et al.* introduced a high throughput microsampling unit capable of meticulous selecting very low abundant targets from complex media.[24] In their work, a microfluidic device composed of poly(methylmethacrylate) employing many parallel high aspect ratio microstructures was functionalized via UV exposure providing a carboxylated scaffold amenable to antibody immobilization. The immunoslection of the cells was affected through the use of monoclonal antibodies specific for the epithelial cell adhesion molecule (EpCAM), which is over-expressed in a number of adenomacarcinomas. The immobilized antibodies were used to selectively isolate low abundant MCF-7 breast cancer cells through a cascade of antibody:antigen complex

formations sufficient to remove the cells from unprocessed whole blood with 97% recovery efficiencies. The devices were capable of high throughput operation at the optimal capture velocity of 2 mm s^{-1} such that 1 mL samples could be exhaustively interrogated in approximately 37 min. Further, these devices required no sample pretreatment by removing the red blood cell fraction via centrifugation or fluorescent staining of the cells due to on-chip integration using a conductance-based sensor capable of discriminating wild-type cells from the low abundant cancerous targets with near 100% detection efficiency.

Table 1.2 Figures of Merit for CTC Isolation on Macro and Micro-Scale Platforms.

Cell Isolation Methods and Description	Preprocessing Requirement	Throughput	Sample Purity	Enumeration
Magnetophoretic-Immunoaffinity[20]	Density gradient centrifugation	High (mL/min)	Low (40-60%)	Offline-Fluorescence
Nuclear Tracked Membranes[51]	Dilution	High (mL/min)	Medium (60-80%)	Online-Fluorescence
FACS/MACS[11,12]	Density gradient centrifugation	High (mL/min)	Medium (60-80%)	Online-Fluorescence
Microposts[5,19,25]	Dilution	Low (μL/min)	Low (40-60%)	Offline-Fluorescence
HTMSU[24]	--	High (mL/min)	High (> 90%)	Online-Conductivity

The analytical figures of merit for several different cell isolation strategies are detailed in Table 1.2 outlining the advantage and disadvantages for each of the various approaches for isolating CTCs from complex biological samples, such as whole blood. Included in this table are two representative microfluidic platforms directed toward rare

cell isolation. As can be seen from this data, the HTMSU example can process large input volume samples with high recoveries and also, due to the incorporation of the conductivity sensor, does not require cell staining for enumeration.

1.6 Future of Microfluidics

Of the various cell isolating/sorting tools developed to-date, some common procedural characteristics make many of them prohibitively difficult to implement; such as, the ability of many of the platforms to only sort the mononucleated cell fractions of whole blood. This criterion dictates the need for performing density gradient centrifugation prior to the enrichment procedure. In addition, these methods often have low throughput such that the probability of isolating the rare event is reduced due to the device capabilities of processing less than 50 μL of sample. Subsequently, the use of either fluorescence activated cell sorting or fluorescence microscopy is performed such that the target cells can be enumerated. This adds additional sample processing of the enriched CTCs via reactions with combinations of fluorescent markers. These supplemental steps necessitate sample handling and transfer, which can induce CTC loss or introduce contamination that can dramatically affect the assay results. This is especially prominent when dealing with low frequency events. To date there have been only two reports of self-contained systems capable of meticulously separating intact CTCs from peripheral blood samples allowing for the direct quantification of the CTC levels once enriched.[5,24]

1.7 References

(1) Ruestow, E. G. *Journal of the history of biology* **1983**, *16*, 185-224.

(2) Loberg, R. D.; Fridman, Y.; Pienta, B. A.; Keller, E. T.; McCauley, L. K.; Taichman, R. S.; Pienta, K. J. *Neoplasia* **2004**, *6*, 302-309.

(3) Meadows, A. L.; Kong, B.; Berdichevsky, M.; Roy, S.; Rosiva, R.; Blanch, H. W.; Clark, D. S. *Biotechnol. Prog.* **2008**, *24*, 334-341.

(4) Pitot, H. C.; Goldsworthy, T.; Moran, S. *J. Supramol. Struct. Cell. Biochem.* **1981**, *17*, 133-146.

(5) Nagrath, S.; Sequist, L. V.; Maheswaran, S.; Bell, D. W.; Irimia, D.; Ulkus, L.; Smith, M. R.; Kwak, E. L.; Digumarthy, S.; Muzikansky, A.; Ryan, P.; Balis, U. J.; Tompkins, R. G.; Haber, D. A.; Toner, M. *Nature* **2007**, *450*, 1235-U10.

(6) Li, Y.; Mao, Y.; Rosal, R. V.; Dinnen, R. D.; Williams, A. C.; Brandt-Rauf, P. W.; Fine, R. L. *Int. J. Cancer* **2005**, *115*, 55-64.

(7) Rao, C. G.; Chianese, D.; Doyle, G. V.; Miller, M. C.; Russell, T.; Sanders, R. A.; Terstappen, L. W. M. M. *Int. J. Oncol.* **2005**, *27*, 49-57.

(8) Ghosh, A.; Wang, X.; Klein, E.; Heston, W. D. W. *Cancer Res.* **2005**, *65*, 727-731.

(9) Gross, H. J.; Verwer, B.; Houck, D.; Hoffman, R. A.; Recktenwald, D. *Proc. Natl. Acad. Sci. U. S. A.* **1995**, *92*, 537-541.

(10) Cristofanilli, M.; Budd, G. T.; Ellis, M. J.; Stopeck, A.; Matera, J.; Miller, M. C.; Reuben, J. M.; Doyle, G. V.; Allard, W. J.; Terstappen, L.; Hayes, D. F. *New Engl. J. Med.* **2004**, *351*, 781-791.

(11) Bauer, J. *Journal of Chromatography B-Analytical Technologies in the Biomedical and Life Sciences* **1999**, *722*, 55-69.

(12) Pappas, D.; Wang, K. *Anal. Chim. Acta* **2007**, *601*, 26-35.

(13) Lybarger, L.; Dempsey, D.; Franek, K. J.; Chervenak, R. *Cytometry* **1996**, *25*, 211-220.

(14) Chein, R. Y.; Yang, Y. C.; Lin, Y. S. *Electrophoresis* **2006**, *27*, 640-649.

(15) Balic, M.; Dandachi, N.; Hofmann, G.; Samonigg, H.; Loibner, H.; Obwaller, A.; van der Kooi, A.; Tibbe, A. G. J.; Doyle, G. V.; Terstappen, L.; Bauernhofer, T. *Cytometry Part B-Clinical Cytometry* **2005**, *68B*, 25-30.

(16) Carnes, E.; Wilkins, E. *Am. J. Appl. Sci.* **2005**, *2*, 607-613.

(17) Chang, W. C.; Lee, L. P.; Liepmann, D. *Lab Chip* **2005**, *5*, 64-73.

(18) Fehm, T.; Solomayer, E. F.; Meng, S.; Tucker, T.; Lane, N.; Wang, J.; Gebauer, G. *Cytotherapy* **2005**, *7*, 171-85.

(19) Mohamed, H.; Murray, M.; Turner, J. N.; Caggana, M. *NSTI Nanotech 2005, NSTI Nanotechnology Conference and Trade Show, Anaheim, CA, United States, May 8-12, 2005* **2005**, *1*, 1-4.

(20) Furdui, V. I.; Harrison, D. J. *Lab Chip* **2004**, *4*, 614-618.

(21) Kameneva, M. V.; Watach, M. J.; Borovetz, H. S. *Clin. Hemorheol. Microcirc.* **1999**, *21*, 357-363.

(22) Mohamed, H.; McCurdy, L. D.; Szarowski, D. H.; Duva, S.; Turner, J. N.; Caggana, M. *IEEE Trans. NanoBiosci.* **2004**, *3*, 251-256.

(23) Law, P.; Dooley, D. C.; Alsop, P.; Smith, D. M.; Landmark, J. D.; Meryman, H. T. *Transfusion* **1988**, *28*, 145-150.

(24) Adams, A. A., Okagbare, P. I. and Soper, S. A. *J. Am. Chem. Soc.* **2008**, *(in press)*.

(25) Irimia, D.; Toner, M. *Lab Chip* **2006**, *6*, 345-352.

(26) Crowley, T. A.; Pizziconi, V. *Lab Chip* **2005**, *5*, 922-929.

(27) Auroux, P. A.; Iossifidis, D.; Reyes, D. R.; Manz, A. *Anal. Chem.* **2002**, *74*, 2637-2652.

(28) Pittman, J. L.; Henry, C. S.; Gilman, S. D. *Anal. Chem.* **2003**, *75*, 361-370.

(29) Zhao, Q.; Cui, D. F.; Wang, L.; Wang, M.; Chen, X. *International Journal of Nonlinear Sciences and Numerical Simulation* **2002**, *3*, 203-206.

(30) Ocvirk, G.; Munroe, M.; Tang, T.; Oleschuk, R.; Westra, K.; Harrison, D. J. *Electrophoresis* **2000**, *21*, 107-115.

(31) Liu, Y.; Fanguy, J. C.; Bledsoe, J. M.; Henry, C. S. *Anal. Chem.* **2000**, *72*, 5939-5944.

(32) Gaudioso, J.; Craighead, H. G. *J. Chromatogr.* **2002**, *971*, 249-253.

(33) Witek, M. A.; Wei, S. Y.; Vaidya, B.; Adams, A. A.; Zhu, L.; Stryjewski, W.; McCarley, R. L.; Soper, S. A. *Lab Chip* **2004**, *4*, 464-472.

(34) Harrison, D. J.; Manz, A.; Fan, Z. H.; Ludi, H.; Widmer, H. M. *Anal. Chem.* **1992**, *64*, 1926-1932.

(35) Llopis, S. L.; Osiri, J.; Soper, S. A. *Electrophoresis* **2007**, *28*, 984-993.

(36) Soper, S. A.; Henry, A. C.; Vaidya, B.; Galloway, M.; Wabuyele, M.; McCarley, R. L. *Anal. Chim. Acta* **2002**, *470*, 87-99.

(37) Vaidya, B.; Soper, S. A.; McCarley, R. L. *Analyst* **2002**, *127*, 1289-1292.

(38) Witek, M. A.; Llopis, S. D.; Wheatley, A.; McCarley, R. L.; Soper, S. A. *Nucleic Acids Res.* **2006**, *34*, e74/1-e74/9.

(39) Henry, A. C.; Tutt, T. J.; Galloway, M.; Davidson, Y. Y.; McWhorter, C. S.; Soper, S. A.; McCarley, R. L. *Anal. Chem.* **2000**, *72*, 5331-5337.

(40) Ford, S. M.; Kar, B.; McWhorter, S.; Davies, J.; Soper, S. A.; Klopf, M.; Calderon, G.; Saile, V. *J. Microcolumn Sep.* **1998**, *10*, 413-422.

(41) Ford, S. M.; Davies, J.; Kar, B.; Qi, S. D.; McWhorter, S.; Soper, S. A.; Malek, C. K. *Journal of Biomechanical Engineering-Transactions of the Asme* **1999**, *121*, 13-21.

(42) Hupert, M. L.; Guy, W. J.; Llopis, S. D.; Shadpour, H.; Rani, S.; Nikitopoulos, D. E.; Soper, S. A. *Microfluid. Nanofluid.* **2007**, *3*, 1-11.

(43) Hruby, J. *MRS Bull.* **2001**, *26*, 337-340.

(44) Furdui, V. I.; Harrison, D. J. *Micro Total Analysis Systems 2002, Proceedings of the mTAS 2002 Symposium, 6th, Nara, Japan, Nov. 3-7, 2002* **2002**, *2*, 700-702.

(45) Grodzinski, P.; Yang, J.; Liu, R. H.; Ward, M. D. *Biomed. Microdevices* **2003**, *5*, 303-310.

(46) Wilding, P.; Pfahler, J.; Bau, H. H.; Zemel, J. N.; Kricka, L. J. *Clin. Chem.* **1994**, *40*, 43-47.

(47) Vona, G.; Sabile, A.; Louha, M.; Sitruk, V.; Romana, S.; Schutze, K.; Capron, F.; Franco, D.; Pazzagli, M.; Vekemans, M.; Lacour, B.; Brechot, C.; Paterlini-Brechot, P. *Am. J. Pathol.* **2000**, *156*, 57-63.

(48) Balic, M.; Dandachi, N.; Hofmann, G.; Samonigg, H.; Loibner, H.; Obwaller, A.; van der Kooi, A.; Tibbe Arjan, G. J.; Doyle Gerald, V.; Terstappen Leon, W. M. M.; Bauernhofer, T. *Cytometry B Clin Cytom* **2005**, *68*, 25-30.

(49) Ghossein, R. A.; Osman, I.; Bhattacharya, S.; Ferrara, J.; Fazzari, M.; CordonCardo, C.; Scher, H. I. *Diagn. Mol. Pathol.* **1999**, *8*, 59-65.

(50) Bosma, A. J.; Weigelt, B.; Lambrechts, A. C.; Verhagen, O. J. H. M.; Pruntel, R.; Hart, A. A. M.; Rodenhuis, S.; Van't Veer, L. J. *Clin. Cancer. Res.* **2002**, *8*, 1871-1877.

(51) Zabaglo, L.; Ormerod, M. G.; Parton, M.; Ring, A.; Smith, I. E.; Dowsett, M. *Cytometry A* **2003**, *55A*, 102-108.

(52) Belov, L.; Huang, P.; Barber, N.; Mulligan, S. P.; Christopherson, R. I. *Proteomics* **2003**, *3*, 2147-2154.

(53) Blankenstein, G.; Larsen, U. D. *Biosens. Bioelectron.* **1998**, *13*, 427-438.

(54) Blankenstein, G.; Scampavia, L. D.; Ruzicka, J.; Christian, G. D. *Cytometry* **1996**, *25*, 200-204.

(55) Fu, A. Y.; Spence, C.; Scherer, A.; Arnold, F. H.; Quake, S. R. *Nat. Biotechnol.* **1999**, *17*, 1109-1111.

(56) Wood, D. P.; Banerjee, M. *J. Clin. Oncol.* **1997**, *15*, 3451-3457.

(57) Fiedler, S.; Shirley, S. G.; Schnelle, T.; Fuhr, G. *Anal. Chem.* **1998**, *70*, 1909-1915.

(58) Muller, T.; Gradl, G.; Howitz, S.; Shirley, S.; Schnelle, T.; Fuhr, G. *Biosens. Bioelectron.* **1999**, *14*, 247-256.

(59) Li, P. C. H.; Harrison, D. J. *Anal. Chem.* **1997**, *69*, 1564-1568.

(60) Becker, F. F.; Wang, X. B.; Huang, Y.; Pethig, R.; Vykoukal, J.; Gascoyne, P. R. C. *Proc. Natl. Acad. Sci. U. S. A.* **1995**, *92*, 860-864.

(61) Pohl, H. A. *J. Appl. Phys.* **1951**, *22*, 869-71.

(62) Chu, F.; Graillat, C.; Guillot, J.; Guyot, A. *Colloid Polym. Sci.* **1997**, *275*, 986-991.

(63) Yang, J.; Huang, Y.; Wang, X. B.; Becker, F. F.; Gascoyne, P. R. C. *Anal. Chem.* **1999**, *71*, 911-918.

(64) Simonnet, C.; Groisman, A. *Anal. Chem.* **2006**, *78*, 5653-5663.

(65) Shevkoplyas, S. S.; Yoshida, T.; Munn, L. L.; Bitensky, M. W. *Anal. Chem.* **2005**, *77*, 933-937.

Chapter 2 Cell Transport via Electromigration in Polymer-Based Microfluidic Devices

2.1 Introduction

The ability to fabricate microscale analytical devices on planar substrates with dimensions similar to those of biological cells has recently attracted significant attention in the field of bioanalysis (i.e., identification and quantification of specific cellular contents, such as DNA, RNA, or protein). Microfluidic devices are attractive for cellular analyses since many processing steps can be integrated into a single platform, minimizing dilution of intracellular components following lysis. The feasibility of handling biological cells in microfluidic devices using various physical forces has already been demonstrated in glass.[1-5] Cell transport and sorting on microfabricated devices have been reported where hydrodynamic,[4,6] electroosmotic,[2,7] and dielectrophoretic[8,9] forces have been used. For example, Li and Harrison[2] used electroosmotic pumping in glass microdevices to transport cells within a network of channels. On-chip manipulations such as plug formation and flow switching in the channel were demonstrated. Chang et al.[10] performed electrical characterization of microorganisms in microdevices. Electrophoretic movement of live and heat-inactivated bacteria confirmed the presence of negative charges on the surface of the cell membrane of the live microorganisms. The dead cells accumulated at the negative electrode suggesting alteration in the charge state of the cells upon heat inactivation. Cell lysis, PCR amplification, and electrophoretic analysis of the genetic amplicons were executed sequentially on a monolithic glass microchip by Waters et al.[3] The entire microchip was thermally cycled to lyse cells and to amplify the DNA, which was carried out in a fabricated well located on the chip. Heo et al.[11] entrapped viable *E. coli* cells in hydrogel micropatches within microfluidic systems. Small molecules, such as dyes and surfactants, were able to

diffuse into the gel, which caused cell lysis and released the cell contents. The cell debris, being sufficiently large, was retained within the gel matrix.

The majority of research on cell transport and manipulation performed in microdevices has been done primarily in glass or silicon. Glass offers important features for cell transport because the EOF is very well characterized and has a magnitude that is typically greater than the electrophoretic mobility of most analytes, leading to migration of all materials, irrespective of charge, *toward the cathode.* The large electroosmotic flow in glass is due to the high surface charge of this material (i.e., deprotonated silanol groups).

Polymers are viewed as attractive materials for microfluidic devices due to their flexibility in micromanufacturing structures, ability to pattern high aspect ratio microstructures, and the low cost of replicating daughters from masters using embossing or injection molding.[12] Unfortunately, many polymers (e.g., poly(methylmethacrylate), high and low density polyethylene, polystyrene, polypropylene, polycarbonate) do not contain ionizable functional groups and, as such, produce much smaller EOFs compared to glass.[13,14] In terms of cell transport, small EOFs can be problematic due to a lack of well-defined transport control.

The EOF, however, can be altered by chemical modification of the polymer substrate leading to the introduction of new ionizable groups on the surface. Successful chemical modification of PMMA and PC has been reported previously in our lab.[15,16] The EOF of amine-terminated PMMA microchannels was shown to be reversed compared to that in unmodified channels. Another way to modify polymers is exposure to UV light. UV irradiation causes photo-oxidation, resulting in a thin surface layer of oxidized polymer.[17-20] For example, PC exposed to 254-300 nm light results in the formation of polymer phenyl salicylates and hydroxybenzophenones.[18,19] Also, hydroxyl-containing

and keto-containing products have been reported.[18,19] In general a wide range of carbonyl-containing functionalities is produced during UV-modification resulting in highly oxygenated surfaces even though the carbonate groups are depleted. PMMA photo-oxidation produces alcoholic groups that are both hydrogen-bonded to ester groups, and/or self-associated.[17] Such photo-processes are easy to perform and introduce additional groups on the polymer surface with fairly high quantum yields. Therefore, UV exposure of polymers can be viewed as a simple method to induce changes in the EOF.[14,21,22]

The goal of the work presented herein was to characterize the electrokinetic transport properties of whole cells in polymeric microfluidic devices. The channels of the polymer microdevices were either pristine or UV-modified in order to change the chemistry of the walls, and consequently changing the EOF. We report on chip transport and monitoring of bacterial (*Escherichia coli)* and baker's yeast cells (*Saccharomyces cerevisiae*). Two important analytical features will be presented; (i) control of cell transport (i.e., flow direction and velocity) by electroosmotic/electrokinetic forces, and (ii) sorting of *Escherichia coli* cells from *Saccharomyces cerevisiae* using differential migration in appropriately prepared material and buffer conditions.

2.2 Materials and Methods

2.2.1 Cells and Reagents. Baker's yeast cells type II (*Saccharomyces cerevisiae*) and nonpathogenic *Escherichia coli* type B cells were obtained from Aldrich (Milwaukee, WI). The stock solutions of phosphate buffer saline (PBS, 100 mM pH=3.0, 7.4, and 9.0, Aldrich) were reagent-grade quality. Concentrations of 0.5, 1.0 and 20 mM PBS were prepared by dilution of the stock PBS solution with deionized (DI) water (17.9 MΩ) from an E-pure water purification system (Barnstead, Dubuque, IA). Cells were washed two times with DI water and centrifuged (1000 rpm). Next, they were placed in buffer and

stored in a refrigerator at 4°C until used (≤ 4 hrs). Cell suspensions for baker's yeast and *E. coli* were 0.30 and 0.33 mg/mL, respectively, unless stated otherwise. Before each measurement, cells were vortexed (Vortex-2 Genie, VWR Scientific, and Westchester, PA) for ~5-7 min.

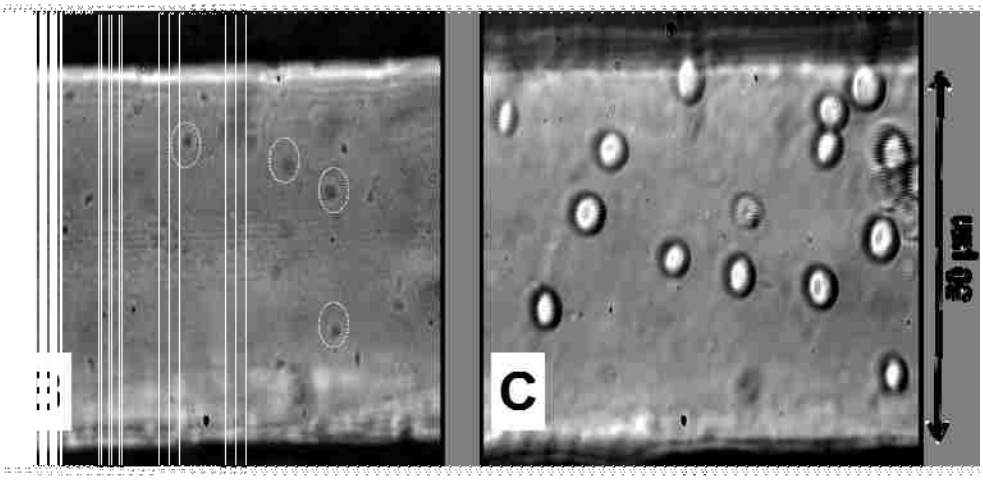

Figure 2.1 A) Photograph of a polymer microdevice with 200 μL buffer reservoirs and interconnects attached to the inlet and outlet ports. Microdevice parameters: channel length = 4 cm, side channel lengths = 0.5 cm, channel width = 50 μm, and channel depth = 80 μm. The solid black line represents the device topology. B) Optical micrograph of a PMMA microdevice channel filled with *E. coli* and C) baker's yeast cells (*S. cerevisiae)* in 1 mM PBS, pH=7.4. These images were obtained using a 100x immersible objective. The observed area under the microscope was 60 x 80 μm. The dotted circles in B) highlight *E. coli* cells contained within the device.

2.2.2 Microchip Fabrication. Polymer microchips were fabricated using LIGA as previously reported.[12,23,24] The procedure involved fabricating a metal molding die, which consisted of raised microstructures of Ni on a stainless steel base plate. The device used in these studies possessed a 50 μm wide and 80 μm deep channel of 4 cm total length and configured in a cross with side channels of 0.5 cm in length.

Devices were prepared in polycarbonate (PC) and poly(methylmethacrylate) (PMMA). PC and PMMA stock sheets of 5.0 mm thickness (Goodfellow, Berwyn, PA) were cut into 133 mm diameter round disks. Discs were washed with 2-propanol and distilled water and dried in an oven at 80°C overnight. The microchannel pattern was hot embossed into the polymer plates using a PHI Precision Press model number TS-21-H-C (4A)-5 (City of Industry, CA). A vacuum chamber was installed into this press to remove air (pressure <0.1 bar) so complete filling of the die could take place. Embossing was performed at 1000 lbs pressure for 4 min at 190°C for PC and 150°C for PMMA.

Before final assembly, chips were washed with soap, rinsed with DI water and 2-propanol, and then ultrasonicated for 15 min in DI water. The channels were examined under a microscope to ensure they were not filled with debris. The embossed devices were assembled by heat annealing a coverplate made from the same material to the substrate. The coverplate and substrate were clamped together and placed in a convection oven for ~20 min at 150°C for PC and 105°C for PMMA. After successful heat annealing, 1 mm holes were drilled into the coverplates and the microfluidic reservoirs/ports were attached with epoxy resin to the inlet and outlet holes. High volume reservoirs (~200 μL) minimized loss of buffer due to evaporation and reduced

the movement of cells due to capillary or hydrodynamic forces. Figure 2.1A shows a photograph of a fabricated device.

2.2.3 Surface Modification. The hot-embossed PC and PMMA microchannels and coverplates were modified prior to assembly by exposure to UV radiation (15 mW/cm^2) for 30-40 min using a UV lamp (ABM, Inc., San Jose, CA). After illumination, all of the polymer parts were rinsed with 2-propanol and sonicated for 5-10 min in DI water. The devices were assembled also by heat annealing, however, at lower temperatures compared to the non-exposed materials (144°C for PC and 98°C for PMMA). It was observed that UV modification of the polymer lowered its glass transition temperature (T_g), thus requiring a lower annealing temperature.

In an effort to simplify device production a post annealing UV treatment was attempted, whereby the devices would undergo thermal annealing as detailed earlier prior to UV modification. In order to test the protocol planar PMMA substrates were UV modified using incrementally increasing UV exposure doses. Water contact angle measurements were performed on both the incident and opposing sides of the modified PMMA to determine water contact angles. Pristine PMMA has a water contact angle of 85º and depending on the UV dose the water contact angle can be significantly decreased indicating the formation of a hydrophilic surface.[25] We observed no change in the hydrophilicity of the opposing side of the planar PMMA indicating that the surface modification was limited to the incident side of the exposed PMMA (see Figure 2.2).

2.2.4 Derivatization of UV-modified PMMA and PC. UV-exposed PMMA and PC surfaces were derivatized with a diamine crosslinking agent followed by covalent attachment of an amine-selective dye to determine the presence and identity of functional groups using the procedure described herein (see Scheme 2.1).[25]

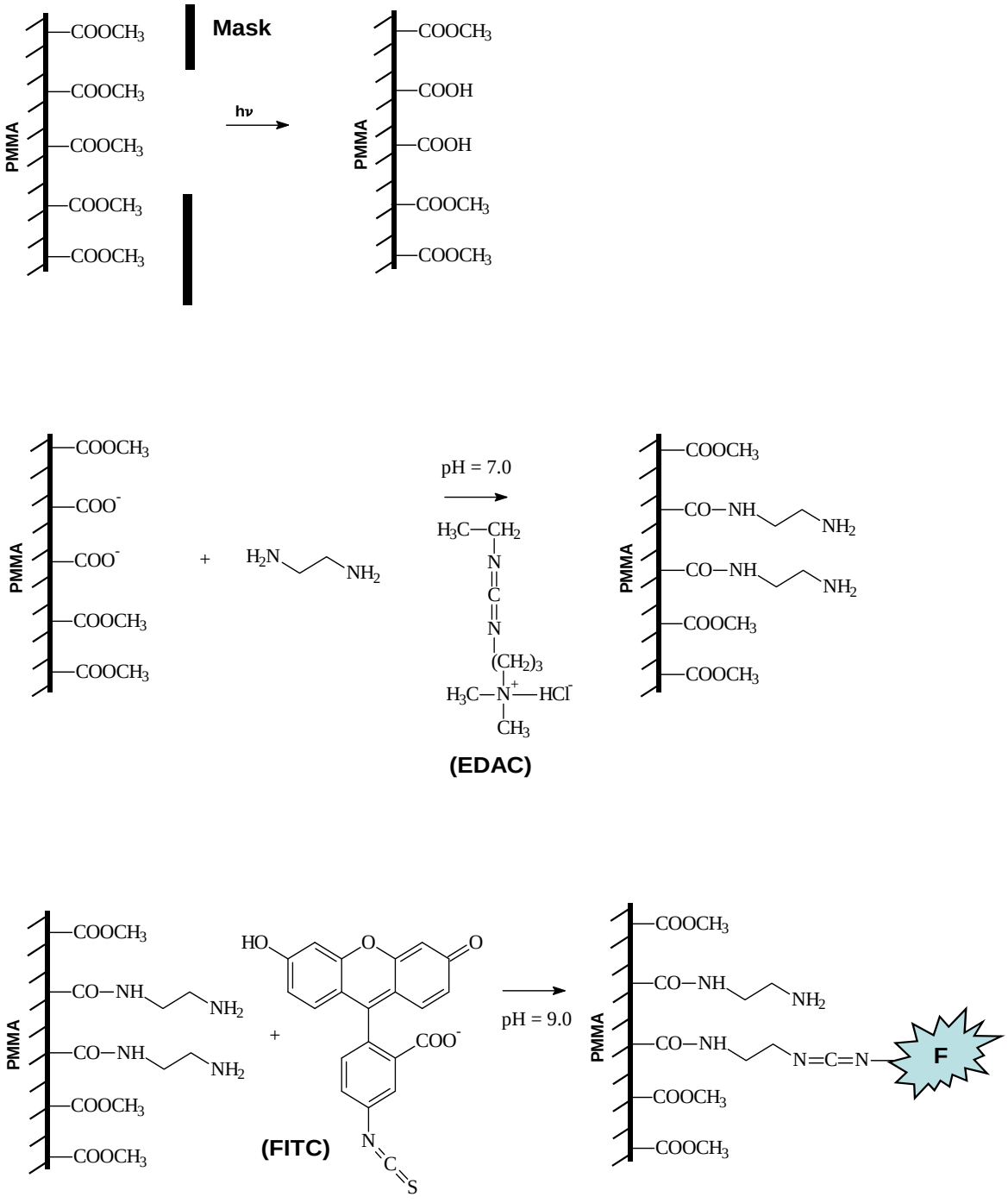

Scheme 2.1 Modification protocol of PMMA and PC surfaces. The material was first exposed to UV radiation through a photomask. The groups formed as a result of exposure were derivatized with ethylene diamine in the presence of EDAC. Any surface-bound primary amines were subsequently reacted with FITC to produce fluorescence. F = fluorescein.

Precut pieces of 0.5-mm-thick PC (Goodfellow) and PMMA (AIN Plastics) were sonicated in 2 propanol for 15 min and subsequently rinsed again with 2-propanol, then dried with high-purity nitrogen. A 500-mesh Ni grid was placed over the PC and PMMA pieces, then the masked pieces of the polymer sheets were placed 1 cm from the UV source and subsequently irradiated for 30 min in air.

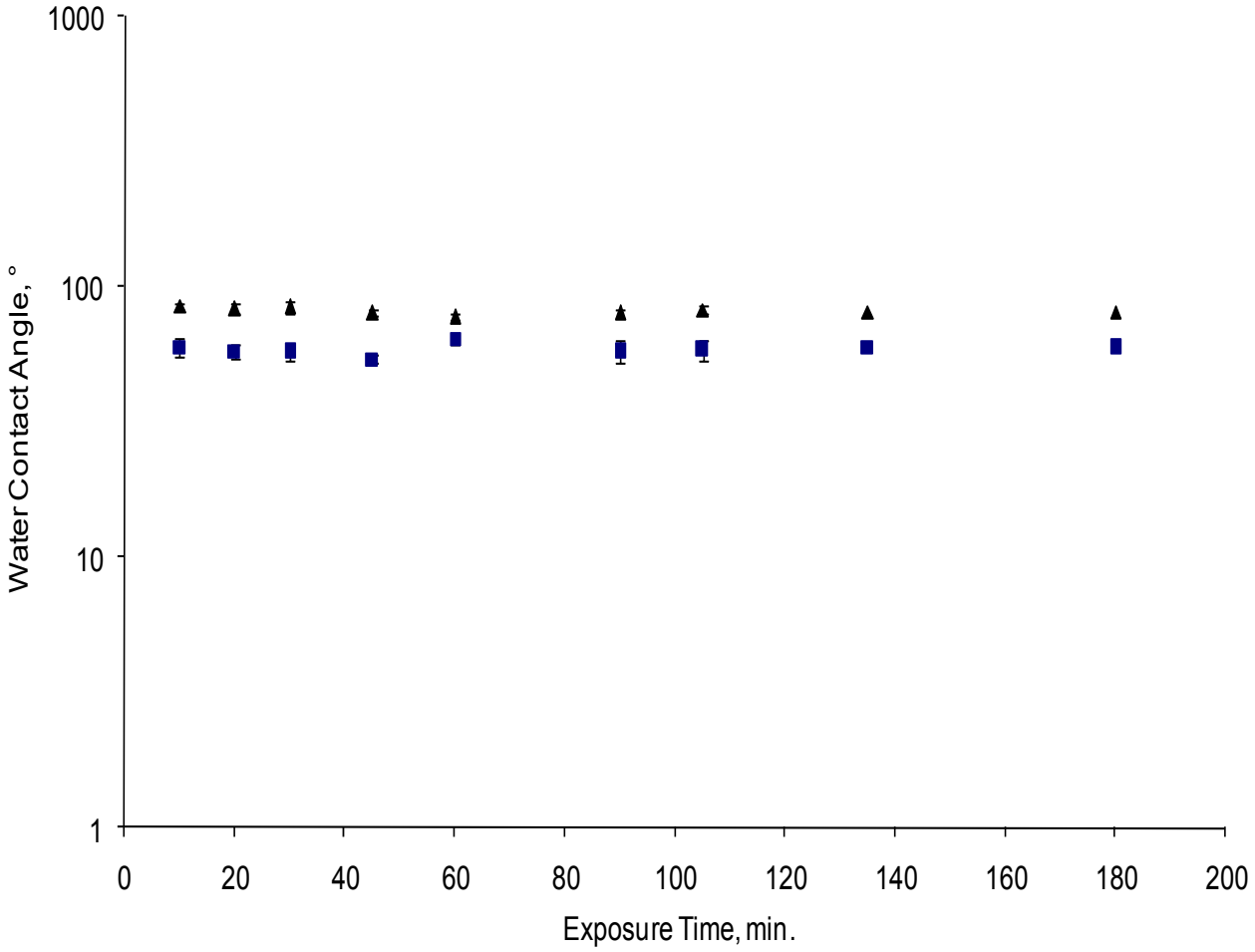

Figure 2.2 Plot of water contact angles of the incident and opposing sides of PMMA taken immediately after modification. The black triangles indicate the water contact angles of the opposing sides of PMMA which are equal to that of unmodified pristine PMMA. The blue squares show the moderate reduction in water contact angle resulting from the incident irradiation. Data points and error bars reflect the average of three measurements and the associated standard deviation from that average, respectively.

Upon removal from the UV source, the PC and PMMA pieces were sonicated in nanopure water for 5 min. The cleaned, exposed pieces were then incubated with agitation for 11 h in a 5 mM EDAC (1-ethyl-1-(3-dimethylaminopropyl)carbodiimide) with 100 mM phosphate buffer (pH=7.0) containing 5 mM ethylenediamine (Aldrich). The resulting amine-terminated surfaces were then rinsed with Nanopure water and placed in a 2 mM FITC (fluorescein isothiocyanate) solution in pH 9.0, 0.1 M borate buffer for 4 h, after which they were rinsed with borate buffer and dried in air. Examination of the derivatized surfaces was achieved with a Nikon Miphot-FXA microscope with a 20X fluorescence objective equipped with a 510 nm excitation filter and a 520 nm barrier filter.

The surface morphology of pristine and UV-modified PMMA and PC surfaces was interrogated using atomic force microscopy (AFM), (Nanoscope III, Digital Instruments/Veeco Metrology Group, Santa Barbara, CA) in the non-contact (tapping) mode.

2.2.5 Measurement of the Electroosmotic Flow (EOF). The EOF in assembled devices was measured using the method described by Zare and co-workers.[26] The procedure involved filling the entire chip with a 20 mM buffer. After filling the chip, one reservoir was emptied and filled with the same type of buffer but of lower ionic strength (18 mM). An electric field (150 V/cm) was then applied to the reservoirs containing the low and high ionic strength buffers and the current was monitored continuously using a strip-chart recorder (Kipp and Zonen Inc., Bohemia, NY). The time needed for the current to reach a plateau was measured from the plot and the linear velocity calculated. Dividing the linear velocity by the electric field strength produced EOF values (cm^2/Vs). The electric field was supplied by a Spellman high-voltage power supply (CZ1000R, Plainview, NY). The electroosmotic flow measurements were carried out through pH

values of 4-10 on both pristine and UV-modified PMMA and PC microchips. Three different buffers were used over the investigated pH range; acetate buffer (pH=4.0, pH=5.0, and pH=6.0); phosphate buffer (pH=7.0 and pH=8.0); and borate buffer (pH=9.0 and pH=10.0).

2.2.6 Cell Transport. Observations of cell transport were performed using a Nikon Optiphot 2 microscope (Nikon, Melville, NY) equipped with a JAI CV 252 monochrome video camera capable of capturing 30 fps. The images were captured directly to the hard drive of a Dell Precision 500M workstation via a Pinnacle Systems DV500 video capture card that was interfaced to a Pinnacle Systems Bluebox (Pinnacle Systems, Inc., Mountain View, CA). The Bluebox served as a conduit for the video transfer to the computer. Adobe Premiere 6.0 (Adobe Systems, Inc., San Jose, CA) was used for data acquisition and subsequent data processing.

The programmable high voltage power supply (PHV) was assembled in-house. The unit consisted of 4 individual power supplies (Model UR5PN, Matsusada Precision Inc., Santa Clara, CA) capable of delivering +5 to -5 kV, ground, and floating potentials. Each power supply was equipped with an independent Reed relay (Model RR1A07P06, Ross Engineering Corporation, Campbell, CA) that was used to toggle the polarity, ground, and floating states of the power supply. The power supply was computer controlled with a 4 channel 12 bit digital to analog board (Model CYDDA 04P, CyberResearch Inc., New Haven, CT) with peripheral component interface (PCI) and software written in Labview (National Instruments, Austin, TX). All experiments were carried out at room temperature. *Caution! The electrophoresis uses high voltages and special care should be taken when handling the electrodes.*

2.2.7 Backscatter Cell Detection. The detection system used for monitoring cell transport via backscatter detection has been described in detail previously.[27] It

consisted of a diode laser (LDH 680, PicoQuant, Berlin, Germany) lasing at 680 nm. The diode head was coupled directly to a single-mode fiber for transporting the light to the detector head. The collimated laser light was directed by a dichroic mirror (Omega Optical, Brattleboro, VT), which reflected the laser light when the mirror was positioned at a 45º angle of incidence. The laser light was then focused into the microdevice channel using a 40X, 0.65 numerical aperture (Θ= 40.5º) microscope objective (Nikon, Melville, NY). The scatter signal was collected by this same objective, transmitted through the dichroic, and focused onto a multimode fiber using an objective of the same power (1:1 imaging). The multimode fiber carried the resulting signal to the detector. An interference band-pass filter (710AF30, Omega Optical, Brattleboro, VT) and long-pass filter (705AELP, Omega Optical, Brattleboro, VT) were used to isolate the appropriate signal. The scattered signal was then focused by a 20X objective (Nikon) onto a SPAD (SPCM-200 single-photon avalanche diode, EG&G optoelectronics, Vaudreuiel, Canada). The output pulses produced from the SPAD were amplified (6954 B5 amplifier, Phillips Scientific, Ramsey, NJ) and fed into a counting board resident on the PC bus (PicoQuant SPC 430).

2.3 Results and Discussion

The cell types studied herein varied in size and shape. Baker's yeast cells (*Saccharomyces cerevisiae*) are spherical eukaryotic cells with 5-10 μm diameters. *Escherichia coli* are bacteria cells with rod-like shape and dimensions of about 1-2 μm. These cells posses a net negative charge at physiological pH, which along with its size determines its electrophoretic mobility.[2] This charge is a result of protonation/deprotonation of membrane bound materials. Thus, cell charge can be controlled by altering the properties of the buffer solution (i.e., pH, ionic strength, salt composition). It has previously been observed that cells suspended in an isotonic salt

solution start to move toward a positively charged electrode upon application of an electric field.[28] The speed of the movement (i.e., electrophoretic mobility) was found to be proportional to the density of charges located on the cell surface.

Figure 2.1B and 2.1C present photomicrographs of *E. coli* (B) and baker's yeast cells (C) in a PMMA microfluidic device. Cell velocities in the present study were calculated by measuring the time a cell migrated a distance of 80 μm, which was the field of view for the objective used in these studies. The average velocity was based on values obtained from 5-7 different cells.

2.3.1 Electroosmotic Flow in Polymeric Devices. The most common mechanism of pumping in microfluidic devices is electrokinetic, which utilizes the electroosmotic flow of the solution and the electrophoretic mobility of the material being transported. The linear velocity at which the material moves is governed by Eq. 2.1;

$$\nu_{app} = (\mu_{eof} + \mu_{ep})E \qquad (2.1)$$

where ν_{app} is the apparent linear velocity (cm/s) and is determined from the sum of the electroosmotic mobility (μ_{eof}) and the material electrophoretic mobility (μ_{ep}) multiplied by the field strength (E). Throughout this work, mobilities reported from anode to cathode are positive, and those from cathode to anode are negative.

By modifying the channel surface, we could control the magnitude and direction of the EOF, resulting in control of transport rate and direction. A simple way to modify polymers is through exposure by UV light. UV irradiation causes photo-oxidation of the surface and leaves the bulk material unmodified.[14,17-22] While previous studies[14,20-22] utilized UV lasers (excimer) to induce these surface charge density changes during ablative processes, we used a broadband UV source with moderate photon densities, which would be expected to minimize any polymer ablation.

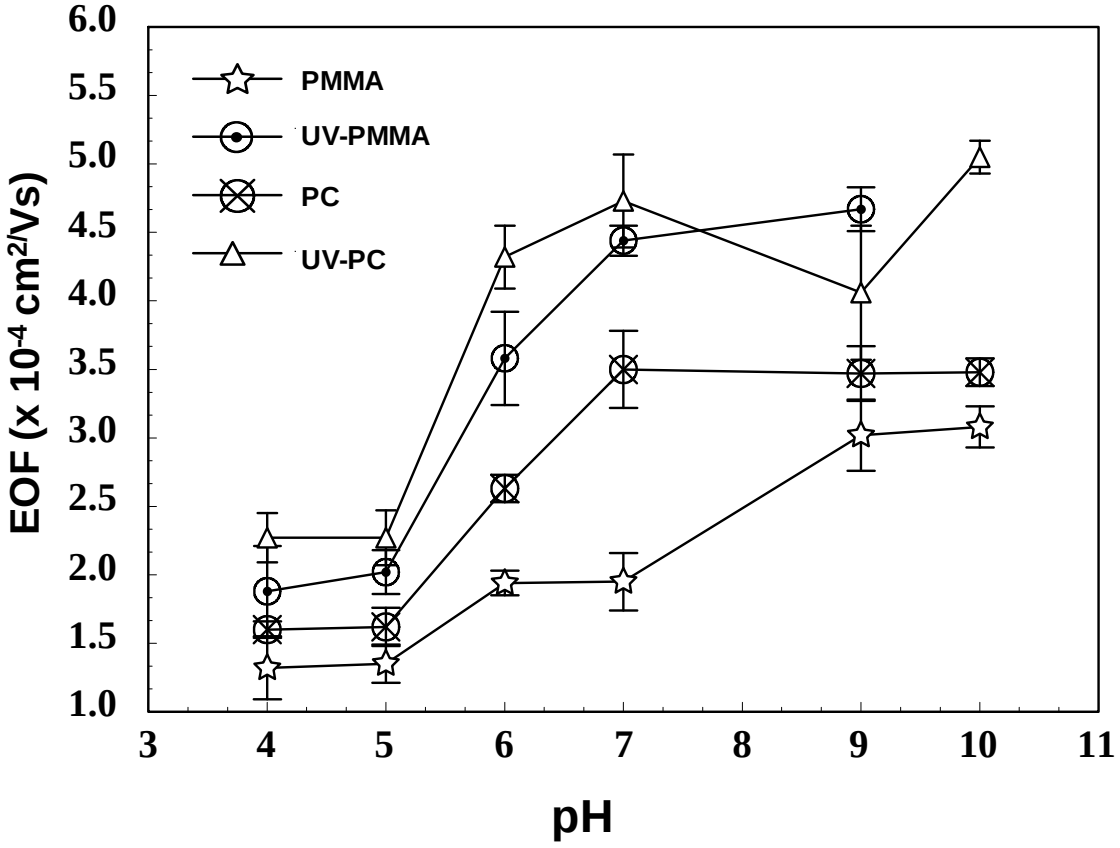

Figure 2.3 Plot of EOF vs. pH for unmodified and UV-modified PMMA and PC. The electroosmotic flow measurements were carried out through pH values of 4-10. Three different buffers were used; acetate buffer (pH=4.0, pH=5.0, and pH=6.0); phosphate buffer (pH=7.0 and pH=8.0); and borate buffer (pH=9.0 and pH=10.0). The low concentration of buffer was 18 mM and the higher concentration was 20 mM. The field strength used was 0.15 kV/cm. The EOFs were measured using the chips described in Figure 2.1. For the UV-modified chips, both the coverplates and substrates were exposed prior to chip assembly.

The EOF values for pristine and UV-modified polymers as a function of pH are plotted in Figure 2.3. The EOFs for both PMMA and PC as well as for UV-modified PMMA and UV-modified PC were positive, indicating solution flow from anode to cathode and thus, negatively charged walls. For the pristine PMMA microdevice, the observed EOF was 1.72×10^{-4} at pH=4 and increased to 3.02×10^{-4} cm^2/Vs at pH=9,

consistent with our previous data.[15,16,29] A much larger EOF was seen for the UV-modified PMMA devices (e.g., 1.88×10^{-4} at pH=4 and 4.67×10^{-4} cm^2/Vs at pH=9). EOFs measured in the UV-modified PC microchannel showed higher values than in unmodified PC as well (e.g., 4.73×10^{-4} and 3.50×10^{-4} cm^2/Vs at pH=7.0 for UV-modified and pristine PC, respectively). These results can be explained by the production of higher negative charge densities on the UV-modified material due to the presence of ionizable groups with lower pK_a values than the terminal phenolic groups found in pristine PC.[18,14,21,22] The first derivative of the plots of EOF vs. pH for both UV-modified PMMA and PC revealed an apparent surface pK_a value of 4.2 for UV-modified PMMA and 4.3 for UV-modified PC. Based on these results, we can speculate that carboxylate groups are present on both the UV-modified PMMA and PC, since typical literature values of pK_a for alkyl or aryl carboxylic acids are in the range of 4-5.

In order to determine the identity of these charged groups on the surface of PMMA and PC exposed to low intensity broadband UV illumination, both PC and PMMA sheets were subjected to UV radiation through a TEM grid and the resulting material reacted with a diamine in the presence of EDAC, which selectively labels carboxylate groups to create an amine-terminated scaffold that could be subsequently reacted with FITC. Following derivatization, the material was imaged using a fluorescence microscope. The resulting images (brightfield and fluorescent) are shown in Figure 2.4. From these images, it can clearly be seen that only those areas exposed to the UV radiation through the TEM grid produced substantial amounts of fluorescence. Since EDAC coupling of the diamine to the surface is a good indicator of the presence of carboxylate groups, it can assumed that UV exposure induced a photo-oxidation reaction, similar to that observed by Locascio and co-workers for laser ablated polymer surfaces.[14] A brightfield image of the PC surface, which can provide information on surface

morphology, showed no distinct features following UV exposure, indicative of no significant amounts of surface ablation induced by this dose.

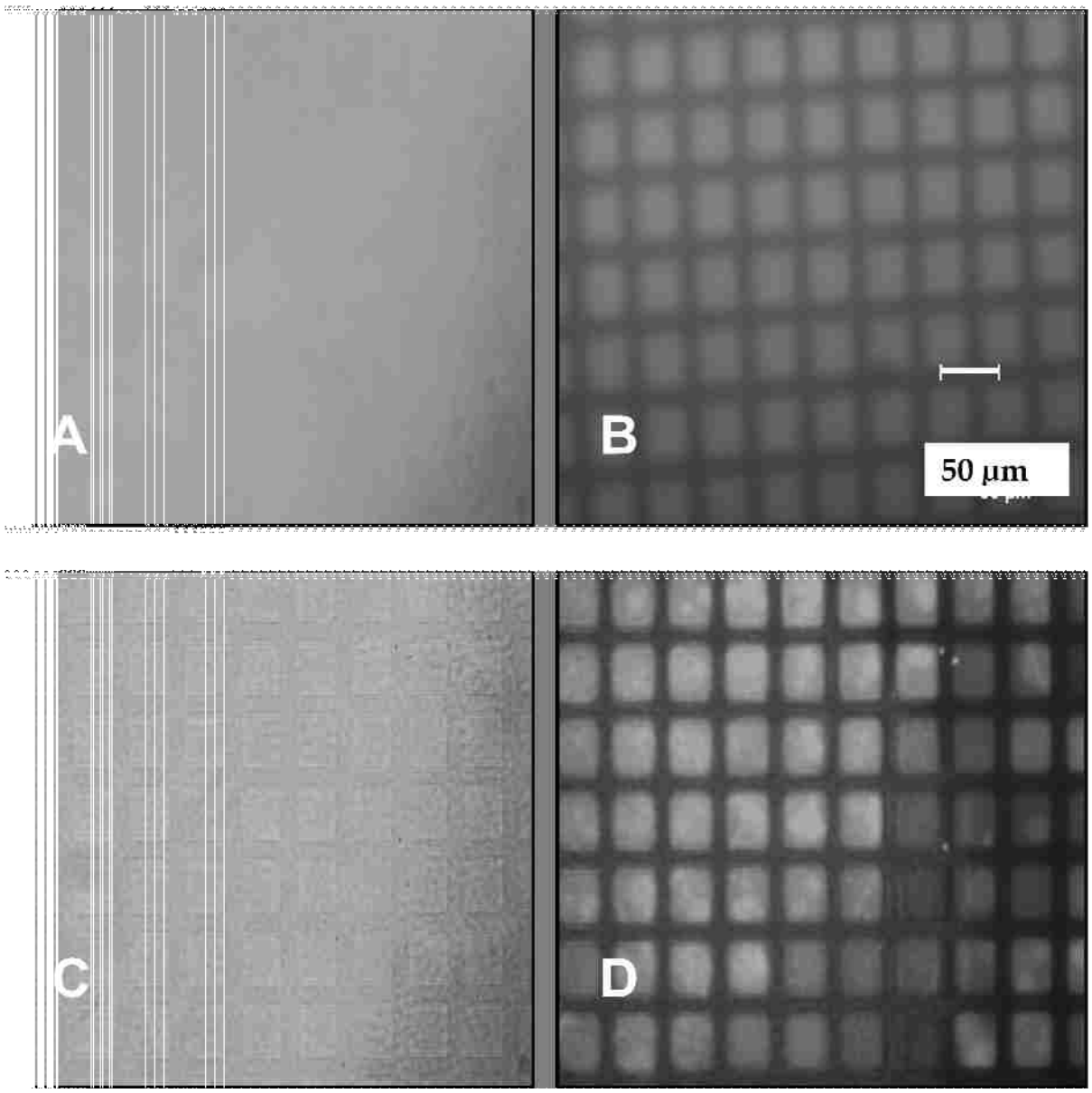

Figure 2.4 Brightfield **A, C)** and fluorescence **B, D)** images of PC **A, B)** and PMMA **C, D)** surfaces exposed to broadband UV radiation through a TEM grid and subsequently reacted with ethylene diamine in the presence of EDAC. Prior to fluorescence imaging, the functional amine scaffold was reacted with FITC. The fluorescence images were acquired using 510 nm excitation with the emission monitored at ~520 nm. The PMMA and PC sheets were exposed to broadband UV radiation (15 mW/cm^2) for 35 min.

However, in the case of PMMA, evidence of slight morphological changes were apparent following UV exposure as indicated by the presence of features defined by the TEM grid. However, in the case of PMMA, evidence of slight morphological changes were apparent following UV exposure as indicated by the presence of features defined by the TEM grid. AFM images of this surface (see Figure 2.5) indicated a trough depth of approximately 75 nm.

2.3.2 Cell Transport in Pristine PMMA and PC. Figures 2.6A and 2.6B shows the linear velocity dependence upon the applied field for baker's yeast cells in PC (A) and PMMA (B) with 0.5, 1.0, and 20 mM PBS at pH=7.4. The negatively charged cells would be expected to migrate in the direction of the anode due to electrophoretic effects, however, at each buffer concentration in both PC and PMMA baker's yeast cells migrated toward the cathode (same direction as EOF).

Clearly, the mobility of these cells is smaller than the EOF resulting in net flow toward the cathode. It was also observed that the flow velocity of baker's yeast cells in these polymer devices decreased with increasing buffer concentration. It is well known that increasing the concentration of the electrolyte will decrease the EOF due to compression of the double layer.[30] Because the apparent mobility is dependent on the EOF, decreases in the EOF result in lower mobilities when the apparent mobility is in the same direction as the EOF, as observed here.

Plots of linear velocity versus electric field were used to extract the apparent mobilities (μ_{app}) for both types of cells. Table 1 shows a summary of the estimated μ_{app} for both *Escherichia coli* and baker's yeast (*Saccharomyces cerevisiae*) for pristine polymers in PBS at pH=7.4. The μ_{app} of the yeast cells in PC were $+2.84 \times 10^{-4}$, $+1.87 \times 10^{-4}$, and $+0.70 \times 10^{-4}$ cm^2/Vs in 0.5, 1.0, and 20 mM PBS, respectively, where the positive sign indicates migration in the same direction as the EOF.

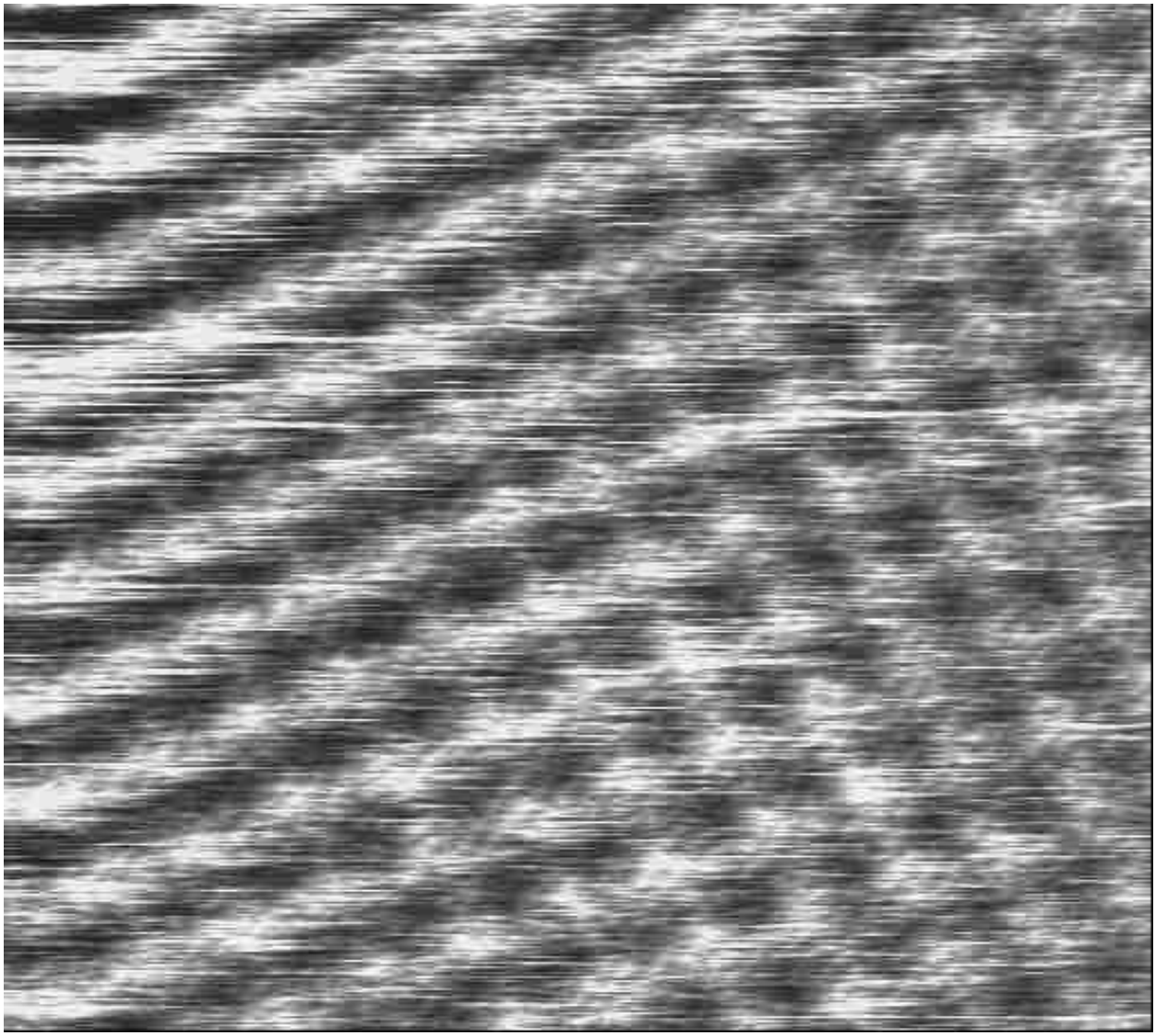

Figure 2.5 AFM images of PMMA following exposure to broadband UV radiation. See Materials and Methods section for experimental details.

The μ_{app} of these cells in PMMA were lower compared to PC due to the lower EOF in PMMA but still migrated toward the cathode.[12,16,29] Figures 2.6C and 2.6D show the flow velocity dependence on the applied potential for *E. coli* cells in PC (C) in 0.5, 1.0, and 20 mM PBS and PMMA (D) in 0.5 and 1.0 mM PBS at pH=7.4. *E. coli* cells show opposite behavior to that observed for baker's yeast in both polymeric materials with 0.5 mM and 1 mM PBS (pH=7.4).

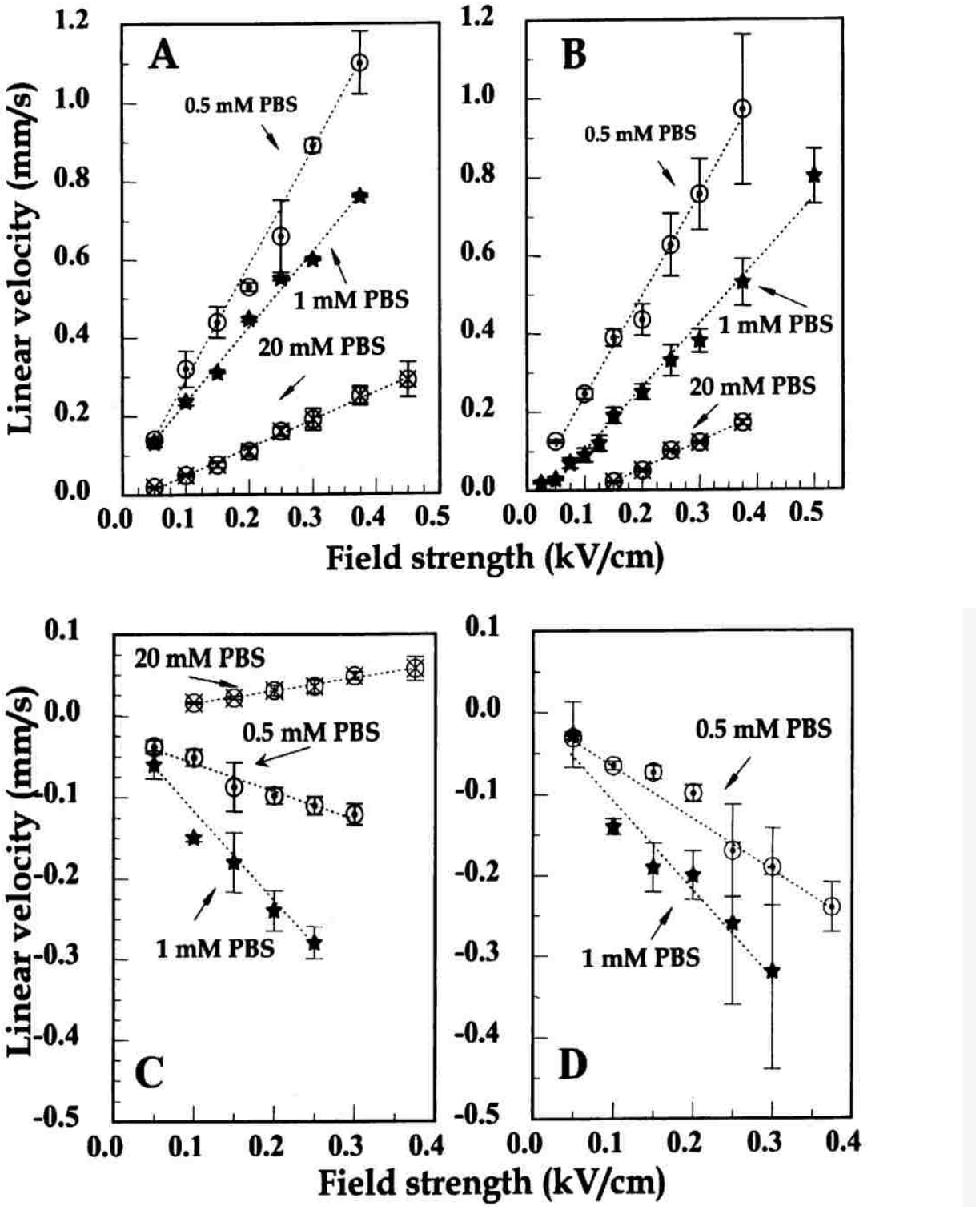

Figure 2.6 Flow velocity versus applied field strength for baker's yeast cells on PC **(A)** and PMMA **(B)** microdevices, and *E. coli* cells on PC **(C)** and PMMA **(D)** microdevices. Channel dimensions the same as stated in Figure 2.1. All velocities were obtained in PBS buffer (pH = 7.4) at concentrations of 0.5, 1.0, and 20.0 mM.

At these conditions, the electrophoretic mobility of *E. coli* cells was greater than the EOF and resulted in migration toward the anode. Interestingly, in 20 mM PBS the direction of cell movement in PC (as well as in UV-modified PC and UV-modified PMMA) was reversed, and the cells migrated in the direction of the cathode. In pristine PMMA at 20 mM PBS, mixed mobilities were observed; some cells moved toward the cathode and some in the direction of the anode. Clearly, there is some additional factor that governs or influences the transport of *E. coli* in 20 mM PBS. One would expect that since the EOF would be reduced at higher ionic strength compared to 0.5 and 1.0 mM PBS the cell apparent mobility would decrease if its μ_{app} was positive.

Table 2.1 Values of apparent electrophoretic mobility (μ_{app}) for *E. coli* and baker's yeast (*S. cerevisiae*) cells in pristine and UV-modified polymers with phosphate buffer saline (PBS) pH=7.4.

Cell type	PBS pH=7.4	μ_{app} in PMMA	μ_{app} in PC	μ_{app} in UV-PMMA	μ_{app} in UV-PC
		x 10^4 cm^2 V^{-1} s^{-1}			
S. cerevisiae	0.5 mM	(+) 2.57±0.11	(+) 2.84±0.12	(+) 3.64±0.05	(+) 4.83±0.80
	1.0 mM	(+) 1.62±0.06	(+) 1.87±0.10	(+) 1.96±0.16	(+) 2.53±0.21
	20 mM	(+) 0.66±0.07	(+) 0.70±0.02	(+) 0.71±0.02	(+) 0.92±0.04
E. Coli	0.5 mM	(-) 0.84±0.04	(-) 0.53±0.05	(-) 0.80±0.06	(-) 0.56 ±0.10
	1 mM	(-) 1.04±0.01	(-) 0.66±0.05	(-) 0.88±0.04	(-) 0.76±0.10
	20 mM	mixed flow directions	(+) 0.16±0.01	(+) 0.14±0.04	(+) 0.28±0.01

Note: (+) mobility indicates flow toward cathode, and (-) mobility indicates flow toward anode.

The electrophoretic behavior (i.e., electrophoretic mobility) of cells is mainly controlled by pH and ionic strength of the medium. Both the degree of dissociation of the functional groups on the cell surface and the thickness of the double layer surrounding a cell are determined by the medium pH and ionic strength, respectively, which can change the electrophoretic mobility.[31] For a rigid colloidal particle with a constant surface potential, Smoluchowski theory predicts that electrophoretic mobility of particles will *decrease proportionally to the square root of the increase in ionic strength*.[32] This model, however, may not be applicable in the present case since biological cells are considered to be non-rigid.[33-38] Ohshima and co-workers pointed out that the electrokinetic behavior of microbes with extracellular polymer layers (i.e., "soft" particles) will be different from that of rigid particles.[33,35] Levine et. al. found that the electrophoretic mobility of red blood cells is smaller than that calculated according to the Smoluchowski equation.[34] Recently, the electrophoretic mobility of a biological cell was studied by Hsu et al.[36] The authors investigated the effect of pH and ionic strength of the medium on the electrophoretic mobility of the cell. They concluded that for *"soft" particles, the electrophoretic mobility decreases with an increase in ionic strength* due to a thinner double layer surrounding the cell and the stronger shielding effect of counter-ions.[36]

Results for *E. coli* cells suggest that at low ionic strength (i.e., 0.5 and 1.0 mM PBS) the electrophoretic mobility was greater than the EOF and resulted in migration toward the anode. At high ionic strength cell electrophoretic mobility decreased faster than the EOF in PC resulting in cell migration toward the cathode. In pristine PMMA with 20 mM PBS, the EOF is suppressed by high buffer concentrations causing some cells to migrate with the EOF and others against it due to differences in individual cell's electrophoretic mobility giving rise to mixed mobility directions.

2.3.3 Cell Transport in UV-Modified PMMA and PC. In both UV-modified polymers, baker's yeast cells moved toward the cathode. The μ_{app} of baker's yeast cells decreased with increasing buffer concentration consistent with a lower EOF at higher ionic strength. The apparent mobility of baker's yeast in UV-modified PC was $+4.83 \times 10^{-4}$, $+2.53 \times 10^{-4}$, and $+0.92 \times 10^{-4}$ cm^2/Vs in 0.5, 1.0, and 20 mM PBS, respectively. These μ_{app} are higher than those obtained in unmodified PC, consistent with a larger EOF for mobilities that are electroosmotically dominated. The μ_{app} of baker's yeast cells in UV-modified PMMA was higher than those in pristine PMMA.

The μ_{app} for *E. coli* cells in UV-modified PC was found to be -0.56×10^{-4}, -0.76×10^{-4}, and $+0.28 \times 10^{-4}$ cm^2/Vs in 0.5, 1.0, and 20 mM PBS, respectively. As can be seen, the sign of μ_{app} indicates cell travel toward the anode, opposite to the EOF, except with the highest ionic strength buffer where the cells migrated toward the cathode, similar to what was observed in unmodified PC. In the case of UV-modified PMMA, the μ_{app} of these cells was -0.80×10^{-4}, -0.88×10^{-4}, and $+0.14 \times 10^{-4}$ cm^2/Vs in 0.5, 1.0, and 20 mM PBS, respectively. The μ_{app} of *E. coli* migrating in UV-modified PMMA was lower than in unmodified PMMA. For example, in 1 mM PBS at pH=7.4 μ_{app} was $-0.88 \times 10^{-4}$and -1.04×10^{-4} cm^2/Vs in UV-PMMA and PMMA microchannels, respectively.

It was found that the EOF in both pristine and UV-modified polymeric devices showed an increase in magnitude at higher pH values (see Figure 2.3). We therefore tested the behavior of the cell mobility in microfluidic channels of different buffer pHs in 1 mM PBS. It was observed that the μ_{app} of baker's yeast increased with increasing pH. For example, in PC with 1 mM PBS μ_{app} were $+1.05(\pm0.10) \times 10^{-4}$, $+2.25(\pm0.20) \times 10^{-4}$, and $+2.40(\pm0.40) \times 10^{-4}$ cm^2/Vs; and for UV-PC they were $+1.15(\pm0.20) \times 10^{-4}$, $+2.65(\pm0.40) \times 10^{-4}$, and $+2.80(\pm0.4) \times 10^{-4}$ cm^2/Vs, at pH 3, 7.4, and 9.5, respectively. The μ_{app} increased for both pristine and UV-modified PC with increases in pH, consistent with

larger EOF values at higher pHs. However, the extent of the increase was more significant for UV-modified PC due to its larger increase in EOF at higher pH values compared to pristine PC. Similar trends were also observed for PMMA and UV-PMMA.

The EOF in glass has a magnitude that is typically greater than the electrophoretic mobility of most analytes or cells. Thus all materials, irrespective of charge, tend to migrate toward the cathode. The μ_{app} measured in 200 mM PBS (pH=7.4) in glass by Li et al.[2] for baker's yeast cells was $+3.50(\pm0.57)x10^{-4}$ and $+2.00(\pm0.36)x10^{-4}$ cm^2/Vs for *E. coli*. In glass, both types of cells migrated with the EOF. For the polymers investigated herein, only baker's yeast cells (regardless of polymer or the buffer ionic strength) migrated with the EOF. The largest μ_{app} of baker's yeast cells in polymer microdevices was observed for UV-modified PC in 0.5 mM PBS (see Table 1). We have found that the largest μ_{app} for *E. coli* cells was observed in PMMA in 1 mM PBS (see Table 1). The largest μ_{app} for cells moving with the EOF was observed in UV-modified PC in 20 mM PBS ($+0.28$ $x10^{-4}$ cm^2/Vs). This value is an order of magnitude lower than that observed in glass.[2]

Chip-to-chip reproducibility of the measured EOFs and cell flow velocities varied slightly, however, the direction of the cell transport was reproducible from chip-to-chip. For example, in 3 different PMMA microdevices, RSD values for the velocities were approximately 10-12% for both types of cells. For a single microdevice, the RSDs for flow velocities were usually 5-10% with up to 20% at high applied fields. It was found generally that the RSD for *E. coli* cells were higher than those for baker's yeast. Similar values for the relative standard deviations have been observed for glass chips (RSD=10-18%).[2]

2.3.4 Cell Adsorption. Cell adhesion and adsorption in a microfluidic device can lead to flow problems mainly due to clogging of the device. Bare silicon and glass surfaces are

particularly prone to cell adhesion, promoting biofouling under both static and flow conditions.[28] Such problems are especially pronounced when high cell counts are used.[2] The hydrophilic nature of the glass surface makes them unsuitable in many cases for cell assays without modification. Cell adhesion has been shown to be reduced by modification of the glass channel walls with trichlorohexadecylsilane,[2] or poly(dimethylacrylamide).[39,40] Covalent and non-covalent modification of the channel surfaces has been performed with silane coupling agents, such as octadecyltrimethoxysilane (ODTMS),[28,39] N-(triethoxysilylpropyl)-O-polyethylene oxide urethane (TESP),[28] and (tridecafluoro-1,1,2,2-tetrahydrooctyl)-1-dimethylchlorosilane (F13) to minimize cell adsorption.[39] The TESP coating was effective at inhibiting glial cell biofouling, allowing the device to operate for several minutes without failure. The ODTMS coatings, on the other hand, promoted glial cell adhesion leading to restricted flow within a few minutes.[28] In studies with *E. coli* cells, ODTMS and F13 were found to be too hydrophobic for use with aqueous solutions.[39]

Unmodified PMMA and PC possess more hydrophobic surfaces compared to glass.[16] UV-radiation of these polymers modifies the surface making them more hydrophilic and potentially more susceptible to cell adhesion.[2,39] Indeed, we noticed minimal cell adhesion/adsorption to the channel wall, channel bottom or coverplate for the unmodified materials. Even after 1 hr of operation, the channels in unmodified polymeric microdevices remained unclogged and functional. Although the clogging of the channels in UV-modified polymers was also not experienced after 1 hr of operation, it was observed that more yeast cells adhered to these channel surfaces. It was noticed during microdevice operation that some of the immobilized/adsorbed cells could be removed by applying higher fields. This was partially caused by an increase in the number of collisions between flowing and stagnant cells as well as stronger fields that

were able to “lift” cells from the polymer surface, suggesting that the adhesion forces of the cell to the polymer surface (UV-modified) were not strong enough to withstand drag forces produced by the EOF.

2.3.5 Cell Sorting. Figures 2.7A and 2.7B show light scattering signals generated for two separate suspensions of unlabeled baker’s yeast cells (A) and *E. coli* (B) in 1 mM PBS (pH=7.4) using a PMMA microchip. Cells were driven separately using electrophoretic/electroosmotic forces in the device with a field strength of 0.2 kV/cm. *E. coli* cells migrated toward the anode and baker’s yeast cells toward the cathode. Each scatter signal most likely represents passing of a single cell through the laser beam. Histograms built for each run are presented in Figure 2.7C. It is evident that the scattering signal for baker’s yeast cells is larger than that for *E. coli*. The average signal was 1,350±432 and 268±86 cps for baker’s yeast and *E. coli,* respectively. The observed difference in the magnitude of the scatter signal is mainly due to differences in size of these two types of cells, but may also reflect shape or surface roughness differences.[6,7,39,41-43]

The observed differential cell migration behaviors in polymeric devices suggested the possibility of presorting these two types of cells electrophoretically. Nano-particles and biological cells have been shown to be sorted on the basis of their dielectric properties.[44] Sorting was based on the fact that when particles are placed in an AC electric field, polarized particles experience a variable translational force, which depends on the applied frequency. Since the polarization is frequency dependent, the net force is also dependent on frequency. Thus, by manipulation of the medium conductivity and applied frequency one can separate the particles based on their dielectric properties.[44]

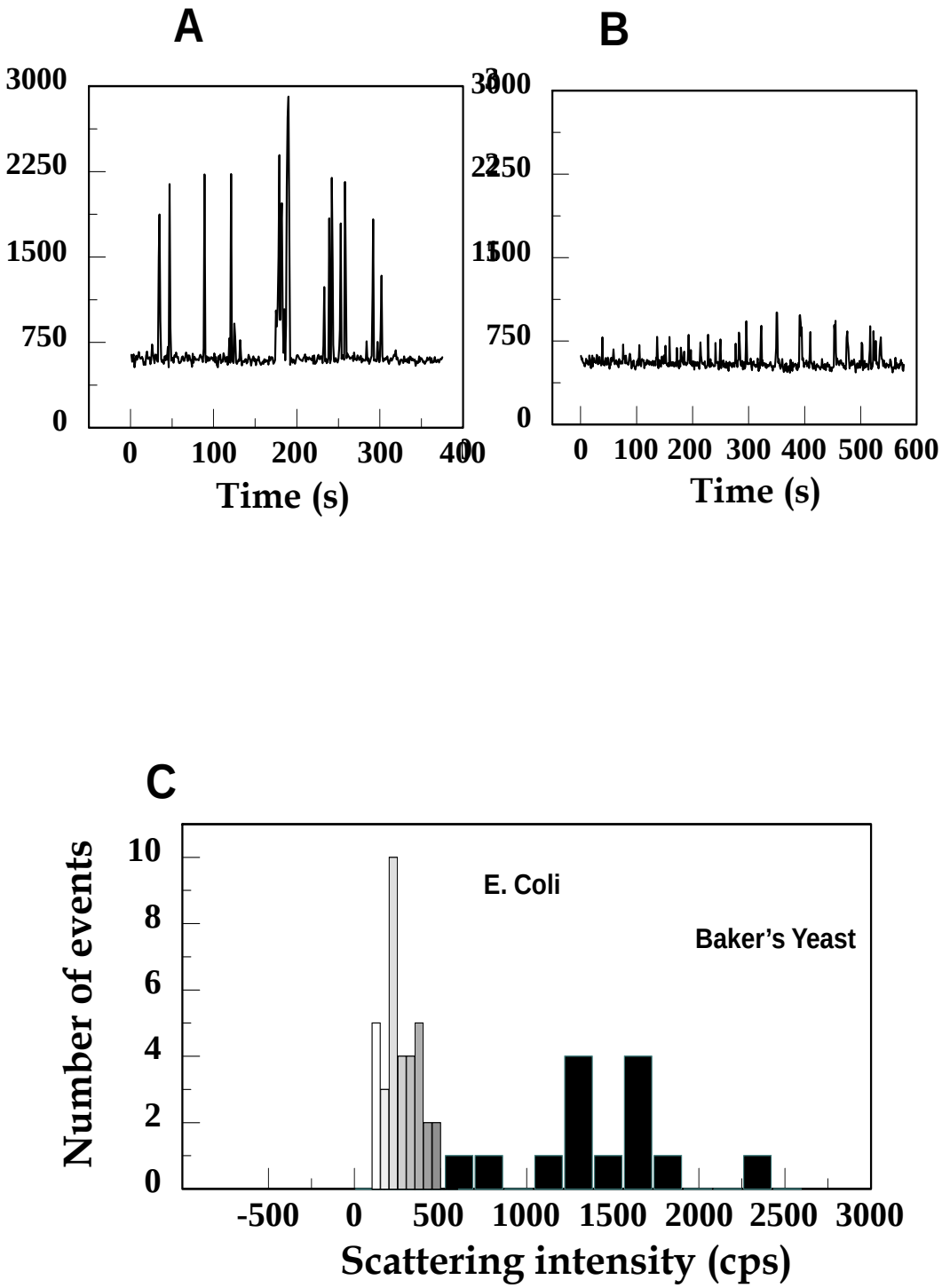

Figure 2.7 Light scattering signals generated for a suspension of unlabeled baker's yeast cells **(A)** and *E. coli* cells **(B)** in 1 mM PBS, pH=7.4 in a PMMA microchip. The two types of cells were run separately. Also shown in **(C)** are histograms of frequency versus scattering signal intensity obtained from baker's yeast and *E. coli* cells constructed from the data in **(A)** and **(B)**. Scattering data were generated with the 680 nm laser at a power of 0.25 mW with a sampling time of 0.5 s. The cells were electrophoretically/electroosmotically driven at 0.2 kV/cm using the chip described in Figure 2.1.

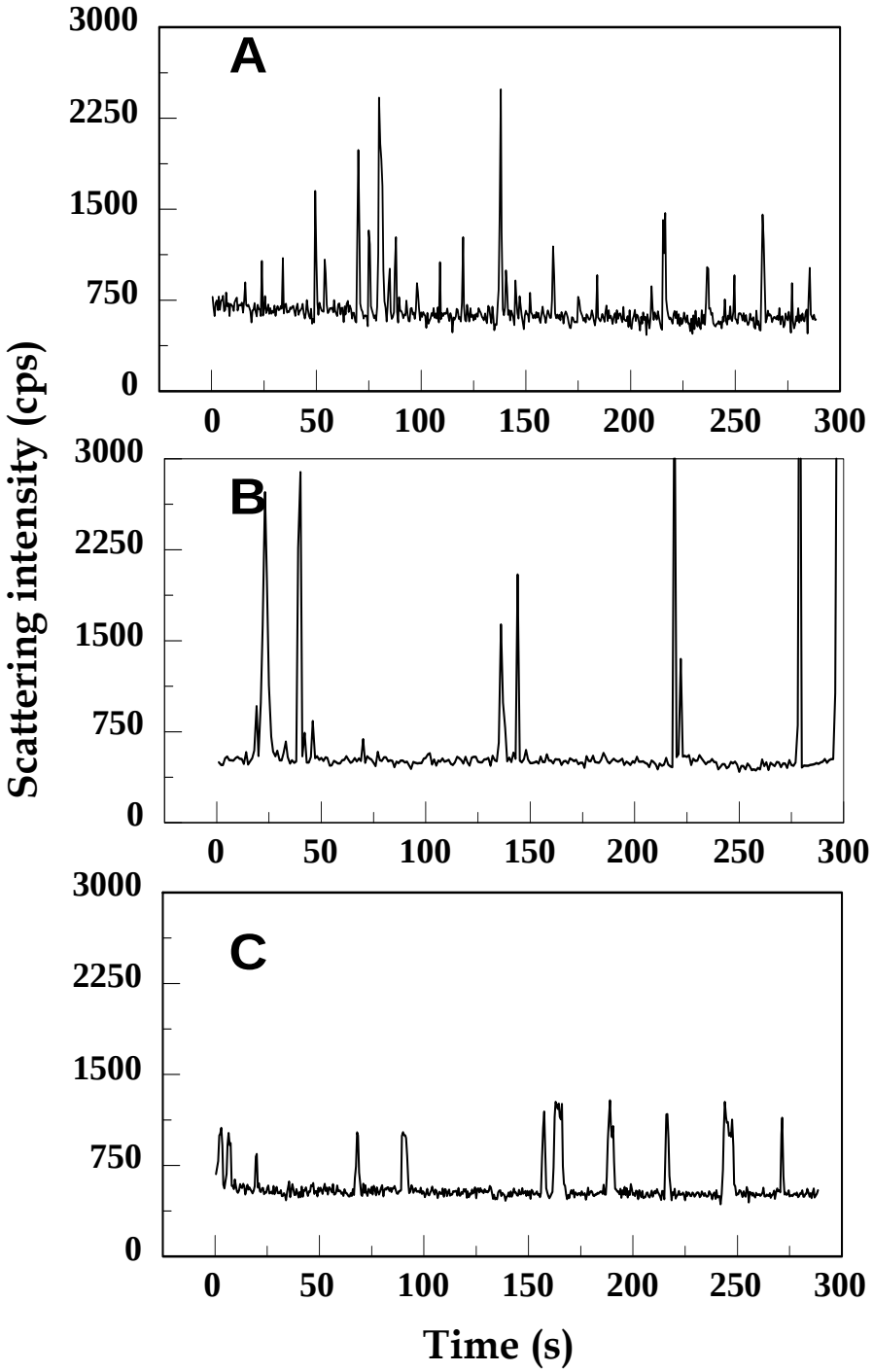

Figure 2.8 Light scattering signals generated for a suspension of an unlabeled mixture of baker's yeast and *E. coli* cells in PBS (pH=7.4) in a PMMA microchip. **A)** The anodic reservoir was filled with baker's yeast and *E. coli* cell suspensions prepared in 20 mM PBS, **B)** the anodic reservoir was filled with baker's yeast and *E. coli* cell suspensions prepared in 1 mM PBS, and **C)** the cathodic reservoir was filled with both cell types in 1 mM PBS (pH=7.4). See Figure 2.7 for experimental details.

We present a simple method of sorting two types of cells based solely on their electrophoretic mobilities. By judicious choice of; (i) the buffer concentration in which the cell suspension is prepared and; (ii) the polymer material and preparation, we can selectively introduce a certain cell type into a microfluidic device from a mixed population of cells. Figures 2.8A-C show scatter data collected for a mixture of electrically driven baker's yeast and E. coli cells in an unmodified PMMA microchannel. In Figure 2.8A, the anodic reservoir was filled with both baker's yeast and E. coli cells suspended in 20 mM PBS. At these conditions, the scattering signal was collected for both baker's yeast and E. coli cells, since both types of cells enter the microchannel. When the anodic reservoir was filled with the mixed cell population (baker's yeast and E. coli) and suspended in 1 mM PBS (pH=7.4), only high intensity signals were observed (Figure 2.8B). The observed scattering signal ranged from 1,500 to 4,000 cps, suggesting that the scatter signal was produced predominately from baker's yeast cells (see Figure 2.7C). As expected, at these conditions we were able to presort E. coli cells from baker's yeast cells based on their differential mobilities. Figure 2.8C shows data obtained in a similar experiment as in Figure 2.8B with the exception that the cathodic reservoir was filled with the mixed population of cells in 1 mM PBS. The scatter signal with low intensity peaks indicated that only E. coli cells entered the microdevice (see Figure 2.7C).

2.4 Conclusions

The use of plastics can increase the utility and diversity of devices due to differences in their surface chemistry and the fact that simple modification chemistries can be imposed on the material to affect changes in its EOF properties. Electrokinetic transport of *Escherichia coli* and *Saccharomyces cerevisiae* (baker's yeast) cells was evaluated in microdevices fabricated in pristine and UV-modified PMMA and PC. The cell

velocities ranged between a few μm/s to several mm/s. For example, the largest flow velocity for baker's yeast cells in these microdevices was observed for UV-modified PC with 0.5 mM PBS, and the lowest was measured in PMMA with 20 mM PBS. Baker's yeast cells migrated with the EOF because their electrophoretic mobility was smaller than the EOF. The largest flow velocity for *E. coli* cells was observed in PMMA with 1 mM PBS and the lowest in UV-modified PC with 0.5 mM PBS. *E. coli* cells migrated toward the cathode only when the cell suspension was prepared in 20 mM PBS. Our results demonstrated the feasibility of manipulating the electroosmotic flow by changing the ionic strength of the buffer and/or modifying the polymer material through UV exposure, which allowed cell sorting electrokinetically. Therefore, selective introduction of only one type of cell into a microdevice device from a mixed population could be performed.

2.5 References

(1) Carlson, R. H.; Gabel, C. V.; Chan, S. S.; Austin, R. H.; Brody, J. P.; Winkelman, J. W. M. D. *Physical Review Letters* **1997**, *79*, 2149-2152.

(2) Li, P. C. H.; Harrison, D. J. *Analytical Chemistry* **1997**, *69*, 1564-1568.

(3) Waters, L. C.; Jacobson, S. C.; Kroutchinina, N.; Khandurina, J.; Foote, R. S.; Ramsey, J. M. *Analytical Chemistry* **1998**, *70*, 158-62.

(4) Blankenstein, G.; Larsen, U. D. *Biosensors & Bioelectronics* **1998**, *13*, 427-438.

(5) Blankenstein, G.; Spohn, U.; Preuschoff, F.; Thoemmes, J.; Kula, M.-R. *Biotechnology and Applied Biochemistry* **1994**, *20*, 291-307.

(6) Blankenstein, G.; Scampavia, L. D.; Ruzicka, J.; Christian, G. D. *Cytometry* **1996**, *25*, 200-204.

(7) Fu, A. Y.; Spence, C.; Scherer, A.; Arnold, F. H.; Quake, S. R. *Nature Biotechnology* **1999**, *17*, 1109-11.

(8) Fiedler, S.; Wirth, R. *Analytical Biochemistry* **1988**, *170*, 38-44.

(9) Muller, T.; Gradl, G.; Howitz, S.; Shirley, S.; Schnelle, T.; Fuhr, G. *Biosensors & Bioelectronics* **1999**, *14*, 247-256.

(10) Chang, H.; Ikram, A.; Kosari, F.; Vasmatzis, G.; Bhunia, A.; Bashir, R. *Journal of Vacuum Science & Technology, B: Microelectronics and Nanometer Structures* **2002**, *20*, 2058-2064.

(11) Heo, J.; Thomas, K. J.; Seong, G. H.; Crooks, R. M. *Analytical Chemistry* **2003**, *75*, 22-26.

(12) Soper, S. A.; Ford, S. M.; Qi, S.; McCarley, R. L.; Kelly, K.; Murphy, M. C. *Analytical Chemistry* **2000**, *72*, 643A-651A.

(13) Shadpour, H.; Musyimi, H.; Karki, M.; Soper, S. A. *unpublished results* **2003**.

(14) Ross, D.; Johnson, T. J.; Locascio, L. E. *Analytical Chemistry* **2001**, *73*, 2509-2515.

(15) Soper, S. A.; Henry, A. C.; Vaidya, B.; Galloway, M.; Wabuyele, M.; McCarley, R. L. *Analytica Chimica Acta* **2002**, *470*, 87-99.

(16) Vaidya, B.; Soper, S. A.; McCarley, R. L. *Analyst (Cambridge, UK)* **2002**, *127*, 1289-1292.

(17) Siampiringue, N.; Leca, J. P.; Lemaire, J. *European Polymer Journal* **1991**, *27*, 633-41.

(18) Adams, M. R.; Garton, A. *Polymer Degradation and Stability* **1993**, *42*, 145-51.

(19) Adams, M. R.; Garton, A. *Polymer Degradation and Stability* **1993**, *41*, 265-73.

(20) Johnson, T. J.; Waddell, E. A.; Kramer, G. W.; Locascio, L. E. *Applied Surface Science* **2001**, *181*, 149-159.

(21) Johnson, T. J.; Ross, D.; Gaitan, M.; Locascio, L. E. *Analytical Chemistry* **2001**, *73*, 3656-3661.

(22) Locascio, L. E.; Perso, C. E.; Lee, C. S. *Journal of Chromatography, A* **1999**, *857*, 275-284.

(23) Ford, S. M.; Kar, B.; McWhorter, S.; Davies, J.; Soper, S. A.; Klopf, M.; Calderon, G.; Saile, V. *Journal of Microcolumn Separations* **1998**, *10*, 413-422.

(24) Qi, S.; Liu, X.; Ford, S.; Barrows, J.; Thomas, G.; Kelly, K.; McCandless, A.; Lian, K.; Goettert, J.; Soper, S. A. *Lab on a Chip* **2002**, *2*, 88-95.

(25) Vaidya, B.; Soper, S. A.; McCarley, R. L. *Analyst* **2002**, *127*, 1289-1292.

(26) Huang, X.; Gordon, M. J.; Zare, R. N. *Analytical Chemistry* **1988**, *60*, 1837-8.

(27) Zhu, L.; Stryjewski, W.; Lassiter, S.; Soper, S. A. *Analytical Chemistry* **2003**, *75*, 2280-2291.

(28) Cox Jimmy, D.; Curry Mark, S.; Skirboll Stephen, K.; Gourley Paul, L.; Sasaki Darryl, Y. *Biomaterials* **2002**, *23*, 929-35.

(29) Henry, A. C.; Tutt, T. J.; Galloway, M.; Davidson, Y. Y.; McWhorter, C. S.; Soper, S. A.; McCarley, R. L. *Analytical Chemistry* **2000**, *72*, 5331-5337.

(30) Grossman, P. D.; Colburn, J. C. *Capillary Electrophoresis. Theory and Practice.*; Academic Press, Inc., 1992.

(31) Desai, M. J.; Armstrong, D. W. *Microbiology and Molecular Biology Reviews* **2003**, *67*, 38-51.

(32) Morisaki, H.; Nagai, S.; Ohshima, H.; Ikemoto, E.; Kogure, K. *Microbiology (Reading, United Kingdom)* **1999**, *145*, 2797-2802.

(33) Ohshima, H. *Maku* **1994**, *19*, 284-91.

(34) Levine, S.; Levine, M.; Sharp, K. A.; Brooks, D. E. *Biophysical Journal* **1983**, *42*, 127-35.

(35) Ohshima, H. *Electrophoresis* **1995**, *16*, 1360-3.

(36) Hsu, J.-P.; Hsieh, T.-S.; Young, T.-H.; Tseng, S. *Electrophoresis* **2003**, *24*, 1338-1346.

(37) Hsu, J.-P.; Fan, Y.-P. *Journal of Colloid and Interface Science* **1995**, *172*, 230-41.

(38) Van Loosdrecht, M. C. M.; Lyklema, J.; Norde, W.; Schraa, G.; Zehnder, A. J. B. *Applied and Environmental Microbiology* **1987**, *53*, 1898-901.

(39) McClain, M. A.; Culbertson, C. T.; Jacobson, S. C.; Ramsey, J. M. *Analytical Chemistry* **2001**, *73*, 5334-8.

(40) Hjerten, S. *J. Chromatogr.* **1985**, *347*, 191-8.

(41) Scampavia, L. D.; Blankenstein, G.; Ruzicka, J.; Christian, G. D. *Analytical Chemistry* **1995**, *67*, 2743-9.

(42) Schrum, D. P.; Culbertson, C. T.; Jacobson, S. C.; Ramsey, J. M. *Analytical Chemistry* **1999**, *71*, 4173-4177.

(43) Sohn, L. L.; Saleh, O. A.; Facer, G. R.; Beavis, A. J.; Allan, R. S.; Notterman, D. A. *Proceedings of the National Academy of Sciences of the United States of America* **2000**, *97*, 10687-10690.

(44) Green, N. G.; Morgan, H. *Journal of Physics D: Applied Physics* **1997**, *30*, L41-L44.

Chapter 3 Highly Efficient Circulating Tumor Cell Isolation from Whole Blood and Label-free Enumeration Using Polymer-Based Microfluidics with an Integrated Conductivity Sensor*

3.1 Introduction

It is generally accepted that most cancer-related mortalities result from metastatic disease.[1] While the process of metastasis is not well understood, a number of chemical, physical and molecular events occur that ultimately result in the dissemination and deposition of tumor cells into targeted organs using the circulatory system and/or bone marrow as the carrier(s). This "seed and soil" process was proposed as early as 1889 by Paget[2] and was later modified with the caveat that shed tumor cells consist of a heterogeneous population with sub-populations possessing different metastatic potentials.[3] The fundamental entities primarily responsible for spawning metastatic disease are circulating tumor cells (CTCs), which can be produced during early stages of tumorigenesis.[4] Elucidating the quantity of CTCs in peripheral blood or bone marrow can serve as an indicator for the clinical management of several cancer-related diseases by providing information on the success/failure of therapeutic intervention and disease stage forecasting.[5,6]

The isolation and enumeration of exfoliated CTCs in peripheral blood or bone marrow for a variety of cancer-related diseases has already been reported, such as breast,[7-9] colorectal,[10] prostate,[11] renal,[12] bladder,[13] and non-small cell lung[14] cancers. As an example of the clinical utility of CTC information, Cristofanilli *et al.* recently reported a study of 177 breast cancer patients using the amount of CTCs in peripheral blood as an indicator of survival.[7] Patients with ≥5 CTCs per 7.5 mL of whole blood possessed a median progression-free survival of 2.7 months versus 7.0 months for those patients containing <5 CTCs in 7.5 mL of their peripheral blood.

*Reprinted with permission from JACS.

The major issue with securing viable clinical information via quantification of CTC levels is the extremely low abundance or rare-event nature of these cells amongst a high number of spectator cells in peripheral blood.[6,15-18] For example, it is clinically useful to quantitatively enumerate 0-10 CTCs in whole blood composed of $>10^9$ erythrocytes and $>10^6$ leukocytes per mL.[7]

For sampling rare events in a large population, three important metrics must be assessed: (1) throughput, the number of cell identification or sorting steps per unit time; (2) recovery, an indicator of the fraction of target cells collected from the input sample; and (3) purity, which depends on the number of "interfering" cells excluded from the analysis.[19] In addition to these three metrics, highly efficient quantification of the number of enriched cells must be provided as well.

The approaches used to date to enrich CTCs from clinical samples have either provided lower-than-desired recoveries with high purity, relatively poor purity but with high recoveries, or in other cases, highly specialized sample processing and handling whose success is laboratory dependent.[20-25] For example, immunomagnetic approaches for CTC enrichment using ferromagnetic micrometer-sized particles coated with molecular recognition elements specific for antigenic-bearing target cells can interrogate diluted blood samples typically yield modest recoveries (~70%) but extremely favorable purity.[22] In the case of size-based separations employing nuclear tracked membranes, polycarbonate membranes with varying pore sizes (8 – 14 μm) can filter large volumes (9.0 – 18 mL) of blood and recover nearly 85% of the CTCs, but significant numbers of leukocytes are also retained (*i.e.*, low purity) potentially complicating the enumeration process.[26] Investigations utilizing reverse-transcription PCR, in which mRNAs are used as surrogates to report CTC levels, have the ability to

detect one CTC in an excess of 10^6 mononucleated cells.[27] However, these assays are prone to high inter-laboratory variability and require extensive sample handling and manipulation.

Most of the CTC isolation/sorting tools currently in use possess some common procedural characteristics that make them prohibitively difficult to implement, such as the ability to sort only the mononucleated fraction of whole blood requiring density gradient centrifugation prior to enrichment and the use of either flow cytometry or fluorescence microscopy following cell staining to enumerate the number of enriched CTCs. These additional steps require sample handling and transfer, which can induce cell loss or contamination that can dramatically affect the assay result, especially when dealing with low numbers of targets.

Microfluidics provides a venue for producing integrated systems that can process clinical samples in closed architectures to minimize sample contamination and loss. However, high throughput sampling of relatively large volumes (>1 mL) has not been a mainstay for microfluidics due to the macro-to-micro dilemma resulting from the small dimensional features associated with these devices. For example, exhaustively sampling a 1.0 mL volume input using a microchannel of 30 μm × 30 μm at a linear velocity of 1.0 mm s^{-1} would require 309 h (12.9 days). This sampling bottleneck was recently addressed by studies with a glass-based microfluidic fabricated using deep reactive ion etching.[28] The high-surface area immunological capture bed consisted of microposts (100 μm diameter x 100 μm tall) arranged in an equilateral triangular format; the device was capable of capturing ~60% of CTCs from untreated whole blood with enumeration achieved by cell staining and microscopic visualization.

Herein we report our efforts aimed toward the development of a self-contained system capable of meticulously separating intact CTCs from peripheral blood and directly quantifying the CTC level upon isolation and enrichment. As a result of careful fluidic design rules and system integration methods, we have successfully employed a microfluidic system capable of exhaustively and rapidly interrogating >1.0 mL of unprocessed whole blood possibly harboring low-abundant CTCs. At the heart of the system were carefully engineered, exceedingly efficient high-aspect ratio capture beds decorated with mABs specific for antigenic integral membrane proteins expressed in CTCs of epithelial origin and a label-free, highly specific single-cell conductivity sensor. The device operational characteristics were achieved by tailoring the dominant CTC capture dynamics, specific device architecture and suspension linear velocity in a high throughput microsampling unit (HTMSU) containing high-aspect ratio microstructures replicated in a polymeric substrate. Direct single-cell counting of the captured cells was made possible by their release as a result of enzymatic digestion of cell-antigen/antibody-surface complexes. Quantitative assessment of CTC numbers was accomplished using an integrated conductivity sensor capable of specifically detecting CTCs via their electrical signatures without requiring cell staining or microscopic visualization.

3.2 Material and Methods

3.2.1 HTMSU Fabrication. Figure 3.1 shows a schematic of the HTMSU and several micrographs of this polymer-based device. The device consisted of a series of 51 high-aspect ratio channels that were either linear or sinusoidally configured and shared a set of common input/output ports. Devices were replicated from a mold master using hot embossing.

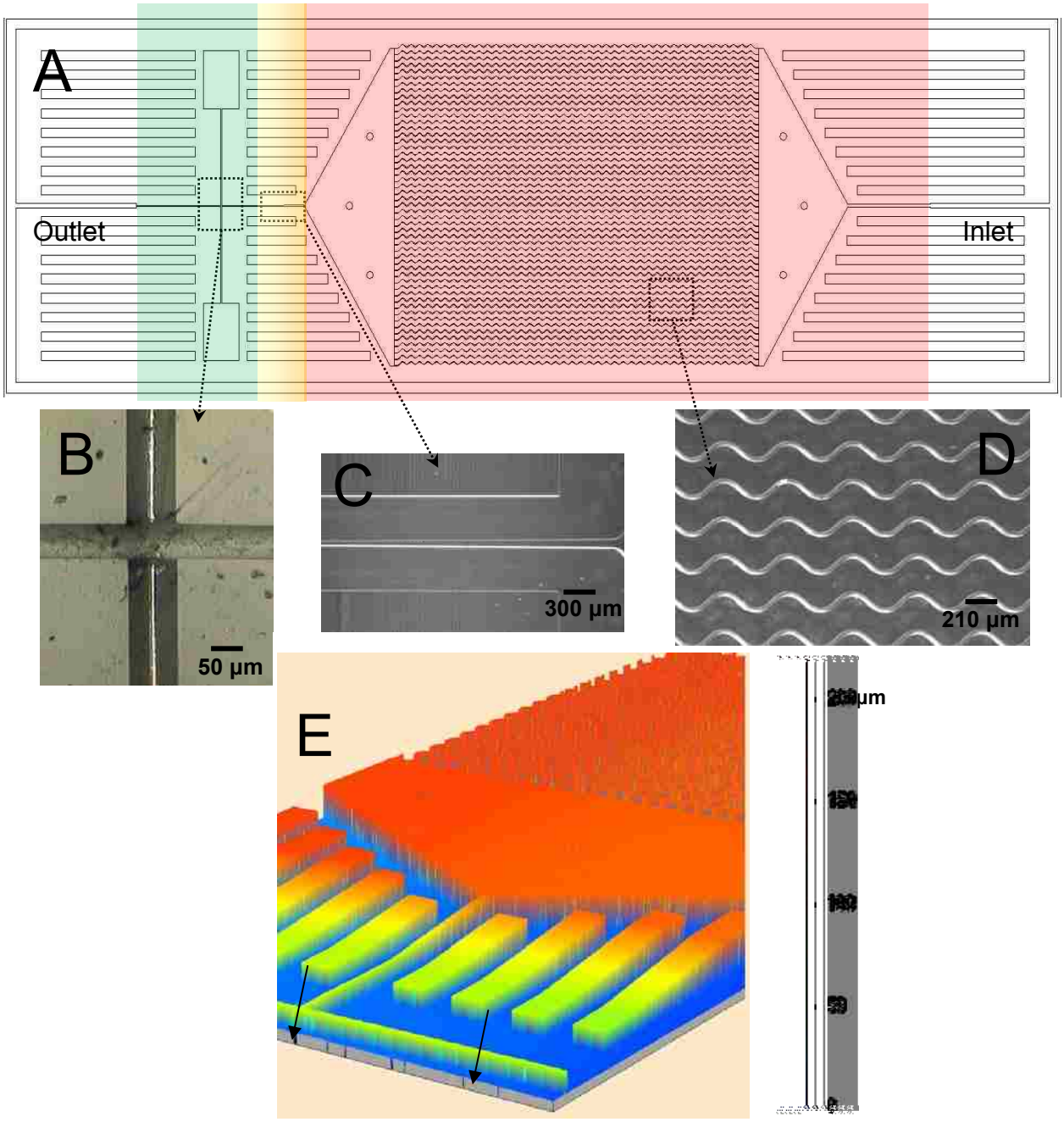

Figure 3.1 Schematics of the HTMSU showing: (A) A scaled AutoCAD diagram of the sinusoidally-shaped capture channels (mould insert feature height: red is 150 µm, green is 80 µm, and orange transitions from 80 to 150 µm over a 2.5 mm length) with brightfield optical micrographs of; (B) the integrated conductivity sensor consisting of cylindrical Pt electrodes that were 76 µm in diameter with a 50 µm gap; (C) single port exit where the HTMSU tapers from 100 µm wide to 50 µm while the depth tapers from 150 µm to 80 µm over a 2.5 mm region that ends 2.5 mm from the Pt electrodes; (D) micrograph taken at 5x magnification showing the sinusoidal cell capture channels; and (E) 3D projection of the topology of the HTMSU obtained at 2.5 µm resolution using non-contact optical profilometry (arrows indicate the platinum electrode conduits).

See the Chapter 4 for details on the fabrication of the mold master and the micro-replication. The substrate selected for the HTMSU was PMMA due to its high fidelity of forming structures with high-aspect ratios via micro-replication, minimal non-specific adsorption of whole blood components to its surface and its ability to generate functional surface-scaffolds through UV irradiation for the attachment of a variety of biological moieties.[29] The HTMSU was manufactured via micro-replication from a metal master. Microstructures were milled onto the surface of a brass plate with a high-precision micromilling machine (KERN MMP 2522, KERN Micro- und Feinwerktechnik GmbH & Co.KG; Germany) following our previously published procedures.[30] The micromilling machine was fitted with a laser measuring system (LaserControl NT, Blum-Novotest GmbH, Germany) for automatic determination of tool length and radius, and an optical microscope (Zoom 6000, Navitar, Inc. Rochester, NY) for monitoring the milling process. Micromilling was carried out at 40,000 rpm. Feed rates were dependent on the size of the milling tool and were typically in the range of 200 mm/min for a 500 µm milling bit, 100 – 150 mm/min for the 200 µm bit, 50 – 75 mm/min for the 100 µm bit and 10-20 mm/min for a 50 µm bit. A typical milling cycle consisted of a pre-cut of the entire surface with a 500 µm milling bit to ensure parallelism between both faces of the brass plate and uniform height of the final milled microstructures over the entire pattern, a rough milling of the microstructures using either a 500 or 200 µm milling bit, and a finishing cut with a smaller diameter milling bit. In the final step of mold master fabrication, burrs were removed by mechanical polishing. Polishing was performed by hand on a 3 µm grain-size polishing paper (Fibrmet Discs - PSA, Buehler, Lake Bluff, IL) followed by polishing on a polypropylene cloth (Engis, Wheeling, IL) with a 1 µm diamond suspension (Metadi Diamond Suspension, Buehler).

Three identical HTMSUs were patterned onto the master enabling production of the units in triplicate during each hot embossing step. In order to accommodate the Pt electrodes used for the conductivity sensor and the inlet/outlet capillaries, the HTMSU was designed with multilevel features.[30] The depth of the HTMSU detection zone was tapered to 80 μm from the 150 μm used in the cell selection beds and throughout the inlet region. The detection channel width was tapered from 100 μm to 50 μm over a 2.5 mm region beginning at the converged outlet and terminating 2.5 mm from the conductivity electrodes scaled for specific detection of CTCs. In the cell selection bed, channel widths (35 μm) that closely matched the average target cell diameter were used to increase the probability of cell-immobilized antibody encounters. To reduce the pressure drops when the device was operated at high volumetric flow rates, the HTMSU was designed with deep (150 μm), high-aspect ratio channels.

Prior to embossing and assembly, PMMA substrates and cover plates were cleaned with reagent grade isopropyl alcohol, IPA (Sigma-Aldrich, St. Louis, MO), rinsed with 18 MΩ nanopure H_2O obtained from a water purification system (D8991, Barnstead/Thermolyne, Dubuque, IA), sonicated for 30 min, rinsed with IPA again and air dried. Hot embossing was performed with a Jenoptik Microtechnik HEX02 (Jena, Germany). For embossing PMMA, the substrate was heated to 140°C and a pressure of 20 kN was applied for 630 s. After the HTMSUs were hot embossed, they were cooled to room temperature and cleaned with IPA.

Regio-specific ultraviolet (UV) modification of the PMMA substrate and cover plate was performed through an aluminum photomask to facilitate the formation of the carboxylated scaffold for directed antibody tethering exclusively within the cell selection beds of the HTMSU. Before final assembly via thermal fusion bonding, the PMMA cover

plate and substrate were locally irradiated at 254 nm with 15 mW cm^{-2} fluence for 10 min using a UV exposure station (ABM, Inc., San Jose, CA). Additionally, into the inlet/outlet ports of the device were inserted 237 μm OD and 150 μm ID polyimide-coated fused silica capillaries and the Pt electrodes fabricated with the required gap (see Materials and Methods). After thermally annealing the cover plate to the substrate, a thin film of epoxy resin was applied to the capillary-device interfaces to prevent leaks.

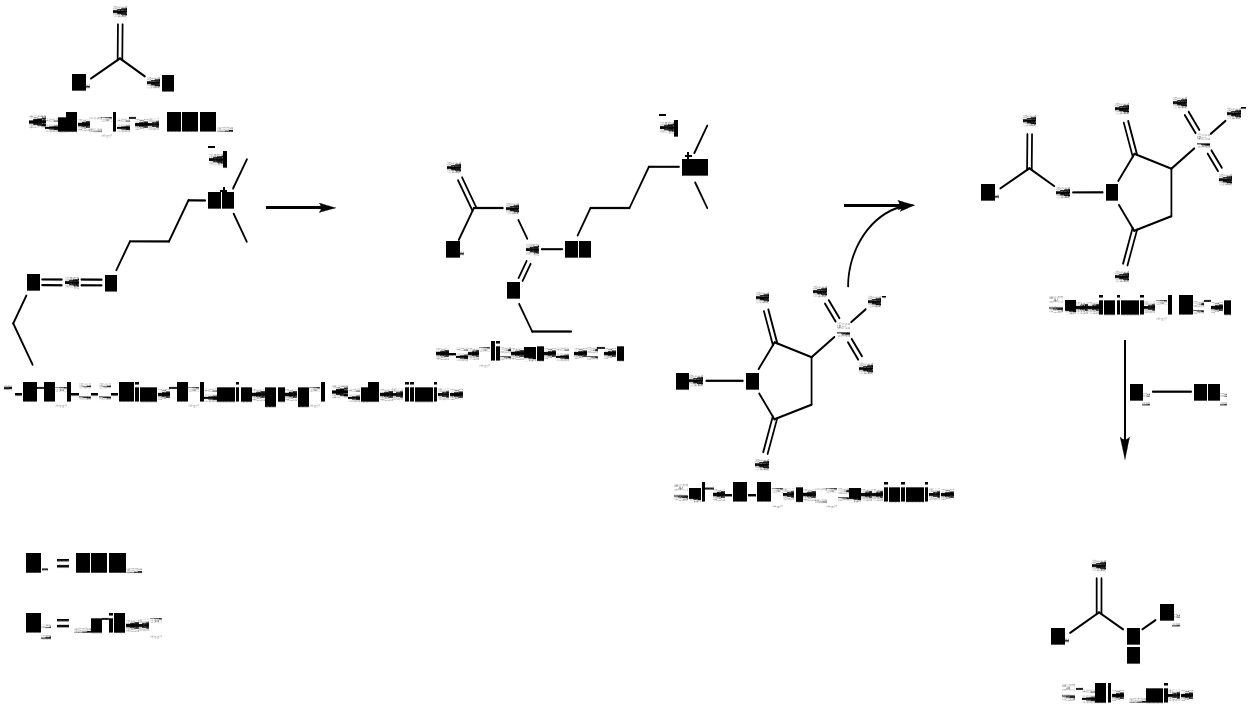

Scheme 3.1 Directed antibody tethering through EDC/NHS coupling. A UV-modified PMMA surface is exposed to a solution containing both EDC and NHS which forms a stable succinimidyl ester that is subsequently reacted with an amine containing antibody ultimately forming a covalent amide bond.

Following UV modification of PMMA, the physicochemical properties of the surface were effectively altered resulting in a moderate reduction of the glass transition temperature (T_g) at the cover plate-substrate interface. The resulting T_g allowed for efficient thermal fusion bonding at 101°C rather than the 106°C T_g of pristine PMMA[31,32], which could

reduce potential thermal deformation of the high-aspect ratio microfeatures. Thermal fusion bonding was carried out in a gas chromatographic (GC) oven (Varian 3400, Palo Alto, CA) using the PMMA cover plate and the open-faced, hot embossed PMMA substrate. The substrate and cover plate were aligned and clamped together between two borosilicate glass plates and the assembly placed into the temperature programmable oven of the GC, where the temperature was increased from 50°C to 101°C at a rate of 20°C/min. The temperature was held at 101°C for 15 min.

3.2.2 Antibody Immobilization. Antibody immobilization was performed using a two step process. Initially, the UV-modified HTMSU device, following thermal assembly, was loaded with a solution containing 4.0 mg/mL of 1-ethyl-3-[3-dimethylaminopropyl] carbodiimide hydrochloride (EDC), 6.0 mg/mL of N-hydroxysuccinimide (NHS) in 150 mM 2-(4-morpholino)-ethane sulfonic acid at pH = 6 (MES, Fisher Biotech, Fair Lawn, NJ) and buffered saline (Sigma-Aldrich, St. Louis, MO) for 1.0 hr to form the succinimidyl ester intermediate. The EDC/NHS solution was then hydrodynamically replaced with a 1.0 mg/mL monoclonal anti-EpCAM antibody (R&D Systems Inc., Minneapolis, MN) solution contained in 150 mM PBS at pH = 7.4 (Sigma-Aldrich, St Louis, MO) and allowed to react for 4 h after which the device was rinsed with a solution of PBS (pH = 7.4) to remove any non-specifically bound anti-EpCAM antibodies.For a complete description of this procedure, see the Appendix.

3.2.3 Apparatus. A PHD2000 syringe pump (Harvard Apparatus, Holliston, MA) was used to hydrodynamically process samples using the HTMSU. In order to interface the HTMSU to the pump, a luer lock syringe (Hamilton, Reno, NV) was fitted with a luer-to-capillary adapter (InnovaQuartz, Phoenix, AZ). The syringe pump was programmed to generate the appropriate volume flow rate to evaluate CTC cell capture efficiency and

post-capture cell retention. The linear velocities were calculated from the cross-sectional area of the respective HTMSU capture channels and the programmed volume flow rate. The flow rates were validated by tracking, via optical microscopy, suspended cells over a fixed 80 μm region.

During evaluative experiments, the HTMSU was fixed to a programmable motorized stage of an Axiovert 200M (Carl Zeiss, Thornwood, NY) microscope, which could monitor the transport of cells in the HTMSU using either fluorescence or brightfield imaging. Videos of cell transport were captured at 30 frames per second (fps) using a monochrome CCD (JAI CV252, San Jose, CA). For fluorescence, excitation was accomplished using a Xe arc lamp and dye-specific filter sets appropriate for the fluorescent dye used for labeling the MCF-7 cells (Carl Zeiss, Thornwood, NY). Each filter cube contained a dichroic mirror, emission filter, and excitation filter.

3.2.4 Integrated Conductivity Sensor. The conductivity electrodes consisted of Pt wires (~76 μm) placed into guide channels that were embossed into the fluidic network and positioned orthogonal to the fluidic output channel (see Figure 3.1). A Pt wire was inserted into these guide channels prior to thermal assembly of the cover plate to the substrate. Once the wire was positioned, the substrate/wire assembly was placed between glass plates and clamped together and finally, heated to slightly higher than the glass transition temperature of PMMA, which embedded the wire into the guide channels and spanned the entire depth of the output channel. To break through the wire to form the electrode pair, a high precision micromilling machine (KERN MMP 2522, KERN Micro- und Feinwerktechnik GmbH & Co.KG; Germany) with a 50 μm bit was used (see Figure 3.1B). Following machining of the Pt wire and UV activation, the cover

plate was aligned to the embossed substrate via alignment marks and clamped together between two glass plates and subjected to thermal fusion bonding.

The conductivity sensor was assembled in-house (for details see Appendix). Conductivity measurements were conducted in TRIS-glycine buffer containing 0.25% (w/w) trypsin, 0.18 mM TRIS, 47 mM glycine and 0.05% (v/v) Tween-20, referred to as the CTC releasing buffer. This CTC releasing buffer was carefully selected in large part for its relatively low conductivity (~50 μS/cm, pH 7.2) and the addition of trypsin to remove the bound CTCs from the capture channel surface for enumeration via single-cell conductometric counting.

3.2.5 Cell Suspensions. Citrated whole rabbit blood was purchased from Colorado Serum Company (Denver, CO). Upon collection, the blood was combined with 10% (w/w) sodium citrate to prevent coagulation. The MCF-7 cells (breast cancer cell line), growth media, phosphate buffered saline, trypsin, and fetal bovine serum was purchased from American Type Culture Collection (Manassas, VA). Adherent MCF-7 cells were cultured to 80% confluence in Dulbecco's modified Eagle's Medium supplemented with high glucose containing 1.5 g L^{-1} sodium bicarbonate ($NaHCO_3$), 15 mM HEPES buffer, and 10% fetal bovine serum (FBS). A 0.25% trypsin solution was prepared in 150 mM PBS and used to harvest the MCF-7 cells.

MCF-7 cells were stained with a fluorescein derivative, PKH67, containing a lipophilic membrane linker for fluorescence visualization experiments (Sigma-Aldrich, St. Louis, Mo). A modified protocol for cell staining was implemented whereby the dye concentration was increased 2-fold resulting in more evenly distributed fluorescent labels over the cell's membrane. Cell counts for seeding experiments into whole blood

were determined by counting three aliquots of cells in succession using a hemacytometer. The cell count accuracy was within 10%.

3.3 Results and Discussion

3.3.1 Model CTC System. The MCF-7 cell line, used as a model for CTC selection and enumeration via the integrated HTMSU, is a breast cancer cell line that possesses an over-expressed membrane antigen termed the epithelial cell adhesion molecule, EpCAM.[33-37] MCF-7 cells are typically 15 – 30 μm in diameter (mean = 24 μm) and have been closely associated with micrometastatic breast cancer.[38] EpCAM occurs at a frequency of 5.1×10^5 molecules per cell.[38] Monoclonal antibodies for EpCAM are available, which can be used to selectively speciate these cells from mixed populations.

3.3.2 Major Considerations. A number of experimental and device operational parameters were investigated to optimize the performance of the HTMSU: (1) Throughput – linear flow velocity, pressure drops, processing time; (2) recovery – capture channel geometry (shape and width), and cell flow dynamics; (3) purity – designing surfaces to minimize non-specific adsorption and provide high selectivity for the target cells.

3.3.3 Pressure Drop. Because the goal of the HTMSU was to process whole blood directly in a high throughput format requiring high volumetric flow rates to reduce processing time, we employed capture channels with high-aspect ratios (aspect ratio = channel height /channel width). For a capture channel width and height similar to the cell dimensions (aspect ratio = 1), capture of a cell within this channel would produce a large pressure drop due to blockage and possibly damage the captured cell making it unavailable for enumeration. Therefore, we adopted a capture channel geometry with an aspect ratio of 4.3; for a 35 μm channel width, the depth was 150 μm, which could

easily be replicated using hot embossing. From Equation 4.6 (see Chapter 4), and a blood viscosity of 4.8 cP (hematocrit = 0.4), the pressure drop for a channel 35 μm x 35 μm (L = 3.5 cm) was calculated to be 7.4 x 10^3 Pa, while a channel that possessed dimensions of 35 μm x 150 μm had a pressure drop of 2.9 x 10^3 Pa, a reduction of greater than 60%.

3.3.4 Flow Dynamics. It has been observed that laminar flow in a tube (capillary) having dimensions greater than 15% that of the cells being transported results in a marginal zone near the tube wall due to migration of the cells toward the central axis of the tube leaving a cell-free layer adjacent to the wall that can be as thick as 4 μm.[39] Because the capture elements (antibodies) are poised on the channel wall, this focusing effect can reduce the number of encounters between the CTCs and their recognition elements. To investigate this phenomenon, we imaged CTCs stained with a membrane-specific fluorescein derivative as they were transported through an unmodified (no mAB) 35 μm wide microchannel that had a straight or sinusoidal configuration (see Figure 3.1). The results of these experiments are given in Figure 3.2; shown in the panels are the effects of channel shape and cell translational velocity (U) on the cells' radial position within the microchannel. Evident in the linear channels (Figure 3.2A and 3.2B) is a cell-free zone, similar to what has been observed in straight capillarie,[40] whose thickness increased with increases in U. However, for the sinusoidally-shaped capture channels, CTC flow dynamics were quite different. First, there was no apparent marginal zone along one edge of the microchannel wall, and secondly, the cell radial distribution seemed to be unaffected by changes in U. The result would be an increase in the antigen/antibody encounter rate as the cells moved through the capture beds at

the relatively high linear velocities required to process large input volumes in reasonable amounts of time using sinusoidal-shaped channels.

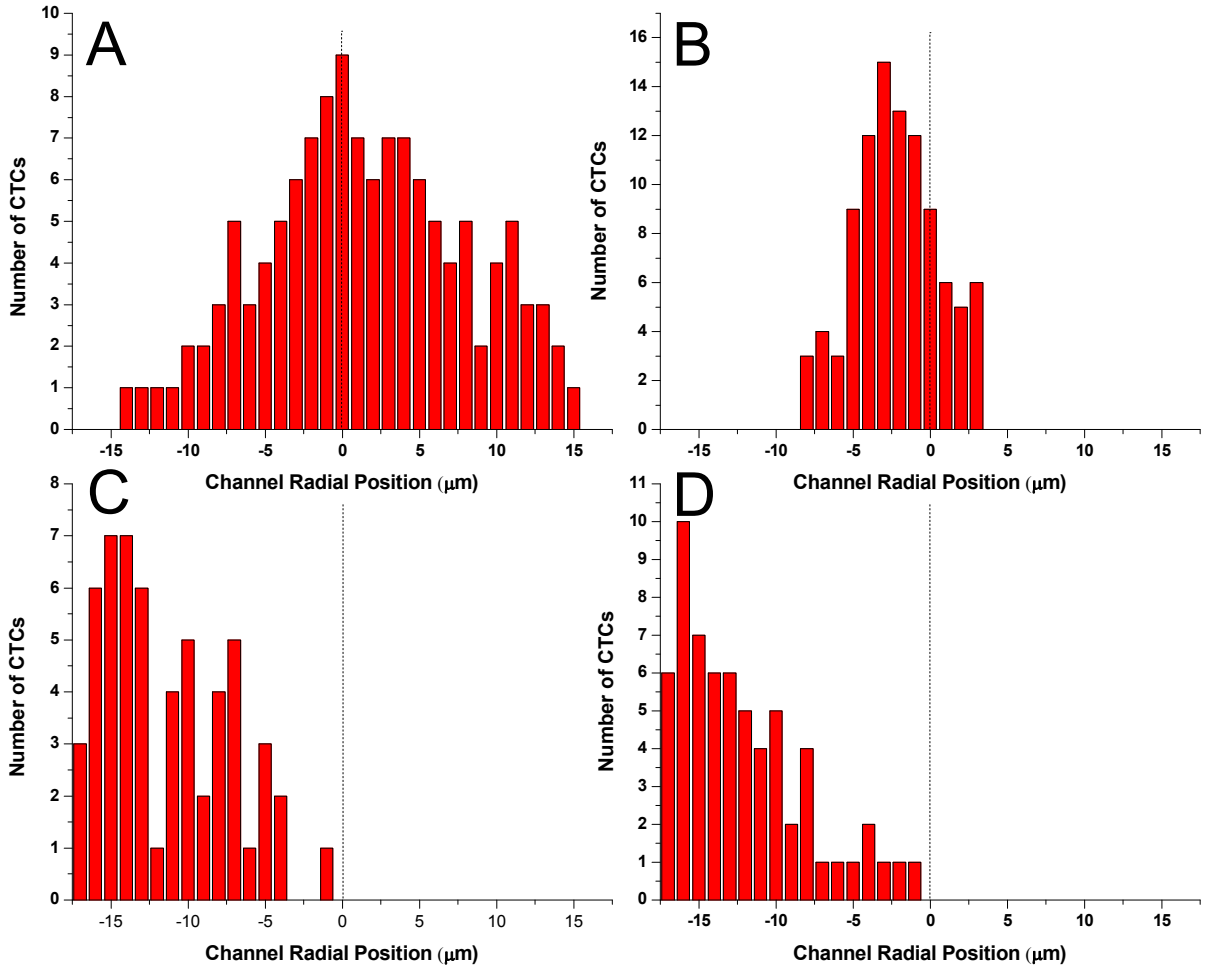

Figure 3.2 Histograms of the radial position of CTCs (centroid) in microchannels with Poiseuille flow at linear velocities (*U*) of 1.0 mm s^{-1} and 10 mm s^{-1} in both straight (A, B) and sinusoidal-configured (C, D) channels. The dashed line represents the microchannel's central axis. (A & B) The radial position of several CTCs histogrammed from micrographs of the straight microchannel with linear flow rates of 1 mm s^{-1} and 10 mm s^{-1}. (C & D) The radial position of several CTCs traversing ¼ of a period of the sinusoidal microchannels with suspension linear velocities of 1 mm s^{-1} and 10 mm s^{-1}. The cells were imaged using fluorescence microscopy with the cells stained using a fluorescein lipophilic membrane dye, PKH67.

3.3.5 Effects of Channel Width and Linear Velocity on Capture Efficiency. In order to maximize the recovery of CTCs from whole blood, the dimensions and layout architecture of the capture channels and the linear flow velocity in which to operate the HTMSU were assessed. Experimental determinations of CTC capture efficiency using cell selection channel widths of 20, 35, and 50 μm (straight channels) were evaluated as well as a 35 μm wide capture channel adopting a sinusoidal pattern. The results of these studies are depicted in Figure 3.3A as plots of CTC capture efficiency (%) versus linear velocity, U (mm s^{-1}).

The 20 μm wide channel yielded 100% capture efficiency at all flow rates investigated. Because the CTCs were often larger than this channel, the cell membranes were in constant proximity to the antibody-coated microchannel walls. Also, most CTCs when observed via fluorescence microscopy did not enter the capture channel because their size was larger than the channel width. Those cells that were able to enter the selection bed, capture occurred within the first 1-2 mm of the 3.5 cm long channel. Due to these effects, the 20 μm device demonstrated consistent failure resulting from microchannel blockage. At higher linear flow velocities these blockages also led to compromising head pressures that resulted in device failure due to cover plate detachment from the embossed substrate. Therefore, adopting a channel width less than the cell average diameter was deemed inappropriate due to device failure and cell selection partly arising from size exclusion effects, which could lead to selection of a large number of leukocytes potentially complicating the enumeration process.

Inspection of the data in Figure 3.3A for capture channels with widths greater than the average CTC cell diameter showed that the capture efficiency increased with increasing linear velocity for all channel widths and shapes until a critical value was

reached (~2 mm s^{-1}) at which point the capture efficiency decreased. For all capture channel widths and shapes when operated at the same linear velocity, improved capture efficiencies were obtained for narrower channels with the highest efficiency demonstrated for the sinusoidal-shaped 35 μm wide channel (97%).

A

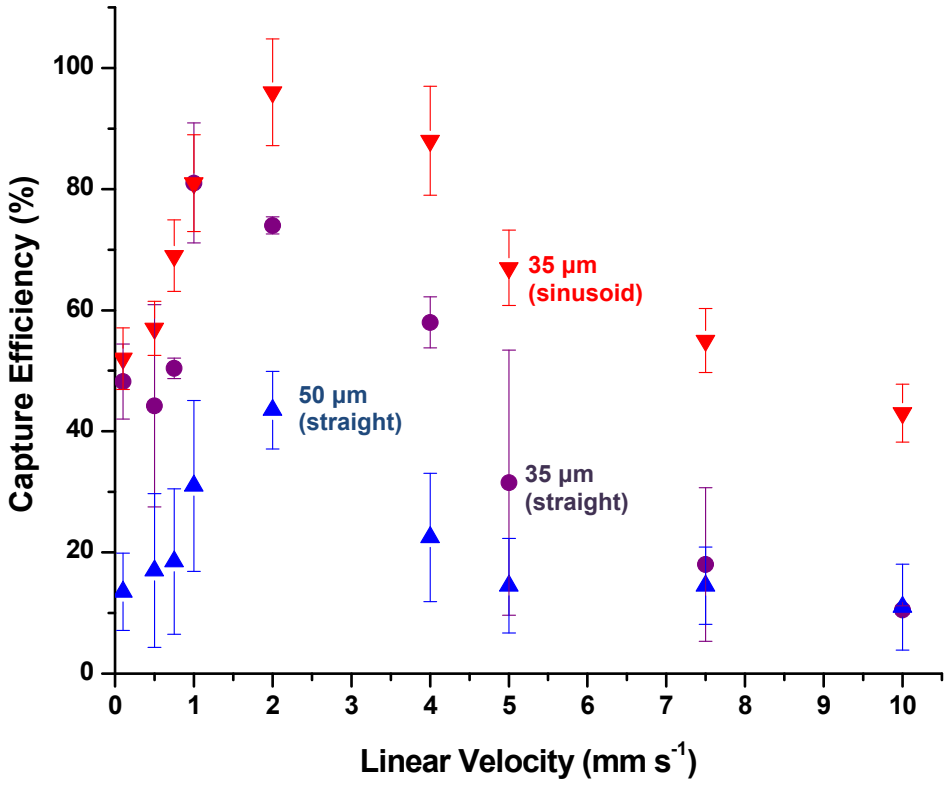

Figure 3.3 Data showing the capture efficiency of CTCs as a function of the cells' translational velocity using 20 (black squares), 35 (red down triangles, sinusoid; purple circles, straight), and 50 μm (blue up triangles) wide microchannels. (A) The microfluidic device consisted of a single channel with the appropriate width and a depth of 150 μm. Following processing of the input buffer containing the MCF-7 cells, the number of captured cells was determined via brightfield microscopy by interrogating the entire length of the capturing channel. (B) The capture efficiency data as a function of the CTC translational velocity was replotted using Equation 4.10 (see Chapter 4) with this data fit to $k_f \times C_\infty \times N_r$ using the fitting parameter, k_{in} (EpCAM:anti-EpCAM forward rate constant). Error bars represent the average 6 % variance in the capture efficiency. (Continued on next page)

B

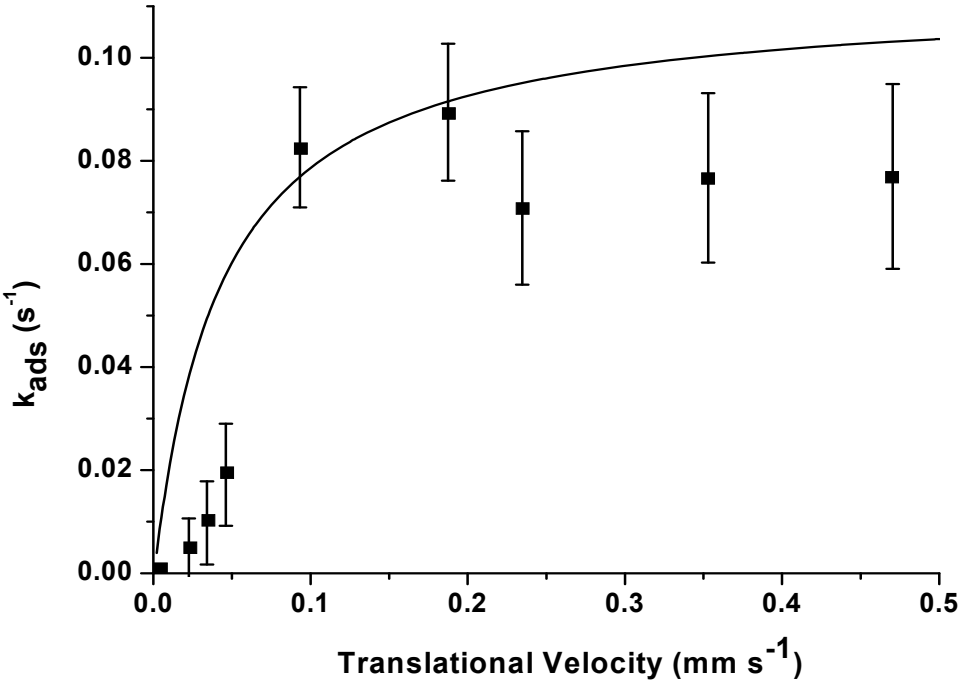

Figure 3.3B See caption above.

This latter observation was consistent with the focusing effects noted for cells moving in a small channel experiencing laminar flow (see Figure 3.2).

To understand the capture efficiency dependence on linear velocity, we evaluated our data according to the Chang and Hammer model for cell adhesion between a surface-tethered antibody and a moving antigen.[41] This model describes a two-state process;

$$A + B \rightleftharpoons A \cdots B \quad (3.1)$$

$$A \cdots B \rightleftharpoons C \quad (3.2)$$

where the first step (Equation 3.1) accounts for transport of the solution antigen to the surface-bound antibody, which describes the encounter rate (k_o), and the second step

(Equation 3.2) gives the probability (P) that an association event will occur during the time the antigen is in close proximity to the tethered antibody. The encounter rate, k_o, increases with increasing linear flow velocity while the probability of a reaction, P, decreases (see Figure 4.2 in Chapter 4). Analytical expressions for k_o and P are provided in Chapter 4 based on the Chang/Hammer model.[41] Below the cell translational velocity of 2 mm s^{-1}, the capture efficiency is determined primarily by k_o, but at U > 2 mm s^{-1}, the capture rate is dominated by P. Plotted in Figure 3.3B is the cell adhesion rate, k_{ads} (see Equation 4.10 in Chapter 4) versus the cells' translational velocity, which shows that k_{ads} asymptotically approaches a limiting value at translational velocities larger than 2 mm s^{-1}. The data plotted in Figure 3.3B were then fit to the velocity-dependent intrinsic adhesion rate constant, k_f, calculated from the product of k_o and P (see Equation 4.7 in the Chapter 4) with one adjustable parameter, k_{in}, which represents the forward rate constant between EpCAM and its anti-EpCAM antibody. Literature values for the MCF-7 cell line and the EpCAM:anti-EpCAM complex were used to calculate P (see Equation 4.9 in Chapter 4 as well as Table 3.1). The best fit was achieved for k_{in} = 1 x 10^7 s^{-1}, which is nearly two orders of magnitude larger than that reported in the literature for the EpCAM:anti-EpCAM forward rate constant (0.99 x 10^5 s^{-1}).[42] This disparity was most likely due to cooperativity effects resulting from the high expression level of EpCAM in this cell line.[43] In addition, the non-deformable nature of cell adhesion assumed in the Chang/Hammer model was not observed in the current experiments (see Figure 4.3 in the Chapter 4).

A device with a single 35 x 150 μm channel operating at the optimal linear flow rate determined above to maximize the capture efficiency would exhaustively process 1 mL of input in 9.5 x 10^5 s (26 h). Simple increases in the linear velocity would not improve

the sampling throughput without sacrificing capture efficiency, so the device was designed to contain multiple capture channels of similar dimensions fanning from a common input. For example, with 51 capture channels, the processing time was reduced to 1.9×10^3 s (31 min). The common output for all of the capture channels allowed for enumeration of cells selected from each channel (190 nL volume) in one step.

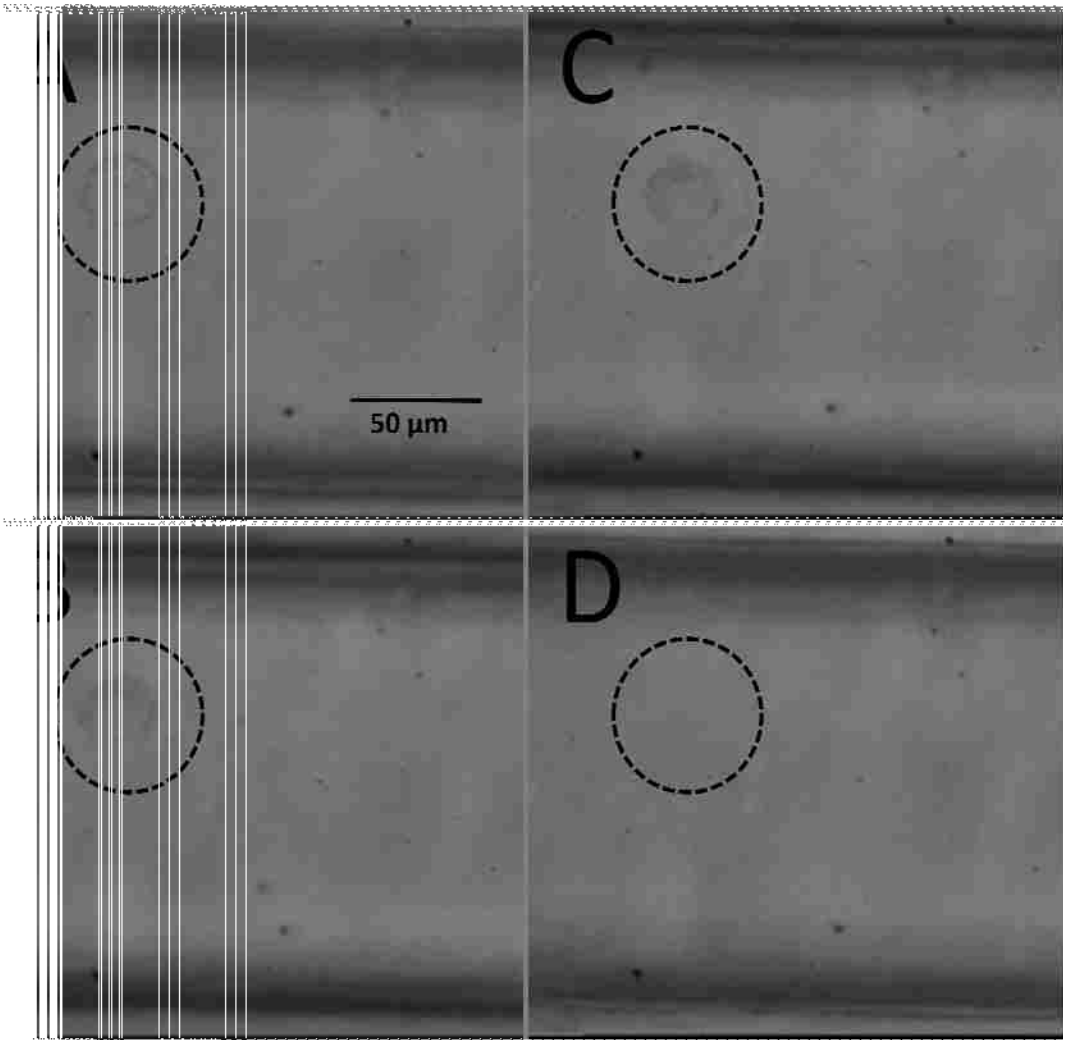

Figure 3.4 Time lapse micrographs of a captured MCF-7 cell: (A) Prior to exposure to the CTC releasing buffer; and (B) exposed to the CTC releasing buffer for ~10 min. (C) The cell appears to be released from the PMMA surface and finally, (D) the cell is swept away when the flow is initiated.

3.3.6 Shear Effects on Captured Cells. It was necessary to evaluate shear forces induced by the fluid traveling through the channels during cell selection and device washing prior to cell counting used to quantitatively enumerate the number of captured cells. Flow-induced shear could either detach the captured cells from the antibody-decorated walls or damage the cell prior to counting.

The total adhesion force (F_A) between the cell and the antibody-decorated PMMA wall was evaluated using the model suggested by Bell.[44] F_A is derived from the product of the contact area, antibody surface density and the adhesion force for a single EpCAM:anti-EpCAM bond, f_c (see Equation 4.12 in Chapter 4). The value determined for f_c was 6.7 × 10^{-6} dynes (see Equation 4.14 in Chapter 4) with a contact area of 16.6 μm^2 for MCF-7 cells assuming the cells upon adhesion to the surface are non-deformable (see Equation 4.13 in Chapter 4). Using these values and an anti-EpCAM antibody PMMA surface density of ~2.3 × 10^{11} cm^{-2} produced a total adhesion force of 0.26 dynes.[45] For cells that are flattened and elongated upon adhesion (see Figure 4.3 in Chapter 4), the contact area was determined to be 456 μm^2 and F_A = 7.0 dynes [46]. When the shear force (F_S) generated by the laminar flow is equal to or greater than F_A, the cell can be removed from the surface. The velocity dependent shear force, F_S, was determined from Stokes' law;

$$F_S = 6\pi\eta r v_c \quad (3.3)$$

where r is the cell radius (12 μm for MCF-7 cells), η is the solution viscosity (4.8 cP for whole blood with a hematocrit level of 0.4) and v_c is the critical linear velocity that can induce cell detachment. Rearrangement of Equation 3.3 produced a value of 2.4 x 10^2 cm s^{-1} for v_c assuming non-deformable contact. Insertion of the contact area and F_A for the flattened and elongated captured cells yielded a value for v_c of 6.4 x 10^3 cm s^{-1}.

Both of these values are significantly greater than the linear velocities used in the present experiments for optimizing the capture efficiency. Several captured cells were observed continuously during experiments in which linear velocities up to 10.0 cm s^{-1} were implemented and no cell damage or disruption of cell:wall adhesion was detected.

3.3.7 Detachment of Intact Cells for Quantitative Enumeration. Due to the strong adhesion force between the captured cells and the antibody-containing capture surface, thermodynamic release from the surface to allow for cell enumeration using the conductivity sensor was deemed in appropriate. The use of the proteolytic enzyme, trypsin, for the release of captured cells without causing cell disassembly, which would complicate single cell counting, was investigated. Figure 3.4 shows time-lapse micrographs of a surface-captured cell that was subjected to trypsin processing. Detachment was facilitated by the proteolytic enzyme in less than a 10 min incubation time. Rigorous evaluation of the trypsin release procedure indicated no cell damage was induced by this process.

3.3.8 Conductivity Sensor for Cell Enumeration. Once the cells were released from the capture surface, they could be swept through the integrated Pt electrodes at the device output. The Pt electrodes were separated by 50 μm producing a cell constant, K (defined as the ratio of electrode gap to the electrode area), of ~0.01 μm^{-1}. The cell constant was scaled to specifically detect CTCs due to their larger size with respect to leukocytes or erythrocytes. As shown in Figure 3.5A, the conductivity sensor with K = 0.01 μm^{-1} did not transduce the presence of leukocytes or erythrocytes due to their smaller size and their characteristic electrical properties. This is particularly attractive, because any non-specific adsorption of leukocytes or erythrocytes during cell selection

will not produce false positive signals providing an additional level of system specificity for the enumeration of CTCs.

A

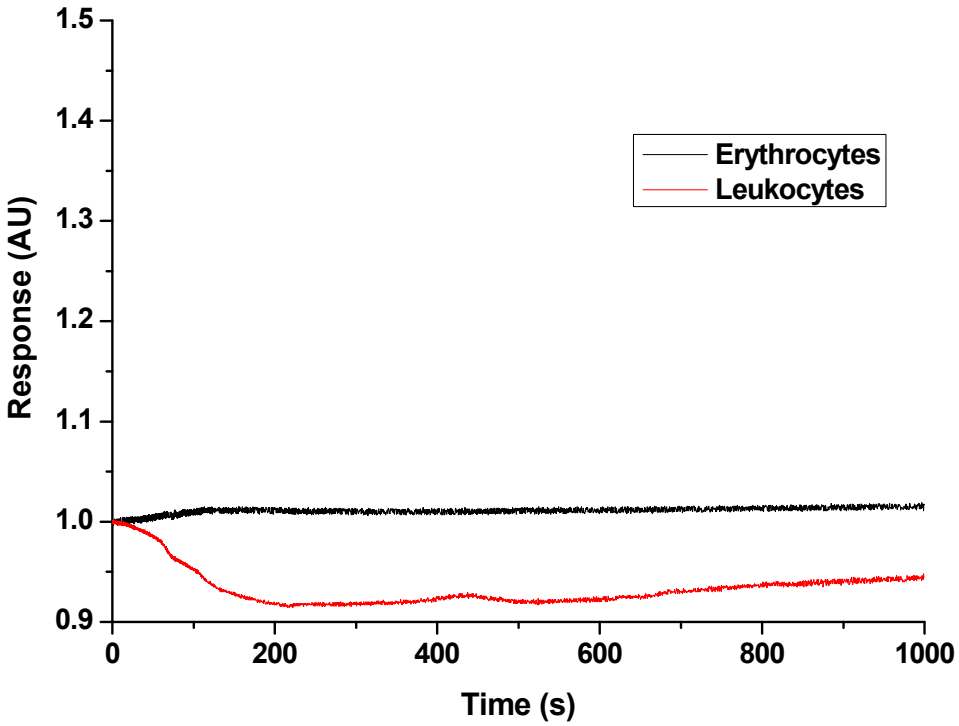

Figure 3.5 Conductance responses (in arbitrary units, AU) and calibration plots for CTCs are shown. (A) Conductometric response for suspensions of leukocytes and erythrocytes (cell density = 150 cells/μL) in TRIS-Glycine buffer transported through the integrated conductivity sensor at a volume flow rate of 0.05 μL/min. (B) Conductometric response of a 1.0 mL aliquot of whole blood spiked with 10 ±1 CTCs and processed in the HTMSU at 2.0 mm/s. The isolated CTCs were released from the PMMA surface using the CTC releasing buffer and transported through the conductivity sensor at a volumetric flow rate of 0.05 μL/min. Peak identification was based on a signal-to-noise threshold of 3:1, which was determined by the peak height of the apparent response and the average peak-to-peak variation in the conductance of the CTC releasing buffer. The arrows designate those peaks scored as CTCs based on the aforementioned criteria. The arrow marked with an "x" possessed a conductivity response lower than the background buffer and as such was not scored as a CTC. (C) Calibration plot for the number of CTCs seeded (10 – 250 cells mL^{-1}) into whole blood versus the conductance responses registered using the conductivity sensor following the processing steps delineated in Figure 3.5B (m=0.945, r^2=0.9988). The data presented in Figure 3.5B was subjected to a 3 point Savitsky-Golay smooth. (Continued on next page)

B

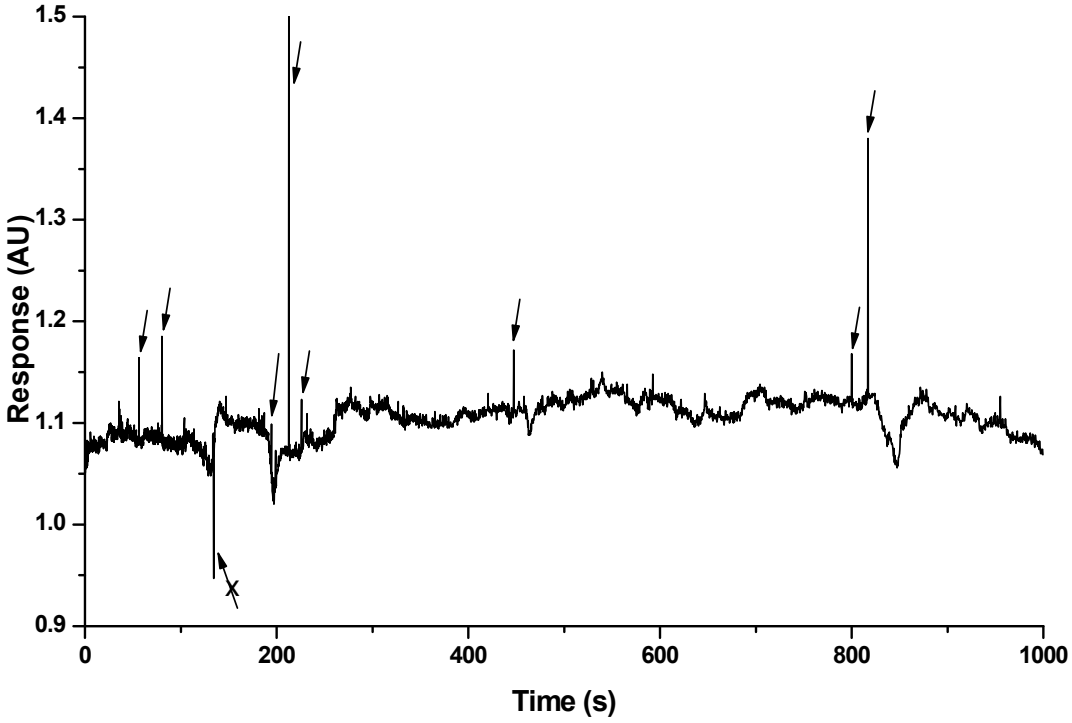

C

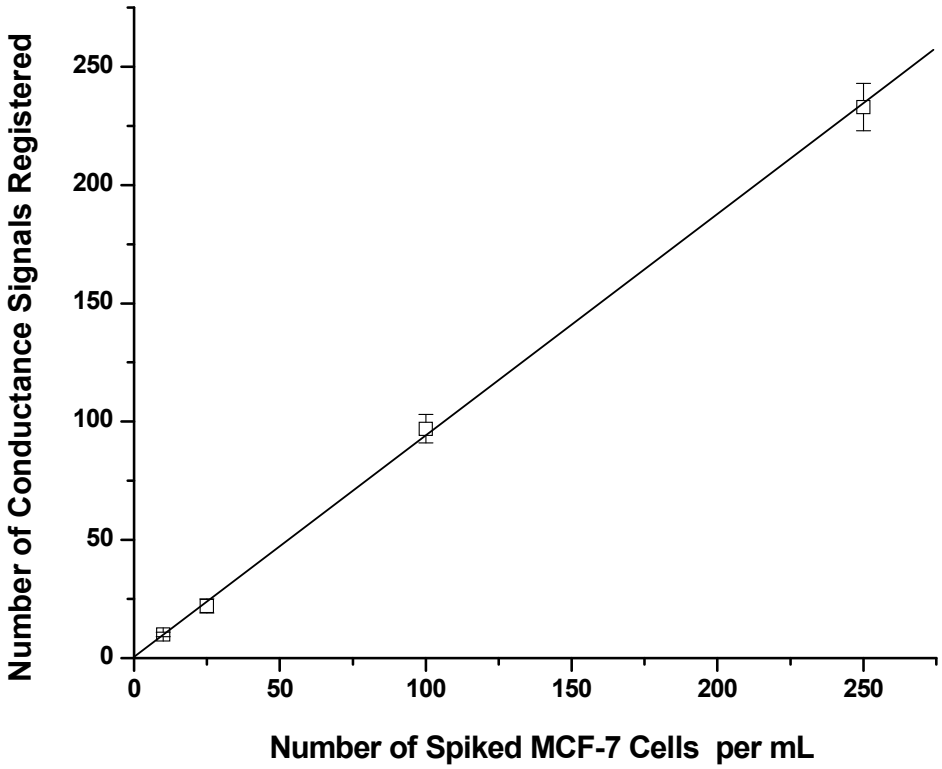

Figure 3.5 (B and C) See caption above.

Following antibody-mediated capture of CTCs seeded into whole blood using the HTMSU, the cells were released from the surface and hydrodynamically driven through the contact conductivity sensor.[32] The chemical composition of CTCs make them ideal candidates for detection using conductivity due to their unique electrical properties compared to erythrocytes or leukocytes. For example, CTCs in general possess very low membrane potential and low impedance resulting from the intracellular migration of sodium ions (Na^+) in compensation for the depleted potassium ion concentration (K^+) of the intracellular fluid. Also, alteration in the cancer cell's membrane content with respect to the types of glycoproteins and antigens they express result in an increase in the number of negatively charged sialic acid molecules that cap the extracellular domains of many integral membrane proteins.[47]

We next analyzed 1 mL of whole blood seeded with 10 ±1 CTCs using the HTMSU, released the enriched cells and quantitatively counted them with the conductivity sensor (see Figure 3.5B). Based on a signal-to-noise threshold of 3 (99.7% confidence level), there were 8 peaks in the conductance trace shown in Figure 3.5B that were assigned to CTCs. As can be seen from Figure 3.5B, only positive conductance spikes were scored as CTCs, while negative spikes were not scored as CTCs. The CTC scoring system was verified through brightfield microscopy, which indicated that CTCs produced positive signals relative to the background conductance generated by the CTC releasing buffer and the negative signals were produced from particulates. In addition, careful microscopic inspection indicated that the positive conductance spikes were indeed due to single cells. The disparity in the peak response for single CTCs was due to differences in cell morphology and composition partly resulting from any one of five mitosis phases of this cell line upon harvest.[48]

For proper enumeration of the recovered CTCs using the HTMSU, the readout phase of the assay required a sampling efficiency near 100% so that every cell released from the capture channels could be detected with sufficient signal-to-noise to be scored as a CTC. To accomplish this and keep the conductivity cell constant (K) at a sufficient level to provide high signal-to-noise for the CTCs, the HTMSU was designed with a multi-level architecture (see Figure 3.1E). The 150 μm deep capture channels were tapered to a depth of ~80 μm at the conductivity sensor to match the Pt electrode diameter to ensure a sampling efficiency near 100%.

To verify the recovery and detection efficiency of the system, the seed number of CTCs in whole blood versus the number of cells enumerated over a broad physiologically-relevant range (10-250 CTCs mL^{-1}) were evaluated (see Figure 3.5C). The best fit line to these data indicated a slope of this calibration curve of 0.945 with an intercept near 0 (r^2 = 0.9988), indicating near 100% recovery and detection of the CTCs seeded into these samples using the HTMSU.

3.4 Conclusions

A novel polymer-based HTMSU was designed, fabricated, and tested for selecting, with high efficiency and specificity, CTCs directly from whole blood using surface-immobilized monoclonal antibodies targeted for membrane proteins unique to this class of cells. Due to the simple and low-cost production of these devices using micro-replication technologies as well as their automated operation with no sample pre-processing required, the HTMSU can be envisioned as an important diagnostic tool for monitoring CTC levels in a variety of adenoma-based cancers for disease detection, cancer staging or evaluating the effectiveness of therapeutic intervention. A compelling attribute of this microfluidic device is the ability to specifically detect the CTCs using an

integrated conductivity sensor. The sensing platform did not respond to potential interferences, which could give rise to false-positive signals, and was simple to implement both operationally (no cell staining as required for fluorescence) and instrumentally (no optical microscope or flow cytometer was required).

The HTMSU was designed to process large input volumes to search for rare events using molecular recognition via integral membrane proteins specific for the target. High throughput processing was realized by using a number of high-aspect ratio microchannels configured in parallel, providing the ability to process 1 mL of input in ~30 min. If the channel depth was increased to 250 – an aspect ratio of 7.14 for 35 μm wide channels – and the number of parallel channels doubled, the sampling time for this same volume input could be reduced to 2.7 min. These changes could provide the ability to select extremely rare events requiring the need for processing larger input volumes (>10 mL).

The HTMSU is flexible in function as well with the ability to change the molecular recognition element to target other rare cells. For example, *E. coli* O157:H7 is a bacterial species typically found in a variety of fresh water bodies with EPA acceptable colony forming unit levels of <20 in waste water and <200 in lakes and rivers per 100 mL. Using monoclonal antibodies specific for this bacterium and scaling the capture channel widths and conductivity sensor appropriate for these cell types, the reported device can be envisioned for field deployment to provide timely results for assisting in bacterial containment.

3.5 References

(1) Leaf, C. *Fortune* **2004**, 76-94.

(2) Paget, S. *Lancet* **1889**, *1*, 571.

(3) Fidler, I. J.; Yano, S.; Zhang, R. D.; Fujimaki, T.; Bucana, C. D. *Lancet Oncology* **2002**, *3*, 53-57.

(4) Loberg, R. D.; Fridman, Y.; Pienta, B. A.; Keller, E. T.; McCauley, L. K.; Taichman, R. S.; Pienta, K. J. *Neoplasia* **2004**, *6*, 302-309.

(5) Braun, S.; Marth, C. *New Engl. J. Med.* **2004**, *351*, 824-6.

(6) Singletary, S. E.; Connolly, J. L. *CA. Cancer J. Clin.* **2006**, *56*, 37-47.

(7) Cristofanilli, M.; Budd, G. T.; Ellis, M. J.; Stopeck, A.; Matera, J.; Miller, M. C.; Reuben, J. M.; Doyle, G. V.; Allard, W. J.; Terstappen, L.; Hayes, D. F. *New Engl. J. Med.* **2004**, *351*, 781-791.

(8) Cristofanilli, M.; Hayes, D. F.; Budd, G. T.; Ellis, M. J.; Stopeck, A.; Reuben, J. M.; Doyle, G. V.; Matera, J.; Allard, W. J.; Miller, M. C.; Fritsche, H. A.; Hortobagyi, G. N.; Terstappen, L. *J. Clin. Oncol.* **2005**, *23*, 1420-1430.

(9) Cristofanilli, M.; Reuben, J. M.; Fritsche, H. A.; Hayes, D. F.; Budd, T. G.; Ellis, M. J.; Stopeck, A.; Miller, C. M.; Matera, J.; Allard, J. W.; Terstappen, L. *Breast Cancer Res. Treat.* **2004**, *88*, S225-S225.

(10) Molnar, B.; Ladanyi, A.; Tanko, L.; Sreter, L.; Tulassay, Z. *Clin. Cancer. Res.* **2001**, *7*, 4080-4085.

(11) Wood, D. P.; Banerjee, M. *J. Clin. Oncol.* **1997**, *15*, 3451-3457.

(12) Uemura, H. *Hinyokika Kiyo.* **1999**, *45*, 571-575.

(13) Soria, J. C.; Morat, L.; Durdux, C.; Housset, M.; Cortez, A.; Blaise, R.; Sabatier, L. *J. Urol.* **2002**, *167*, 352-356.

(14) Kurusu, Y.; Yamashita, Y.; Ogawa, M. *Surgery* **1999**, *126*, 820-826.

(15) Muller, V.; Pantel, K. *Breast Cancer Res. Treat.* **2004**, *6*, 258-61.

(16) Pachmann, K.; Clement, J. H.; Schneider, C.-P.; Willen, B.; Camara, O.; Pachmann, U.; Hoeffken, K. *Clin. Chem. Lab. Med.* **2005**, *43*, 617-627.

(17) Pachmann, K.; Heiss, P.; Demel, U.; Tilz, G. *Clin. Chem. Lab. Med.* **2001**, *39*, 811-817.

(18) Parareda, A.; Gallego, S.; Roma, J.; Llort, A.; Sabado, C.; Gros, L.; De Toledo Josep, S. *Oncol. Rep.* **2005**, *14*, 1021-7.

(19) Chein, R. Y.; Yang, Y. C.; Lin, Y. S. *Electrophoresis* **2006**, *27*, 640-649.

(20) Furdui, V. I.; Harrison, D. J. *Lab Chip* **2004**, *4*, 614-618.

(21) Grodzinski, P.; Yang, J.; Liu, R. H.; Ward, M. D. *Biomed. Microdevices* **2003**, *5*, 303-310.

(22) Balic, M.; Dandachi, N.; Hofmann, G.; Samonigg, H.; Loibner, H.; Obwaller, A.; van der Kooi, A.; Tibbe, A. G. J.; Doyle, G. V.; Terstappen, L.; Bauernhofer, T. *Cytometry Part B-Clinical Cytometry* **2005**, *68B*, 25-30.

(23) Gross, H. J.; Verwer, B.; Houck, D.; Hoffman, R. A.; Recktenwald, D. *Proc. Natl. Acad. Sci. U. S. A.* **1995**, *92*, 537-541.

(24) Vona, G.; Sabile, A.; Louha, M.; Sitruk, V.; Romana, S.; Schutze, K.; Capron, F.; Franco, D.; Pazzagli, M.; Vekemans, M.; Lacour, B.; Brechot, C.; Paterlini-Brechot, P. *Am. J. Pathol.* **2000**, *156*, 57-63.

(25) Yang, J.; Huang, Y.; Wang, X. B.; Becker, F. F.; Gascoyne, P. R. C. *Anal. Chem.* **1999**, *71*, 911-918.

(26) Zabaglo, L.; Ormerod, M. G.; Parton, M.; Ring, A.; Smith, I. E.; Dowsett, M. *Cytometry A* **2003**, *55A*, 102-108.

(27) Ghossein, R. A.; Osman, I.; Bhattacharya, S.; Ferrara, J.; Fazzari, M.; CordonCardo, C.; Scher, H. I. *Diagn. Mol. Pathol.* **1999**, *8*, 59-65.

(28) Nagrath, S.; Sequist, L. V.; Maheswaran, S.; Bell, D. W.; Irimia, D.; Ulkus, L.; Smith, M. R.; Kwak, E. L.; Digumarthy, S.; Muzikansky, A.; Ryan, P.; Balis, U. J.; Tompkins, R. G.; Haber, D. A.; Toner, M. *Nature* **2007**, *450*, 1235-U10.

(29) McCarley, R. L.; Vaidya, B.; Wei, S.; Smith, A. F.; Patel, A. B.; Feng, J.; Murphy, M. C.; Soper, S. A. *J. Am. Chem. Soc.* **2005**, *127*, 842-843.

(30) Hupert, M. L.; Guy, W. J.; Llopis, S. D.; Shadpour, H.; Rani, S.; Nikitopoulos, D. E.; Soper, S. A. *Microfluid. Nanofluid.* **2007**, *3*, 1-11.

(31) Henry, A. C.; Tutt, T. J.; Galloway, M.; Davidson, Y. Y.; McWhorter, C. S.; Soper, S. A.; McCarley, R. L. *Anal. Chem.* **2000**, *72*, 5331-5337.

(32) Galloway, M.; Stryjewski, W.; Henry, A.; Ford, S. M.; Llopis, S.; McCarley, R. L.; Soper, S. A. *Anal. Chem.* **2002**, *74*, 2407-2415.

(33) Ayodele A. Alaiya, B. F. G. A. S. L. *Electrophoresis* **2000**, *21*, 1210-1217.

(34) Crisan, D.; Ruark, D. S.; Decker, D. A.; Drevon, A. M.; Dicarlo, R. G. *Mol. Diagn.* **2000**, *5*, 33-8.

(35) Meng, S.; Tripathy, D.; Shete, S.; Ashfaq, R.; Haley, B.; Perkins, S.; Beitsch, P.; Khan, A.; Euhus, D.; Osborne, C.; Frenkel, E.; Hoover, S.; Leitch, M.; Clifford, E.; Vitetta, E.; Morrison, L.; Herlyn, D.; Terstappen Leon, W. M. M.; Fleming, T.; Fehm, T.; Tucker, T.; Lane, N.; Wang, J.; Uhr, J. *Proc. Natl. Acad. Sci. U. S. A.* **2004**, *101*, 9393-8.

(36) Simon, B.; Podolsky, D. K.; Moldenhauer, G.; Isselbacher, K. J.; Gattonicelli, S.; Brand, S. J. *Proc. Natl. Acad. Sci. U. S. A.* **1990**, *87*, 2755-2759.

(37) Szala, S.; Froehlich, M.; Scollon, M.; Kasai, Y.; Steplewski, Z.; Koprowski, H.; Linnenbach, A. J. *Proc. Natl. Acad. Sci. U. S. A.* **1990**, *87*, 3542-3546.

(38) Rao, C. G.; Chianese, D.; Doyle, G. V.; Miller, M. C.; Russell, T.; Sanders, R. A.; Terstappen, L. W. M. M. *Int. J. Oncol.* **2005**, *27*, 49-57.

(39) Fung, Y. C. *Biomechanics: Mechanical Properties of Living Tissues*; Springer-Verlag: New York, 1993.

(40) Zheng, J. J.; Yeung, E. S. *Anal. Chem.* **2002**, *74*, 4536-4547.

(41) Chang, K. C.; Hammer, D. A. *Biophys. J.* **1999**, *76*, 1280-1292.

(42) Willuda, J.; Honegger, A.; Waibel, R.; Schubiger, P. A.; Stahel, R.; Zangemeister-Wittke, U.; Pluckthun, A. *Cancer Res.* **1999**, *59*, 5758-5767.

(43) Guthrie, J. W.; Hamula, C. L. A.; Zhang, H. Q.; Le, X. C. *Methods* **2006**, *38*, 324-330.

(44) Bell, G. I. *Science* **1978**, *200*, 618-627.

(45) Wei, S.; Soper, S. A.; McCarley, R. L. *Analyst* **2008**, *(submitted for publication)*.

(46) Feng, J.; Soper, S. A.; McCarley, R. L.; Murphy, M. C. In *Lasers in Surgery XIV* Proceedings of the SPIE: San Jose, CA, 2004; Vol. 5312, p 278-293.

(47) Hakomori, S. *Immun. Allergy Clin. N. Amer.* **1990**, *10*, 781-802.

(48) Sherr, C. J. *Science* **1996**, *274*, 1672-1677.

Chapter 4 Theory, Models, and Expansion of Highly Efficient Circulating Tumor Cell Isolation from Whole Blood and Label-free Enumeration Using Polymer-Based Microfluidics with an Integrated Conductivity Sensor*

4.1 Conductivity Detection Electronics

To measure conductance changes in the CTC releasing buffer of the HTMSU induced by single CTCs, a specially-designed circuit was developed (see Figure 4.1). To reduce the effects of parasitic capacitance, $C_{p,}$ due to wiring and the electrode configuration, a synthetic inductor, L, of 132 mH was designed using a gyrator circuit. Gyrators, for a given bandwidth, allow the creation of high Q inductors from RC components. This inductance was placed in parallel with C_p and the sine frequency varied to locate the resonance peak of the voltage across L and C_p. Once this resonance point was found, the voltage across the sample cell was directly sensitive to changes in G_s (solution conductance). A target frequency of 40 kHz was chosen to minimize the impedance due to C_d (double layer capacitance) and hold the inductance to a reasonable value. This signal was fed to a transconductance amplifier, $G_{1,}$ which converted the voltage sinusoid into a current. The gain of G_1 was 10 μA/volt. A current source was needed to drive the sample cell because a voltage source, with its low output impedance, would reduce the circuit's Q. The current was set to ±5 μA for the experiments. The required resonance frequency (*f*) could be approximated by the standard parallel resonance equation;

$$f = {}^{1}/_{2\pi}\,(LC_p)^{1/2} \quad (4.1)$$

The voltage across the sample cell was fed to an Analog Devices AD630 synchronous modulator/demodulator (Norwood, MA) that was configured as a phase sensitive detector. The reference input of the AD630 was driven from a phase-delayed sine wave

*Reprinted with permission from JACS.

oscillator output. This phase adjustment was needed to compensate for phase lags in the detected sample voltage. The sample voltage was fed to a low pass filter with a cutoff frequency of 180 Hz. The filter produced an average dc signal that was sent to a differencing amplifier, A_1. The difference amplifier served to null the output to zero volts while measuring G_S. A high gain amplifier, A_2, could amplify small changes in G_S without saturating the voltage produced by the releasing buffer itself. A National Instruments PCI6071E, 12 bit A/D acquisition card (Austin, TX) was used to convert the analog signal to a 12 bit digital signal.

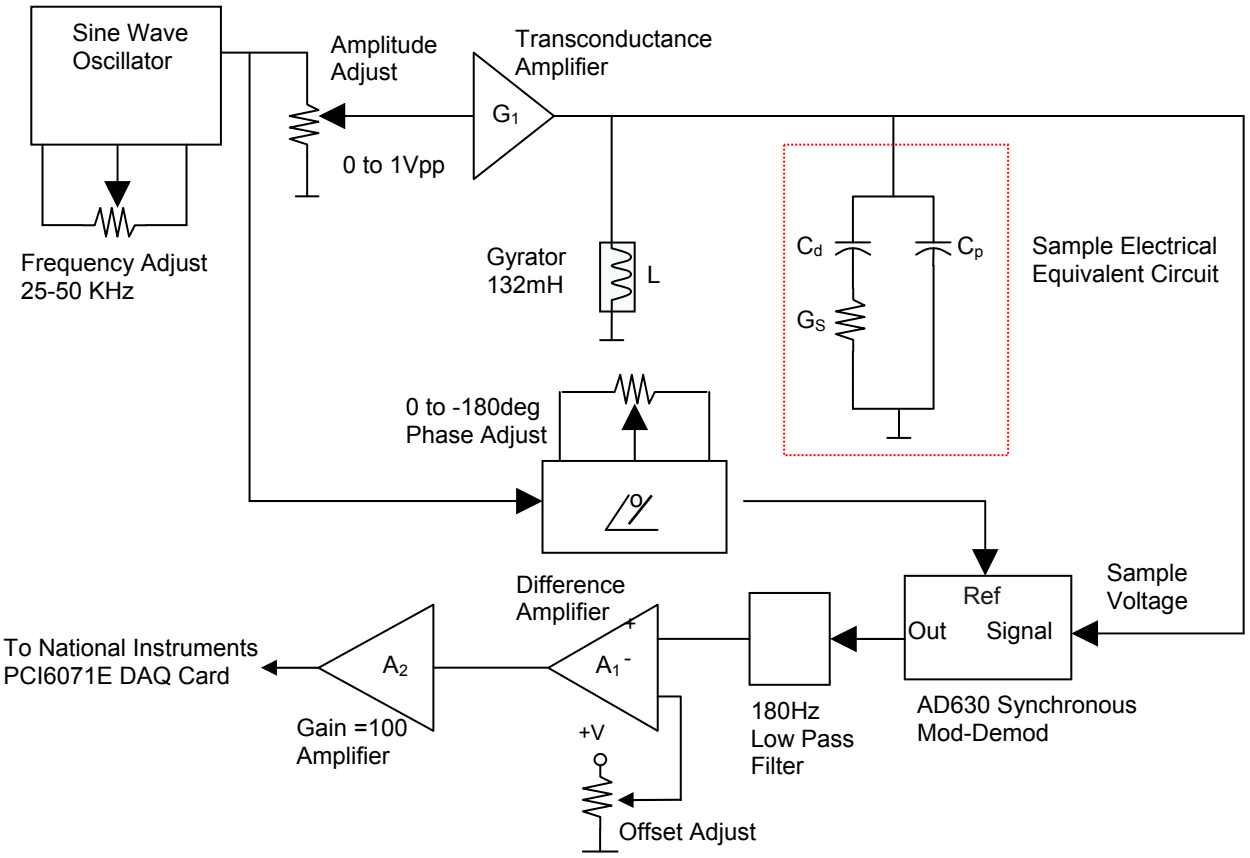

Figure 4.1 Circuit diagram for the conductivity sensor.

4.2 Pressure Drop in a Microchannel with Blood Flow

The volume flow of blood (Q) in an enclosed microchannel can be calculated from a modified version of Poiseuille flow using Equation 3.A2:

$$Q = \frac{\pi d^4}{128\eta} \cdot \frac{dP}{dX} \cdot F(\varepsilon) \quad (4.2)$$

The hydraulic diameter of the microchannel (*d*) is given as $d = 4(A/(2(ht + w)))$, where *A* is the channel cross-sectional area and *ht* and *w* represent the channel height and width, respectively, η is the solution viscosity, dP/dX is the pressure drop (see below) and $F(\varepsilon)$ is calculated from;

$$F(\varepsilon) = 1 - \frac{16}{7}\varepsilon^{1/2} + \frac{4}{3}\varepsilon - \frac{1}{21}\varepsilon^4 \quad (4.3)$$

The term $F(\varepsilon)$ accounts for the viscosity-dependent hematocrit level of whole blood with ε determined from Equation 3.A4;

$$\varepsilon = \frac{4\tau_y}{D} \cdot \left(-\frac{dP}{dX}\right)^{-1} \quad (4.4)$$

where τ_y is the yield stress and is related to the blood hematocrit level (*H*) using;

$$\tau_y = -0.1 \cdot (0.625H)^3 \quad (4.5)$$

From Equation 4.2, the pressure drop (ΔP) in a channel of length *L* can be calculated from;

$$\Delta P = \frac{128\eta L}{\pi d^4 F(\varepsilon)} Q \quad (4.6)$$

4.3 Modeling Cell Capture Data as a Function of the Cell Translational Velocity (U)

To explain the experimental data in terms of capture efficiency versus the linear flow rate, the data for the 35 μm wide sinusoidally-shaped channels was modeled by adopting the 2-state model developed by Chang and Hammer, with the assumption that

transport was dominated by convection (*i.e.*, Pe >> 1, where Pe is the Peclet number and represents the ratio of convective to diffusive mass transport).[1] In this model, the rate of capture of cells at a surface containing immobilized recognition elements depends on the encounter rate and the reaction time. The rate of capture per ligand/receptor pair (k_f, s^{-1}) can be calculated with Equation 3.A7;

$$k_f = k_o P \quad (4.7)$$

where k_o is the encounter rate and describes the rate of transport of cells to the wall where the antibodies are immobilized and *P* is the probability of a reaction occurring between the cell ligand (*i.e.,* EpCAM) and surface receptor. For *Pe* >> 1, as in the current experiments, k_f is primarily reaction limited and is calculated using Equation 4.8;

$$k_f = \pi D Nu P \quad (4.8)$$

where *D* is the cell diffusion coefficient and *Nu* is the Nusselt number, which describes the flux of antigens to immobilized antibodies and can be approximated from $2Pe/\pi$ for *Pe* >> 1. *P* is estimated from Equation 4.9;

$$P = {\Lambda\delta}/{(1 + \Lambda\delta)} \quad (4.9)$$

where δ is the dimensionless Damköhler number ($a^2 k_{in}/D$; k_{in} = intrinsic EpCAM:anti-EpCAM reaction rate; *a* is the encounter radius) and Λ is the dimensionless encounter time and is calculated from $\tau/(a^2/D)$, where $\tau = 8a/(3U\pi)$. A plot of k_o, *P*, and k_f versus the cell slip velocity, where the slip velocity is ~0.47*U*, are depicted in Figure 4.2.

The experimental data (% of input cells bound to the channel wall) can be used to calculate the rate of adsorption, k_{ads}, from;

$$k_{ads} = \frac{-U}{L} \ln [1 - \%bound] \quad (4.10)$$

where *L* is the length of the capture channel and *U* is the translational velocity of the cells within the fluidic channel. Finally, k_{ads} is related to k_f through the relationship;

$$k_f = {}^{k_{ads}}/_{C_\infty N_r} \quad (4.11)$$

where C_∞ is the cell surface antigen density and N_r is the number of antibodies in the encounter area ($2\pi a^2$). Therefore, a plot of U versus k_{ads}, which is obtained from the experimental data, can be fit to Equation 4.8 with one adjustable parameter, k_{in}, that is used for the estimation of *P*.

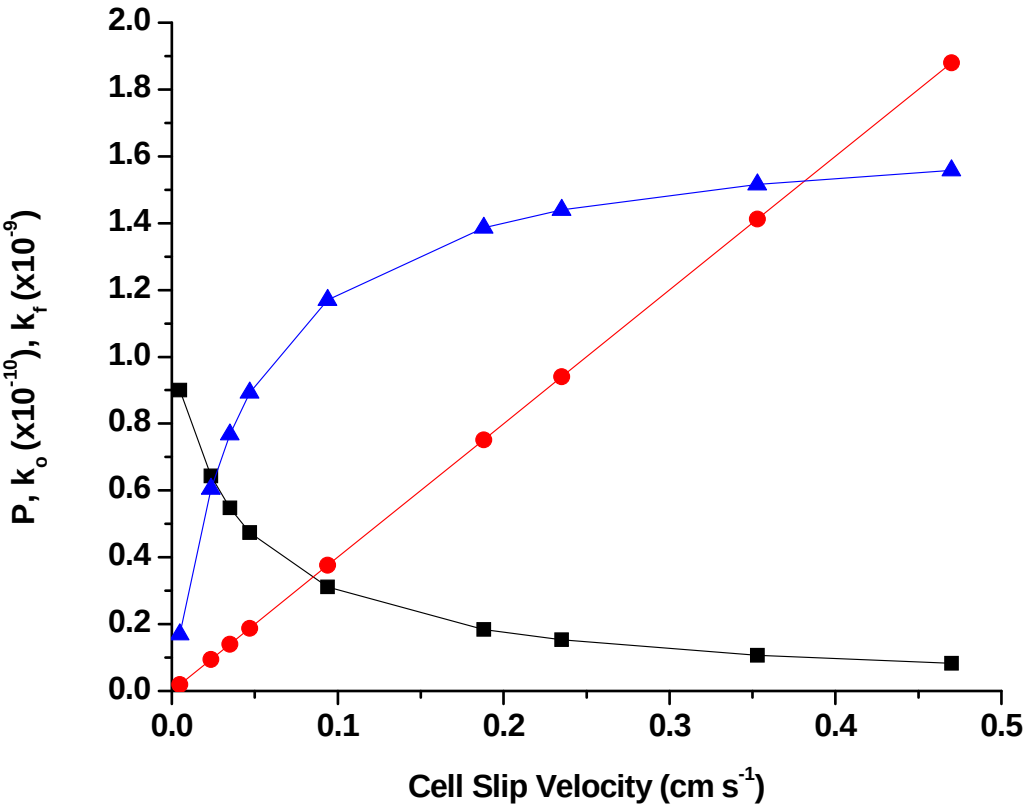

Figure 4.2 Plot of *P* (black rectangles), k_o (red circles) and k_f (blue triangles) as a function of the input cell slip velocity into a fluidic channel of dimensions 35 µm x 150 µm.

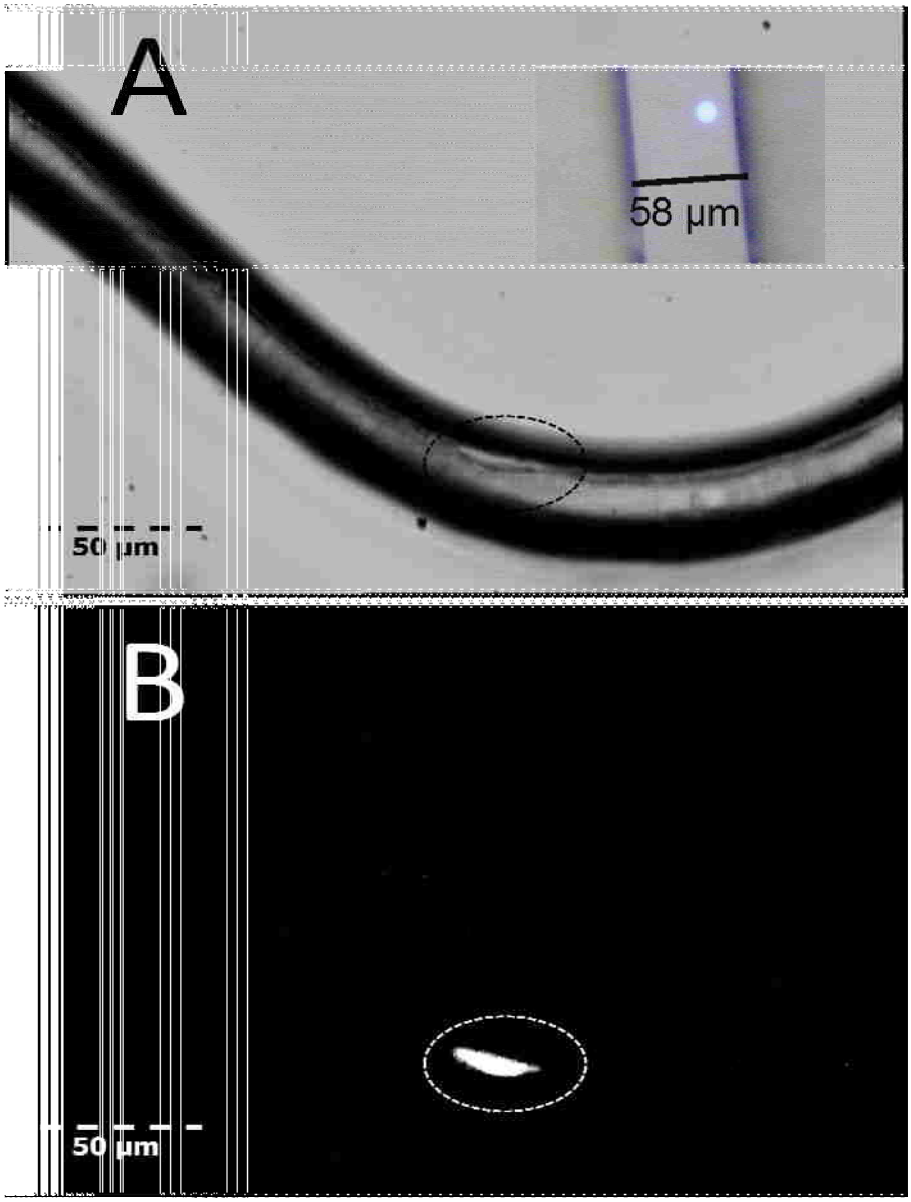

Figure 4.3 Brightfield and fluorescence micrographs showing monoclonal antibody captured CTCs in a PMMA microchannel. (A) Brightfield micrographs taken at 40× magnification and (B) the corresponding fluorescence micrographs verifying the captured cell is the fluorescently labeled CTC. The inset shown in Panel (A) is a fluorescently-stained MCF-7 cell in a PMMA channel that was not decorated with anti-EpCAM antibodies indicating the spherical shape of these cells.

4.4 Adhesion Strength of EpCAM:Anti-EpCAM Antibody Complex on a Surface

The adhesion force (F_A) between the cell and the antibody-decorated surface can be determined from the bond strength between a single antigen:antibody complex (f_c), the

cell contact area with the PMMA surface (A_c) and the number of receptors poised on the PMMA surface within the contact area of the cell (C_s) from:

$$F_A = f_c \times A_c \times C_s \quad (4.12)$$

If the cell is assumed to be a non-deformable object upon adhesion to the capture surface, the contact area can be calculated using Equation 4.13;[2]

$$A_c = \pi r^2 \sin\left(cos^{-1}\left(r - h' + {}^{h}/_{r}\right)\right) \quad (4.13)$$

where *r* is the cell radius and *h* and *h'* represent the characteristic cell separation distances from the surface upon binding. Using *h* and *h'* as 100 Å and 400 Å, respectively,[3] the calculated contact area was determined to be 16.6 μm^2 for the MCF-7 cells. If the cell is assumed to flatten and elongate after contact, as observed experimentally (see Figure 4.3), the resulting contact area A_c is 456 μm^2.[4]

The single EpCAM:anti-EpCAM antibody adhesion force was estimated using the formalism by Bell,[5] who developed the following expression for deriving the critical force required to break a single bond (Equation 4.14);

$$f_c = {}^{kT}/_{r_o}\,\alpha_c \quad (4.14)$$

where *k* is Boltzman's constant, *T* is the absolute temperature, r_o is the separation distance between receptors at the minimum breaking force and $\alpha_c = KC_s$ (K = EpCAM:anti-EpCAM equilibrium constant). Using values from Table 3.1 and T = 298K, a value of 6.7 x 10^{-6} dynes was calculated for f_c. The same result was found using Dembo's binding affinity model.[4,6,7]

Table 4.1 Literature values for the complex between EpCAM and its monoclonal antibody.

Parameter	Description	Value	Reference
a	Encounter radius	5 nm	[1]
k_{in}	Forward rate constant for EpCAM - anti-EpCAM binding	0.99 x 10^5 s^{-1}	[8]
r	MCF-7 average cell radius	12 μm	[9]
H	Blood hematocrit level	0.4	[10]
L	Cell selection bed length	35 mm	
d	Microchannel hydraulic number	56 μm	[11]
D	MCF-7 cell diffusion coefficient	10^{-10} cm^2 s^{-1}	[12]
η	Viscosity of blood (H = 0.4)	4.8 cP	[10]
C_∞	Cell surface density of EpCAM - calculated from the average surface area of MCF-7 cells and the expression level of EpCAM	282 μm^{-2}	[13]
N	Expression level of EpCAM in MCF-7 cells	5.1 x 10^5	[13]
K	EpCAM:anti-EpCAM equilibrium constant	3.3 x 10^8 M^{-1}	[8]
r_o	Separation distance between receptors at min. breaking force	0.5 nm	[1]
N_L	Substratum anti-EpCAM density on UV-modified PMMA	2.3 x 10^{11} cm^{-2}	[14]

4.5 References

(1) Chang, K. C.; Hammer, D. A. *Biophys. J.* **1999**, *76*, 1280-1292.

(2) Cozens-Robert, C.; Quinn, J. A.; Lauffenburer, D. A. *Biophys. J.* **1990**, *58*, 107-125.

(3) Clausen, J. *Immunochemical techniques for the identification and estimation of macromolecules, In Laboratory Techniques in Biochemistry and Molecular Biology*, 1981; Vol. 1.

(4) Feng, J.; Soper, S. A.; McCarley, R. L.; Murphy, M. C. In *Lasers in Surgery XIV* Proceedings of the SPIE: San Jose, CA, 2004; Vol. 5312, p 278-293.

(5) Bell, G. I. *Science* **1978**, *200*, 618-627.

(6) Dembo, M.; Torney, D. C.; Saxman, K.; Hammer, D. *Proceedings of the Royal Society of London Series B-Biological Sciences* **1988**, *234*, 55-83.

(7) Kuo, S. C.; Lauffenburger, D. A. *Biophys. J.* **1993**, *65*, 2191-2200.

(8) Willuda, J.; Honegger, A.; Waibel, R.; Schubiger, P. A.; Stahel, R.; Zangemeister-Wittke, U.; Pluckthun, A. *Cancer Res.* **1999**, *59*, 5758-5767.

(9) Depasquale, J. A.; Samsonoff, W. A.; Gierthy, J. F. *J. Cell Sci.* **1994**, *107*, 1241-1254.

(10) Kameneva, M. V.; Watach, M. J.; Borovetz, H. S. *Clin. Hemorheol. Microcirc.* **1999**, *21*, 357-363.

(11) Chein, R. Y.; Yang, Y. C.; Lin, Y. S. *Electrophoresis* **2006**, *27*, 640-649.

(12) Dieterich, P.; Klages, R.; Preuss, R.; Schwab, A. *Proc. Natl. Acad. Sci. U. S. A.* **2008**, *105*, 459-63.

(13) Rao, C. G.; Chianese, D.; Doyle, G. V.; Miller, M. C.; Russell, T.; Sanders, R. A.; Terstappen, L. W. M. M. *Int. J. Oncol.* **2005**, *27*, 49-57.

(14) McCarley, R. L.; Vaidya, B.; Wei, S.; Smith, A. F.; Patel, A. B.; Feng, J.; Murphy, M. C.; Soper, S. A. *J. Am. Chem. Soc.* **2005**, *127*, 842-843.

Chapter 5 Highly Specific Selection, Isolation, and Enumeration of *Escherichia coli* from Various Water Sources

5.1 Introduction

Escherichia coli (E. coli) are potentially enterohemorrhagic bacteria living in the lower intestines of many mammals, and are typically known as gut flora. Their primary function, when located in the intestines, is assisting in waste processing, vitamin K production and food absorption. There are several hundred strains of *E. coli*; strains like *E. coli* O157:H7 produce powerful "shiga-like" toxins (stx_1, stx_2) responsible for severe illnesses including but not limited to bloody diarrhea, colitis, or even death in animals and humans.[1] *E. coli* O157:H7 also harbors a 43 kb pathogenicity island, termed the locus of enterocyte effacement, which contains virulent attributes required for forming lesions on hosts. Hemolytic-uremic syndrome (HUS) and seizures are presented in infantile cases resulting from exposure of these pathogens to children.[2] Physically, *E. coli* is a rod-shaped bacterial cell with a length of 2 µm and a width of approximately 0.8 µm. In many cases, *E. coli* infiltrate various fresh water bodies by being carried via runoff to tributaries and/or aquifers.[3] These virulent bacteria are typically transmitted via the fecal-oral pathway by ingesting contaminated water or food-stuffs.[4]

The food industry is particularly concerned with cross-contamination due to the proximity of many domestic farm animals to various vegetative food crops in rural areas. The turn-around time for laboratory tests often exceeds 2 wk.[5] Thus, it has become increasingly necessary to screen for these bacteria earlier in the food production cycle in order to reduce the numerous potential health-related issues associated with widespread outbreaks. To decrease the impact, implementation of testing at the earliest possible point of intervention is required. Minimization of the scope of the impact from

such contaminations is inextricably linked to developing portable, sensitive, isolation and enumeration technologies that can be effectively applied by novice end-users.

A common strategy employed for determining the presence of *E. coli* is the ISO 9308-1 method in which water samples are membrane filtrated followed by the growth of the isolated cells using lactose 2,3,5-triphenyltetrazoliumchloride (TTC) agar with Tergitol 7.[6] Coliforms reduce TTC producing a yellow-orange color indicative of rod-shaped bacteria that ferment lactose to produce gas and acid within 48 h at 35°C.[7] However, the major difficulties associated with this methodology are the time required to produce readable results, and the ability for a broad cross-section of users to correctly interpret the results. In addition, other organisms present in the water can elicit a positive response (false positive for *E. coli*) and some *E. coli* strains do not ferment lactose (false negatives).[8] A recent comparison of different growth media for culturing *E. coli* and various coliforms was presented.[9] The results of the comparison study indicated that m-ColiBlu24 and Colilert 18 chromogenic media provided faster and more reliable results compared to the ISO standard media, but still required 22 h and 18 h, respectively, to obtain reliable results compared to 72 h for the ISO 9308-1 method.

A recent report highlighted the ability of a molecular biological assay, BAX, to detect and enumerate the presence of *E. coli* O157:H7 bacteria.[10] In this assay, the capabilities of real time polymerase chain reaction (RT-PCR) are used to specifically test for strain-specific species using molecular markers unique to the strain. The authors reported the ability to detect 10 CFUs in a processing time of 8 h, where CFU is defined as “colony forming unit,” which is the number of viable bacteria. However, the process required pre-concentration of samples containing low abundances of *E. coli* by filtering the water sample using 0.45 μm cellulose ester filters followed by elution of the retained

material. Then, the eluted volume was subjected to immunomagnetic selection using anti-*E. coli* O157:H7 antibodies coated onto magnetic beads. Unfortunately, these multiple processing steps made implementation of this assay for field deployment prohibitive due to the extensive hardware requirements and the required operator expertise. Though these virulent bacteria, impose imminent danger upon consumption there exists no U.S. Food and Drug Administration mandate on maximum levels in any food source.[11] The total bacterial level at which action is taken by the FDA is currently set at 104 CFU g^{-1} of sample (see Table 5.1).

Recreational waters including fisheries, boating, and swimming areas as well as drinking water supplies have in recent years become breeding grounds for potentially virulent bacteria.[1] The US EPA allowable levels of *E. coli* are shown in Table 5.1. Specifically, elevated levels of pathogenic bacteria such as *E. coli* O157:H7 can be correlated to the increased occurrence of most water-related sicknesses, deaths, and/or the development of harmful algal bloom formations.[12] These waterborne pathogens are assessed by first filtering large (100 mL) aliquots of water using porous membrane-based filter paper that can also support the subsequent adherent cell culturing and microscopic inspection of the bacteria such that a determination can be made as to viability and toxicity. Upon harvesting and culturing the bacteria, morphological examinations as well as pathogen specific immunoaffinity is often used.

There are a variety of emerging technologies for isolating cells from heterogeneous samples with selection based on immunoaffinity or distinct reporter molecules that are unique to the targets. The most promising developments include fluorescence assisted cell sorters,[1] flow through filtrations,[13,14] enzyme linked immunosorbent assays (ELISA),[15,16] and immunomagnetic cell sorting.[17-19] The commonality between these

methods is the extensive use of prefiltration and arduous culturing protocols needed to produce detectable levels of the bacteria. The most rapid of these assays can take up to 8 h. In addition, the required equipment and sample preparation phases of these assays make them difficult to implement for wide-scale usage, especially in field-deployable applications.

Table 5.1 Source and acceptable levels of *E. coli*

Source	**Acceptable *E. coli* level, CFU/100 mL**
Drinking[20]	0
Wastewater[20]	20
Lake/River[20]	200(A) 1000(C)*
Meat/Produce[21]	104**

*(A)=Advisory **(C)=Closure. **Represents CFU g^{-1} which is the FDA action level.

In order to successfully analyze rare bacterial strains in complex samples, new approaches are required. The ideal system would provide high specificity for selection of the species/strain/source specific bacteria directly from waters or other complex sample matrices from a variety of sources and also enumerate the number of colony forming units (CFU) over a large dynamic range. The system should be simple to operate and packaged into a compact unit that will permit field deployment. The following characteristics should be associated with the device; (i) high throughput sampling of mL volumes in <10 min of processing time concentrating the bacterial cells to nL volumes; (ii) functionally compatible with immobilization strategies used to fix capture elements to the capture bed; and (iii) amenable to small sensors with high sampling efficiency for automated cell counting strategies. In any case, the volume sampled is typically dictated by the frequency of the events to be assessed. For bacteria the US EPA recommends aqueous sample sizes of 100 mL[20] and the US FDA recommends solid samples sizes of 25 g.[4]

Traditional microfluidic device architectures are encumbered by inherently low throughput; however, when parallelization of features is employed, as in the design delineated herein, it is possible to exhaustively interrogate large samples for rare biological cells in short periods of time (see Fig. 5.1). In this manuscript, we present preliminary results on the use of a novel technology directed toward the unambiguous identification of microbial water supply contaminates using microfluidic devices that enable selective cell isolation and subsequent enumeration using an integrated conductivity sensor.

Figure 5.1 AutoCAD 2008 rendering of a microfluidic device that can provide high throughput miscro-sampling (HTMSU). The device used a series of microchannels that were decorated with antibodies specific for the target cell. The antibodies were immobilized beneath the gray shaded region, which consisted of 37 straight microchannels that were uniformly 3 cm long and 30 µm wide. The entire device was 150 µm deep. The output end contained a conductivity sensor that consisted of a pair of Pt wires placed orthogonal to the fluid flow path.

5.2 Materials and Methods

5.2.1 High-Throughput Microsampling Unit Fabrication. The substrate selected for the high throughput micro-sampling unit (HTMSU) was poly(methyl methacrylate), PMMA, due to its high fidelity for forming structures with high-aspect ratios via micro-replication, minimal non-specific adsorption of *E. coli* cells to its surface and its ability to generate functional surface-scaffolds through UV irradiation for the attachment of a

variety of biological moieties.[22] A molding tool was made via high precison micromilling and the molding tool used to emboss microstructures into PMMA. Embossed PMMA substrates and PMMA cover slips were cleaned with reagent grade isopropyl alcohol (Sigma-Aldrich, St. Louis, MO), rinsed with nanopure H_2O (Model D8991, BarnStead/Thermolyne, Dubuque, IA), sonicated with a model 8890 sonicator (Cole Parmer, Vernon Hills, IL) for 15 min, rinsed with IPA again, and air dried. Then, ultraviolet (UV) modification of the PMMA substrates and cover slips was performed through an aluminum mask to facilitate the formation of carboxylic functional groups on the PMMA surface for antibody immobilization. Both substrates and cover slips were irradiated at 254 nm with 15 mW cm^{-2} for 10 min from the UV source (500W DUV; Model UXM-501 MA; Ushio America, Cypress, CA). After UV modification, the glass transition temperature (T_g) of the substrate was changed from 106 °C to 101°C.[23] The microdevice and cover slips were aligned and clamped between two glass plates and fixed using clips (ACCO Brands, Inc., Lincolnshire, IL). The UV modified areas of the device and cover slips were mated using alignment marks. The clamped unit was then inserted into a programmable oven (Varian 3400, Palo Alto, CA) and the temperature raised from 50°C to 101°C at a rate of 20°C/min with the final temperature held for 15 min. The total annealing time for each HTMSU was 17.6 min. A 15 cm long (inlet) and a 2 cm long (outlet), 237µm O.D. and 100 µm I.D. polyimide coated fused silica capillary (Polymicro Technologies, Ave Phoenix, AZ) was epoxied between the substrate and cover slip on the inlet and outlet sides of the HTMSU, respectively. An AutoCAD rendering of the device is shown in Figure 5.1.

5.2.2 Antibody Immobilization. The HTMSUs were loaded with 4 mg mL^{-1} of 1-ethyl-3-[3-dimethylaminopropyl] carbodiimide hydrochloride (EDC) and 6 mg mL^{-1} of N-

hydroxysuccinimide (NHS) in 150 mM 2-(4-morpholino)-ethane sulfonic acid (MES) (Sigma-Aldrich, St. Louis, MO) at pH 6 for 1 h at room temperature to obtain the succinimidyl ester intermediate of the carboxylated surface. The EDC/NHS solution was removed by rinsing the fluidic network with nanopure H_2O. Then, an aliquot of 1.0 mg mL^{-1} of affinity purified polyclonal anti-*E. coli* O157:H7 antibody (K-log, Inc., Gaithersburg, MD) solution in 150 mM PBS (pH=7.4) (Sigma-Aldrich, St. Louis, MO) was introduced into the HTMSU and allowed to react for 4 h.

5.2.3 Cell Suspension. *E. coli* O157:H7 cells were purchased from K-log, Inc., Gaithersburg, MD. The *E. coli* cells were stained with FITC using a lipophilic membrane linker (PKH67, Sigma-Aldrich, St. Louis, MO). The cell density of the original *E. coli* O157:H7 sample was 3 x 10^9 cells mL^{-1}. Serial dilutions were performed to obtain the desired cell density for each experiment.

5.2.4 Cell Capture Protocol. The HTMSUs were fixed onto the programmable motorized stage of an Axiovert 200M (Carl Zeiss, Thornwood, NY) microscope and videos were captured during each experiment at 30 frames per second (fps) using a monochrome CCD camera (JAI CV252, San Jose, CA). A Xe arc lamp was used to excite the fluorescent dyes incorporated into the cell membrane. A syringe pump was used in an infuse mode to inject cell suspensions and buffers into the HTMSU. The HTMSU was interfaced to a syringe pump (Model PHD2000, Harvard Apparatus, Holliston, MA) using a syringe (Becton, Dickinson, and Company, Franklin Lakes, NJ) and luer-to-CE adapter (InnovaQuartz, Phoenix, AZ). Pre-capture rinses were performed with 0.2 mL of 150 mM PBS at 20 µL/min flow rates (270 mm s^{-1}) to maintain isotonic conditions. Then, 0.1 mL of a 10 cells μL^{-1} cell suspension was introduced at 2.0 mm s^{-1} linear velocity. Next, a post capture rinse was performed with 0.2 mL of 150

mM PBS at 100 mm s^{-1} to remove non-specifically adsorbed cells on the HTMSU surface. Finally, the numbers of cells captured by the antibody immobilized microchannels were counted using brightfield and fluorescence microscopy for confirmation of cell capture to the channel walls. Each experiment was performed in triplicate for each linear velocity studied.

5.3 Results and Discussion

Microdevices with 30 µm wide channels that were 150 µm deep and 3 cm long were used to assess the capture efficiency of the antibody-immobilized microfluidic device for cylindrically-shaped *E. coli* cells (0.8 µm dia. × 2.0 µm long) from 10 µL suspensions with densities of 100 *E. coli* cells μL^{-1}. In order to determine if the antibody was covalently tethered to the microchannel walls, fluorescently labeled antibodies were used. In Figure 5.2, the fluorescence intensity from a microchannel with no labeled secondary antibody, a microchannel loaded with 500 µg mL^{-1} anti-*E. coli* O157:H7 secondary antibody (K-log, Inc., Gaithersburg, MD), and a rinsed microchannel with secondary antibody are shown. From these images, it was found that a buffer rinse following antibody immobilization resulted in an increase in the average fluorescence above background, strongly indicating the presence of tethered antibodies.

Experiments were next conducted in which *E. coli* strain K12 was used as a negative control. Due to genomic differences, strain K12 lacks the capacity to express the antigen targeted by the anti-*E. coli* O157:H7 antibody. As expected no *E. coli* K12 cells were isolated using this microfluidic device with O157:H7 antibodies (see Figure 5.3). In addition, the lack of K12 cells adsorbed to the channel wall provided evidence of a lack of non-specific adsorption of these cells to the channel wall.

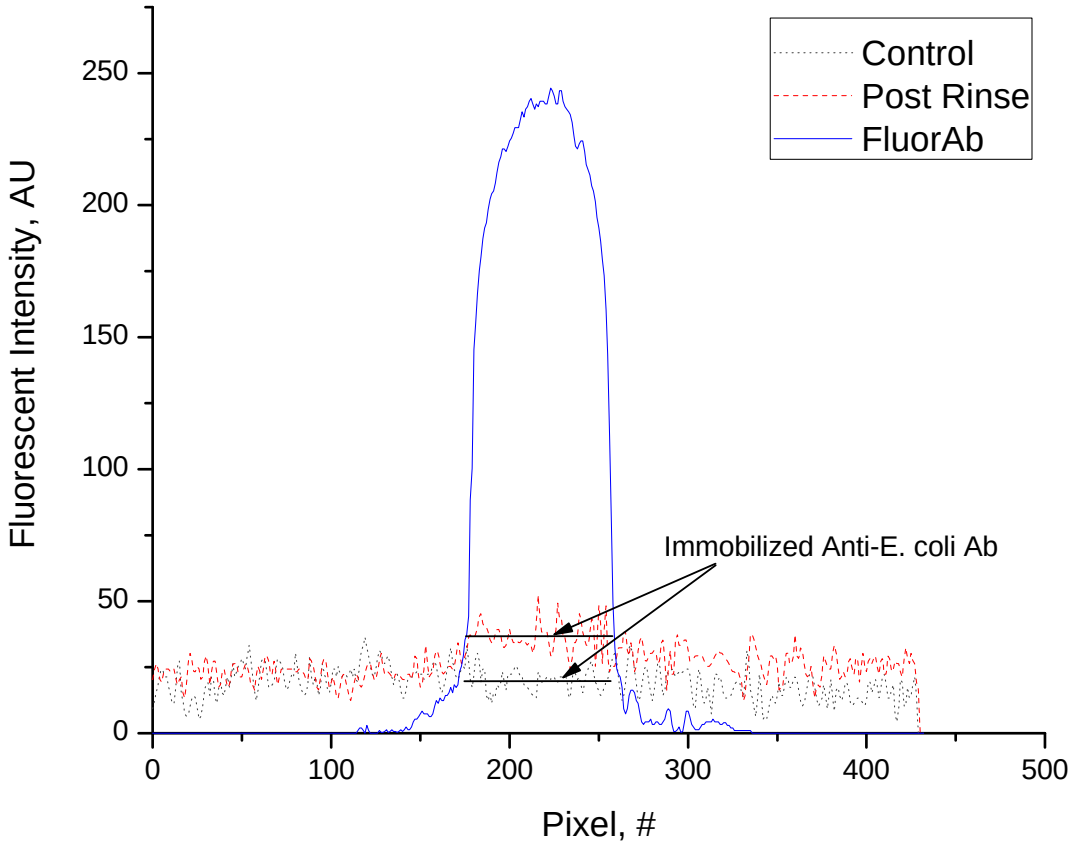

Figure 5.2 Fluorescence image of a 20 µm wide microchannel decorated with surface-immobilized antibodies that were covalently labeled with a fluorophore. The control trace, illustrated by a black dotted line, shows the PMMA microchannel in the absence of the fluorescently-labeled antibody. The solid blue line represents the fully loaded channel after it was infused with a solution containing 500 µg mL^{-1} of FITC labeled anti-*E. coli* antibody in the presence of EDC/NHS. The red dashed trace shows an increase in the fluorescence intensity corresponding to the immobilized antibody immobilized. The two solid black lines represent the average fluorescence intensity before and after the immobilization process.

Finally, the target O157:H7 cells were processed through the antibody immobilized HTMSU. Fluorescently-labeled O157:H7 cells were selectively isolated from suspensions at a 2.0 mm s^{-1} linear velocity. After processing 10 µL of the sample, the captured cells were enumerated via fluorescence microscopy. The capture efficiencies in three successive experiments was found to be 5.3%, 6.1%, and 8.7%. The low capture efficiency can be attributed to the relatively wide linear microchannels used here with respect to the width of these cells. The diameter of the *E. coli* cells was 0.8

μm and the channel width used was >20× that of the targets. We have previously shown, that by designing the capture microchannel width to dimensions similar to that of the target cells can increase the capture efficiency by as much as 10-fold.[24]

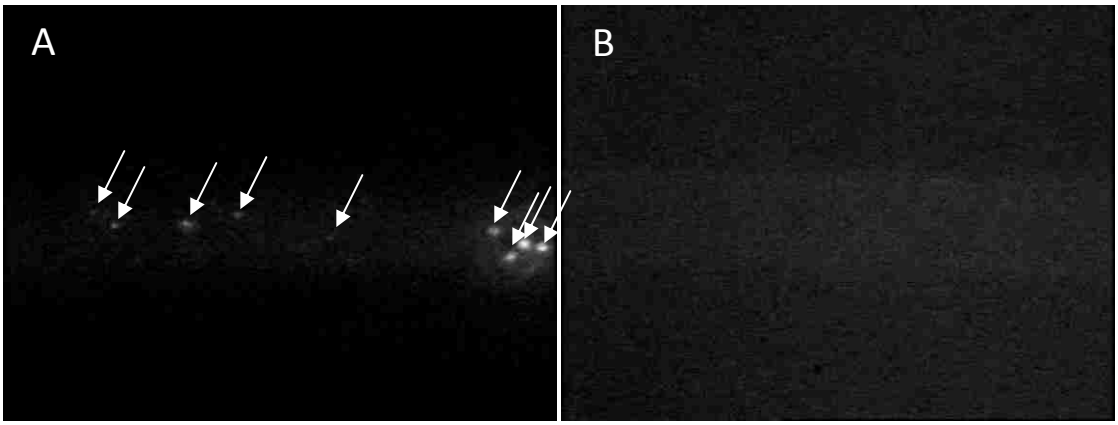

Figure 5.3 A) The micrograph shows 9 captured *E. coli* O157:H7 cells indicated by arrows. The cells were isolated from a suspension with cell density of 100 *E. coli* cells/μL using an antibody immobilized microdevice. B) The panel shows that no *E. coli* strain K12 cells were isolated when a suspension of equal density of the innocuous strain was analyzed.

In addition, previous experiments indicated that linear microchannels are not ideal for capturing cells, because the cell trajectories are parallel to the microchannel walls with cell focusing resulting from hydrodynamic effects resulting in low numbers of "cell-wall" interactions producing fewer capture events. Incorporating curvilinear microchannels can further increase the recovery due in large part to the inertia of the cells, imparted by centripetal forces resulting from traversing the curved region of the microchannels.

5.4 Conclusion

A new approach toward the isolation of low abundant *E. coli* cells has been presented in which the number of cells in mL-scaled samples can be ascertained without the need for long incubation periods and bacterial culturing procedures that

result in analysis times exceeding 48 hrs. The *E. coli* O157:H7 cells were specifically indentified and immobilized using immunoaffinity. Further investigations are warranted for the capture and enumeration of *E. coli* cells to increase the capture efficiency and provide the ability to sample larger volumes in minimal processing times. Micromilling has proven effective in producing devices with multilevel structures for circulating tumor cell isolation and enumeration,[24] yet as evidenced by the low capture efficiencies presented here, this fabrication technique is not suitable for producing architecture appropriate for *E. coli* isolation. The maximum capture efficiencies in the devices presented herein are limited due to the minimum channel widths (~20 μm) that micromilling is commensurate with producing. Future efforts should focus on engineering microdevice designs specifically for *E. coli*. To improve upon capture efficiency, it would be suggested to produce devices with a maximum width of 2 μm and depth of 40 μm corresponding to a minimum aspect ratio of 20, an aspect ratio that can be used to replicate parts in polymers using embossing. Using these parameters, x-ray lithography is ideally suited for production of moulding tools containing these narrow and deep channels required for effective *E. coli* isolation. In addition, to increase throughput thereby reducing analysis time the number of parallel processing channels should be increased. For example, the use of 2,000 parallel channels would allow for a volume flow rate of 19.2 μL min^{-1} maintaining a linear velocity of 2 mm s^{-1} to maximize capture efficiency through the selection channels of the device and producing a 1 mL processing time of 52 min. If the aspect ratio of this device were doubled while maintaining the channel width, the throughput would also double thereby reducing the processing time to 26 min per analysis.

5.5 References

(1) McClain, M. A.; Culbertson, C. T.; Jacobson, S. C.; Ramsey, J. M. *Anal. Chem.* **2001**, *73*, 5334-5338.

(2) Ibekwe, A. M.; Watt, P. M.; Grieve, C. M.; Sharma, V. K.; Lyons, S. R. *Appl. Environ. Microbiol.* **2002**, *68*, 4853-4862.

(3) Reschiglian, P.; Zattoni, A.; Roda, B.; Casolari, S.; Moon, M. H.; Lee, J.; Jung, J.; Rodmalm, K.; Cenacchi, G. *Anal. Chem.* **2002**, *74*, 4895-4904.

(4) Weimer, B. C.; Walsh, M. K.; Beer, C.; Koka, R.; Wang, X. *Appl. Environ. Microbiol.* **2001**, *67*, 1300-1307.

(5) Bennett, A. R., MacPhee, S., Betts, R. P., *Lett. Appl. Microbiol.* **1996**, *22*, 237-243.

(6) Bernasconi, C.; Volponi, G.; Bonadonna, L. *Water Sci. Technol.* **2006**, *54*, 141-145.

(7) Breed, R. S.; Norton, J. F. *American Journal of Public Health* **1937**, *27*, 560-563.

(8) Leclerc, H.; Mossel, D. A.; Edberg, S. C.; Struijk, C. B. *Annual Review Microbiology* **2001**, *55*, 201-234.

(9) Bernasconi, C.; Fermi, V. E. *Water Science and Technology* **2006**, *54*, 141-145.

(10) Bukhari, Z.; Weihe, J.; LeChevalier, M. *Water Science and Technology* **2004**, *50*, 233-237.

(11) Tu, S.-I.; Golden, M.; Paoli, G.; Gore, M.; Gehring, A. *J. Rapid Methods Automat. Micro.* **2004**, *12*, 247-258.

(12) Niemi, R. M.; Heikkila, M. P.; Lahti, K.; Kalso, S.; Niemela, S. I. *J. Appl. Microbiol.* **2001**, *90*, 850-858.

(13) Abdel-Hamid, I.; Ivnitski, D.; Atanasov, P.; Wilkins, E. *Biosensors Bioelectron.* **1999**, *14*, 309-316.

(14) Brewster, J. D.; Mazenko, R. S. *J. Immunol. Methods* **1998**, *211*, 1-8.

(15) Chapman, P. A.; Malo, A. T. C.; Siddons, C. A.; Harkin, M. *Appl. Environ. Microbiol.* **1997**, *63*, 2549-2553.

(16) Johnson, R. P.; Durham, R. J.; Johnson, S. T.; Macdonald, L. A.; Jeffrey, S. R.; Butman, B. T. *Appl. Environ. Microbiol.* **1995**, *61*, 386-388.

(17) DeCory, T. R.; Durst, R. A.; Zimmerman, S. J.; Garringer, L. A.; Paluca, G.; DeCory, H. H.; Montagna, R. A. *Appl. Environ. Microbiol.* **2005**, *71*, 1856-1864.

(18) Furdui, V. I.; Harrison, D. J. *Lab Chip* **2004**, *4*, 614-618.

(19) Karch, H.; JanetzkiMittmann, C.; Aleksic, S.; Datz, M. *J. Clin. Microbiol.* **1996**, *34*, 516-519.

(20) USEPA, 2002, Implementation Guidance for Ambient Water Quality Criteria for Bacteria; EPA-823-B-02-003

(21) Grant, M. A.; Wernberg, J. S.; Van, K. T.; Albert, A. M. *J. AOAC Int.* **2006**, *89*, 1317-1326.

(22) McCarley, R. L.; Vaidya, B.; Wei, S.; Smith, A. F.; Patel, A. B.; Feng, J.; Murphy, M. C.; Soper, S. A. *J. Am. Chem. Soc.* **2005**, *127*, 842-843.

(23) Witek, M. A.; Wei, S. Y.; Vaidya, B.; Adams, A. A.; Zhu, L.; Stryjewski, W.; McCarley, R. L.; Soper, S. A. *Lab Chip* **2004**, *4*, 464-472.

(24) Adams, A. A., Okagbare, P. I. and Soper, S. A. *J. Am. Chem. Soc.* **2008**, *(in press)*.

Chapter 6 Future Work: Continued Biosensor Research at United States Naval Research Laboratory, Washington D.C.

6.1 Introduction

Explosives pose major security and environmental risk in this era of immanent domestic terroristic activity.[1] In addition, the existence of explosive nitroaromatics such as TNT at various military sites and munitions testing grounds throughout the United States require environmental monitoring of residual unexploded ordnance as well as the degradation products of detonated nitroaromatics in groundwater and soil.[2] Finally, forensic investigations, as they pertain to domestic terroristic activities, also dictate that field deployable assessment tools be readily available for untrained field technicians to employ in order to rapidly determine the safety of emergency medical personnel and other first responders.[2]

Off-site chemical analysis has been performed using traditional instrumentation including high performance liquid chromatography,[3] gas chromatography coupled to mass spectrometers,[4] surface enhanced Raman spectroscopy,[5] cyclic voltammetry,[6] and energy dispersive x-ray diffraction[7] in the analysis of various explosives. These methods have successfully delivered high sensitivity and selectivity for the analytes yet these methods offer limited portability which detracts from their potential for being field deployable. Size notwithstanding, these instruments further require the significant expertise to employ. Microarray biosensors that involve the displacement of analogues have been employed in the field with promising results, but the traditional mass transport limitations in conventional microarrays and microfluidics inhibit the ability to reliably detect sub-pg/mL amounts of the analytes from bulk solution reliably.[1] To date, the most prolific field deployable detection system has been the extensively trained canine, but unfortunately, these animals are expensive, require continuous

maintenance, and are subject to fatigue. Further, the canine's strong sense of smell is rendered ineffective when the analyte or target is submerged in groundwater.[2]

The nature of explosives and concern for the safety of the analyst or sample collector suggest the need for sensing these dangerous and potentially toxic (≥ 2 ng/mL) environmental contaminants remotely.[8] This is especially important in the cases where the analytes consist of plumes of unexploded ordnance that has the potential for accidental detonation. Therefore, sensors for explosive nitroaromatic compounds that offer new approaches to the rapid, highly sensitive and selective remote detection of trace levels of various explosives are warranted. Proposed herein is a novel approach with application of high aspect ratio microstructures designed to meet three primary requirements: 1) reduction of false positive and false negative responses in complex matrices, 2) rapid analysis time, and 3) capable of sampling large volumes.

6.2 Materials and Methods

6.2.1 Apparatus and Protocol. Three peristaltic pumps (Lee Company, Westbrook, CT) connected to high aspect ratio microfluidics via fused silica capillaries will be employed to hydrodynamically infuse/effuse samples, regenerate fluorescent surface, and wash the antibody coated device. The custom pumps are designed expressly to be incorporated into field deployable portable devices employing microfluidics as indicated by the design incorporating a small rugged outer casing, low power consumption, capability of delivering as low as 0.1 µL per step, and five hundred total steps for all chamber volumes. The pumps have 0.25 ms response times and can be configured with chambers that range from 10 µL – 1.25 mL. The pumps also allow solution pass through, when the pumps metering piston is in the full open position, to vent or send processed components to waste vessels. Each pump has a vent system designated V1,

V2, and V3 that corresponds to each pumps designation P1 through P3. Two of these pumps (P1 and P2) will be connected to the inlet side of a Y oriented interface designed to accommodate two feeding capillaries with P1 dedicated to delivering the fluorescently labeled analogues, surface regeneration, that adsorb to the antibody immobilized surfaces aiding the establishment of a baseline fluorescence signal from which displaced fluorescence corresponds to bound target.[1] P2 on the inlet side of the device will be used to sample the ambient environment of the system on command in conjunction with P3 which is connected to the effluent side of the microsampling unit. With P2 in the open position P3 will be actuated instituting uptake of the sample. In order to interface the pumps to the high throughput microsampling unit (HTMSU), a PEEK-to-capillary (Hamilton, Reno, NV) adapter kit will be fitted with a luer-to-capillary adapter (InnovaQuartz, Phoenix, AZ). The pumping system will be designed to generate the appropriate volume flow rate to quantitate TNT over a broad linear dynamic range of relevant (subpicomolar – nanomolar)) TNT plume concentrations. The capture efficiency on an antigen flowing over a bed of immobilized antibodies has been shown to be dependent of the flow rate and the length of column used.[9-11] Also critical is the size of the capture bed. In earlier experiments, the amount of antibody bound to a fixed surface increased with increases in capture bed size. Also observed in these experiments was a decrease in the %RSD of measurements in which more analyte was obtained and quantitated implying improvement in measurement precision can be achieved when isolating more analyte.[9,10]

The high throughput microsampling unit (HTMSU) will be fixed to the stage of an inverted microscope initially, allowing for monitoring the release and/or adsorption of the chromophores to the HTMSU using fluorescence imaging via a high sensitivity CCD

with excitation via Xe arc lamp and dye-specific filter sets appropriate for the chosen chromophores. Ultimately, linear dynamic range and limits of detection will be determined using laser induced fluorescence measurements, reported literature values of existing displacement based sensors are 3 orders of magnitude and 1.0 pg/mL, respectively.

In order to reduce the potential for false negatives and positives a multifaceted detection system would be incorporated. First, the analytes would be selected using a displacement immunoassay where antibodies directed toward the nitroaromatics would be covalently tethered to the surface of the microfluidic platforms forming stable capture beds used to selectively isolate the targets while confining these analytes to low nanoliter volumes effectively preconcentrating the analyte. The displacement process is shown in equations below in which the antibody (Ab) is bound to the fluorescently labeled antigen (Ag^*). The binding affinity of the target has a binding affinity that is typically two orders of magnitude greater than that of the analogue thus in the presence of the target the antigen (Ag) displaces the analogue producing the means of signal transduction.

$$\mathrm{Ab} + \mathrm{Ag}^* \rightleftharpoons \mathrm{AbAg}^*$$

$$\mathrm{AbAg}^* + \mathrm{Ag} \rightleftharpoons \mathrm{AbAg} + \mathrm{Ag}^*$$

A CCD would be employed in the displacement based assay to monitor the loss of fluorescence over time. Correlating the displaced fluorescently labeled analogues direct proportionality to the bound analyte thereby allowing for calibration based quantitation with broad linear dynamic range is possible in the displacement assay owing to binding more of the analyte at lower concentrations. In the displacement format, two forms of

quantification will be employed thereby providing both sensitivity and selectivity whereby the elimination of false readings can be reduced or eliminated.

Incorporation of high throughput microfluidic systems as the analysis platform offers high surface area to volume ratios which in turn allows for processing large sample sizes in short time periods. In conventional microfluidics sample injection volumes in the picoliter range are typical allowing for only a small amount of analyte to be processed resulting in lower overall signal to noise than could be realized were the sample size increased to the milliliter range and exhaustively interrogated prior to sensing. This mass sensitive approach to analyzing nitroaromatics would be analogous to “purge and trap” techniques employed by US EPA methods that involve chromatographic analyses of volatile organics. Using anti-TNT antibodies with high binding affinity to select and isolate more target from larger sample sizes provides the potential of unparalleled sensitivity especially when coupled to conductance based detection systems similar to those reported to achieve attomolar sensitivities of proteins on microfluidic platforms.[12] Ultimately, these analyses will take place submerged thus requiring a closed system capable of being isolated from an aqueous environment. The HTMSUs are closed systems that are not prone to leakage and when integrated are capable of withstanding significant outside pressure.[13,14]

6.2.2 High Throughput Microsampling Unit. Microfabricated devices featuring high aspect ratio microstructures offer unparalleled throughput within high surface area to volume ratio conduits. This is particularly attractive when exhaustively interrogating large samples with low analyte concentrations for the purpose of quantitation is desired. The proposed microfluidic will incorporate multiple microfluidic channels to reduce the pressure drop across the device while allowing for high volume throughput over short

time periods. The advantage realized from this type of assay will be manifested in the preconcentration of many analyte molecules from approximately 1 mL samples as opposed to that of traditional microfluidics. For example, traditional microfluidics typically offers picoliter sample volumes, which when considering a sample that has nanomolar analyte concentrations reliable quantitation becomes increasingly prohibitive due to each picoliter only containing only a miniscule 602 molecules. Increasing the sampling efficiency allows for a dramatic increase in the number of analytes molecules available to for transduction at the detector thereby easing the restrictions on applicable detection strategies.

The proposed device will consist of a series parallel high-aspect ratio channels sharing common input/output ports. The devices will be replicated from a mold masters using hot embossing as described in detail elsewhere.[15] Briefly, the substrate selected for the HTMSU is PMMA due to its high fidelity of forming structures with high-aspect ratios via micro-replication, minimal non-specific adsorption of biological components to its surface and its ability to generate functional surface-scaffolds through UV irradiation for the attachment of a variety of biological moieties.[13,16] Initially, microstructures will be milled onto the surface of a brass plate with a high-precision micromilling machine (KERN MMP 2522, KERN Micro- und Feinwerktechnik GmbH & Co.KG; Germany) following our previously published procedures.[15]

Using this technique three identical HTMSUs can be patterned onto the brass master enabling production of the polymeric units in triplicate during each hot embossing step. In order to accommodate the Pt electrodes used for the conductivity sensor and the inlet/outlet capillaries, the HTMSU was designed with multilevel features.[15] As an example of flexibility, in our previous work, the depth of features on an

analogous microfluidic's detection zone was tapered to 80 μm from the 150 μm used in the cell selection beds and throughout the inlet region. The detection channel width was tapered from 100 μm to 50 μm over a 2.5 mm region beginning at the converged outlet and terminating 2.5 mm from the conductivity electrodes scaled for specific detection of CTCs. In the cell selection bed, channel widths (35 μm) that closely matched the average target cell diameter were used to increase the probability of cell-immobilized antibody encounters. In the proposed selection of TNT, initial experiments will be performed in 25 – 75 μm wide channels that are 150 μm deep to evaluate the effect of aspect ratio on the isolation and quantitation of TNT. To reduce the pressure drops when the device was operated at high volumetric flow rates, the HTMSU was designed with deep (150 μm), high-aspect ratio channels. For quantitation a conductivity detector was used. The sensitivity is governed by the cell constant (K) which is defined as L/A where L is the separation distance between the electrodes and A is the total surface area of the electrodes. The total conductance (G) is defined as:

$$G= \frac{(\lambda_+ +\lambda_-)C}{1000K}$$

where C is concentration of the analyte, λ_+ and λ_- are limiting ionic conductance for the cations and anions, respectively. By establishing a baseline conductance for the run buffer the magnitude of perturbations of the baseline conductance in a given assay can be directly related to analyte concentration in the effluent.

6.2.3 Surface Modification. Regio-specific ultraviolet (UV) modification of the PMMA substrate and cover plate is performed through an aluminum photomask to facilitate the formation of the carboxylated scaffold for directed antibody tethering exclusively within the cell selection beds of the HTMSU. Before final assembly via thermal fusion bonding, the PMMA cover plate and substrate will be irradiated at 254 nm with 15 mW cm^{-2}

fluence for 10 min using a UV exposure station (ABM, Inc., San Jose, CA). Additionally, into the inlet/outlet ports of the device were inserted 237 μm OD and 150 μm ID polyimide-coated fused silica capillaries and the Pt electrodes fabricated with the required gap. After thermally annealing the cover plate to the substrate, a thin film of epoxy resin will be applied to the capillary-device interfaces to prevent leaks.

Following UV modification of PMMA, the physicochemical properties of the surface are effectively altered resulting in a moderate reduction of the glass transition temperature (T_g) at the cover plate-substrate interface. The resulting T_g allowed for efficient thermal fusion bonding at 101°C rather than the 106°C T_g of pristine PMMA,[12,17] which reduces potential thermal deformation of the high-aspect ratio microfeatures. Thermal fusion bonding will be performed using a temperature programmable ovensuc as that contained in gas chromatograph (Varian 3400, Palo Alto, CA) using the PMMA cover plate and the open-faced, hot embossed PMMA substrate. The substrate and cover plate will be aligned and clamped together between two borosilicate glass plates and the assembly placed into the temperature programmable oven of the GC, where the temperature will be increased from 50°C to 101°C at a rate of 20°C/min. The temperature was held at 101°C for 15 min.

6.2.4 Antibody Immobilization. Covalent antibody immobilization will be performed using a two step process. Initially, the UV-modified HTMSU device, following thermal assembly, will be loaded with a solution containing 4.0 mg/mL of 1-ethyl-3-[3-dimethylaminopropyl] carbodiimide hydrochloride (EDC), 6.0 mg/mL of N-hydroxysuccinimide (NHS) in 150 mM 2-(4-morpholino)-ethane sulfonic acid at pH = 6 (MES, Fisher Biotech, Fair Lawn, NJ) and buffered saline (Sigma-Aldrich, St. Louis, MO) for 1.0 hr to form the succinimidyl ester intermediate. The EDC/NHS solution will

then be hydrodynamically replaced with a 1.0 mg/mL anti-TNT antibody (Biological Detection Systems, Pittsburg, PA) solution contained in 150 mM PBS at pH = 7.4 (Sigma-Aldrich, St Louis, MO) and allowed to react for 4 h after which the device will be rinsed with a solution of PBS (pH = 7.4) to remove any non-specifically bound moieties from the surface.

6.2.5 Integrated Conductivity Sensor. Conductivity electrodes will consist of Pt wires (25 – 127 μm dia.) placed into guide channels of equal width and depth embossed orthogonal to the fluidic output channel. The Pt wires will be inserted into these guide channels prior to thermal assembly of the cover plate to the substrate. Once the wire is positioned, the substrate/wire assembly will be placed between glass plates and clamped together and finally, heated to a temperature slightly higher than the glass transition temperature of PMMA, once embedded the wire spanned the entire depth of the output channel. To break through the wire to form the electrode pair, a high precision micromilling machine (KERN MMP 2522, KERN Micro- und Feinwerktechnik GmbH & Co.KG; Germany) with a 50 μm bit was used. Following machining of the Pt wire and UV activation, the cover plate will be aligned to the embossed substrate via alignment marks and clamped together between two glass plates and subjected to thermal fusion bonding.

Conductivity measurements will be conducted in the run buffer where the critical components are compatibility with the analyte and fluidic system. The releasing buffer will be carefully selected in large part for its relatively low conductivity (~50 μS/cm, pH 7.2) and the addition of trypsin to digest the antibodies facilitating the removal of the bound TNT from the capture channel surface for conductometric quantitation.

6.3 Expected Results and Significance

The current state of the art displacement based immunological measurements offers at the optimum flow rate of 100 μL/min analysis times of 3 min using a single capillary with 0.55 mm i.d. that was 20 cm long.[9-11,18] These experiments were characterized by less than ideal analyte recovery rates and deviations from linearity in quantitative measurements on samples above 300 ng/mL. Linearity in the previous schemes was limited to 2 to 3 orders of magnitude. Refining the isolation and release of the analytes for secondary measurements the linear dynamic range may be extendable. Tuning the microfluidics to capture the analytes more effectively and incorporating these features on a single chip it is possible to increase the sensitivity and limit of detection of the measurement systems while reducing the overall analysis time. For instance, if an HTMSU were employed with 50 parallel channels with matching cross section to those mentioned above the processing time for a 100 μL sample could be reduced 3 min to 0.06 min. Incorporating high aspect ratio microchannels offers high surface area to volume ratios resulting in more exhaustive interrogation of samples leading to higher capture efficiencies. It stands to reason that if one extracts more of the analyte from the sample that the slope of the subsequent calibration curve would also increase thereby affording higher sensitivity.

6.4 Dissertation Summary

After a brief overview of the recent literature on CTC isolation and enumeration in microfluidic devices in Chapter 1, this dissertation initially focuses on the electrokinetic manipulation of biological cells within polymeric microfluidic devices in an effort to demonstrate the separation of mixed cellular populations. During my early work, I demonstrated that through manipulation of simple parameters such as solution ionic

strength, substrate surface chemistry, and the bulk composition of the substrate used that the apparent mobilities of cells in mixed populations could be exploited to effectively separate mixed populations of cells into its individual constituents. Also shown in my early work was the use of Rayleigh scatter to both distinguish cells based on size and as a means of direct quantitation. The basis for the enumeration and typing in the early work was that the larger particles or cells in suspension scattered more light than the smaller counterparts as indicated in Chapter 2. Though this work represented a significant stride in the community this work had a few drawbacks, primarily related to low throughput, incompatibility with densely populated samples, and enriched cells were of relatively low purity.

In an effort to improve upon some of the initial drawbacks of my early work, in Chapter 3 and 4, I expound on the development of a microfluidic device termed: high throughput microsampling unit (HTMSU), which simplified cell analysis greatly. The devices were micromanufactured with multilevel microstructures via a novel high precision micromilling technique developed in-house. The microstructures possessed aspect ratios greater than four and served to improve throughput by running identical channels in parallel. Further, the devices improved the sample interrogation by increasing the surface area to volume ratio by an order of magnitude, thereby exposing more of the sample to the capture elements improving the overall effectiveness of the protocol. Also within this device was a regiospecifically modified region which served to selectively isolate cells from suspension through an immunoaffinity based interaction between immobilized antibodies and membrane bound antigens expressed in the periphery of the target cells. These devices were used to analyze whole blood samples for low abundant target cells without the need for sample pretreatment.

Finally, I transcended the confines of traditional disease related bioassays, and extended the technology to environmental samples in an effort to improve the turnaround time, sensitivity, and portability of traditional groundwater assessment. As a model analyte *E. coli* was chosen due to its toxicity and its adverse impact on recreational waters in the form of beach closings due to elevated levels. The analysis of *E. coli* using HTMSUs continues to be a challenge due to many factors. The bacteria were much smaller than that of the cancer cells used in the proof of concept discussed in Chapter 3 and 4, hence capture efficiencies of no greater than 14% were obtained in initial experiments. Also, the conductivity sensor had to be modified in order to discern the smaller perturbations at the conductivity cell produced by the much smaller bacterium as it traversed the detector. In addition using brightfield microscopy the *E. coli* were difficult to distinguish when captured on microchannel walls even when fluorescently labeled because of the size and the relatively small depth of field when compared to the total channel depth.

6.5 Immediate Projections

With minor modifications to the devices such as narrowing the channel widths, changing the immobilized antibodies, and optimizing the processing velocity this technology will be widely applicable. Experimental optimization of the parameters will have significant impact on extending the applicability in disease diagnostics and prognostics. In the clinical setting, small relatively inexpensive devices with long shelf lives are required, and the advent of aptamers provide a basis for increased thermal stability with similar K_d values to antibodies directed towards the same target. Also, efforts are underway to facilitate the integration of molecular profiling techniques to the current devices that nondestructively isolate and enumerate the CTCs. By lysing the

cells, capturing the DNA via solid phase reversible immobilization, and performing on-chip continuous flow polymerase chain reaction (cf-PCR) we will someday circumvent the current state of the art screening techniques such as colonoscopy, mammography, and magnetic resonance imaging.[19,20] Further, in the environmental regime, investigation with these devices will yield assessment of environmental samples for low abundant bacterial cells, phytoplankton, and the devices will ultimately be used to trap and quantitate molecules as well as bacteria. Field deployability for environmental analysis and device shelf life will be improved by incorporating aptamers, small oligonucleotides that bind proteins with affinities that compare favorably with antibodies, because they are thermally stable and possess long shelf life.

6.6 References

(1) Rabbany, S. Y.; Lane, W. J.; Marganski, W. A.; Kusterbeck, A. W.; Ligler, F. S. *Journal of Immunological Methods* **2000**, *246*, 69-77.

(2) Sohn, H.; Sailor, M. J.; Magde, D.; Trogler, W. C. *Journal of the American Chemical Society* **2003**, *125*, 3821-3830.

(3) U.S. Environmetal Protection Agency, SW-846 Method 8330.

(4) Hakansson, K.; Coorey, R. V.; Zubarev, R. A.; Talrose, V. L.; Hakansson, P. *Journal of Mass Spectrometry* **2000**, *35*, 337-346.

(5) Sylvia, J. M.; Janni, J. A.; Klein, J. D.; Spencer, K. M. *Analytical Chemistry* **2000**, *72*, 5834-5840.

(6) Krausa, M.; Schorb, K. *Journal of Electroanalytical Chemistry* **1999**, *461*, 10-13.

(7) Luggar, R. D.; Farquharson, M. J.; Horrocks, J. A.; Lacey, R. J. *X-Ray Spectrometry* **1998**, *27*, 87-94.

(8) Ligler, F. S.; Taitt, C. R.; Shriver-Lake, L. C.; Sapsford, K. E.; Shubin, Y.; Golden, J. P. *Analytical and Bioanalytical Chemistry* **2003**, *377*, 469-477.

(9) Narang, U.; Gauger, P. R.; Ligler, F. S. *Analytical Chemistry* **1997**, *69*, 2779-2785.

(10) Narang, U.; Gauger, P. R.; Ligler, F. S. *Analytical Chemistry* **1997**, *69*, 1961-1964.

(11) Whelan, J. P.; Kusterbeck, A. W.; Wemhoff, G. A.; Bredehorst, R.; Ligler, F. S. *Analytical Chemistry* **1993**, *65*, 3561-5.

(12) Galloway, M.; Stryjewski, W.; Henry, A.; Ford, S. M.; Llopis, S.; McCarley, R. L.; Soper, S. A. *Analytical Chemistry* **2002**, *74*, 2407-2415.

(13) Witek, M. A.; Wei, S. Y.; Vaidya, B.; Adams, A. A.; Zhu, L.; Stryjewski, W.; McCarley, R. L.; Soper, S. A. *Lab on a Chip* **2004**, *4*, 464-472.

(14) Adams, A. A., Okagbare, P. I. and Soper, S. A. *Journal of the American Chemical Society* **2008**, *(in press)*.

(15) Hupert, M. L.; Guy, W. J.; Llopis, S. D.; Shadpour, H.; Rani, S.; Nikitopoulos, D. E.; Soper, S. A. *Microfluidics and Nanofluidics* **2007**, *3*, 1-11.

(16) McCarley, R. L.; Vaidya, B.; Wei, S.; Smith, A. F.; Patel, A. B.; Feng, J.; Murphy, M. C.; Soper, S. A. *J. Am. Chem. Soc.* **2005**, *127*, 842-843.

(17) Henry, A. C.; Tutt, T. J.; Galloway, M.; Davidson, Y. Y.; McWhorter, C. S.; Soper, S. A.; McCarley, R. L. *Anal. Chem.* **2000**, *72*, 5331-5337.

(18) Narang, U.; Gauger, P. R.; Kusterbeck, A. W.; Ligler, F. S. *Analytical Biochemistry* **1998**, *255*, 13-19.

(19) Hashimoto, M.; Chen, P. C.; Mitchell, M. W.; Nikitopoulos, D. E.; Soper, S. A.; Murphy, M. C. *Lab Chip* **2004**, *4*, 638-645.

(20) Witek, M. A.; Llopis, S. D.; Wheatley, A.; McCarley, R. L.; Soper, S. A. *Nucleic Acids Res.* **2006**, *34*, e74/1-e74/9.

APPENDIX: PERMISSIONS

André A. Adams

From: Terese Winslow [terese.winslow@mindspring.com]
Sent: Tuesday, June 17, 2008 11:35 AM
To: André A. Adams
Subject: Re: Use of Illustration in Dissertation

Dear Andre,

I'm not sure if I replied to your message. So sorry if I haven't. You may use my figure in your dissertation without charge. Please be sure to contact me for any other usage. And please send me the title of the thesis and date of publication. Many thanks.

Terese

Terese Winslow
Medical Illustrator
714 South Fairfax Street
Alexandria, Virginia 22314

Phone: 703-836-9121
Fax: 703-836-3715
terese.winslow@mindspring.com
www.teresewinslow.com

On Jun 3, 2008, at 1:14 PM, André A. Adams wrote:

In Appendix A (Figure A.6. Gene Transcription, Translation, and Protein Synthesis.) of a 2001 NIH report on stem cells an illustration of the cell based DNA transcription and subsequent protein translation is shown. This figure nicely shows the process of protein production, and would be a nice fit for my dissertation. I am wondering if you permit use of your figures in dissertations, and what the procedure is for obtaining such permission?

Sincerely,

André
André A. Adams
Louisiana State University
Department of Chemistry
202 Choppin Hall
Baton Rouge, LA 70803
Off: (225) 578-7709
Fax: (225) 578-3458
Mob: (225) 938-7528
AOL IM: andre11
Yahoo IM: aadadams
aadam14@lsu.edu
aadadams@yahoo.com
aadadams@gmail.com

PERMISSION REQUEST FORM

Date: 6/3/8

From: To: Copyright Office
Publications Division
American Chemical Society
1155 Sixteenth Street, N.W.
Washington, DC 20036

FAX: 202-776-8112

To: From: André A. Adams
LSU Chemistry
202 Choppin Hall
Baton Rouge LA 70803

Your Phone No. 225-578-7709
Your Fax No. 225-578-3458

I am preparing a paper entitled:
Novel Devices and Protocols Enabling Isolation and Enumeration...

to appear in a **(circle one)** book, magazine, journal, proceedings, other Dissertation
entitled: Novel Devices and Protocols Enabling Isolation and Enumeration...

to be published by: Louisiana State University Library System

I would appreciate your permission to use the following ACS material in print and other formats with the understanding that the required ACS copyright credit line will appear with each item and that this permission is for only the requested work listed above:

From ACS journals or magazines (for ACS magazines, also include issue no.):

ACS Publication Title	Issue Date	Vol.	No.	Page(s)	Material to be used*
Analytical Chemistry	1997	69	6	1564-1568	Figure 2
Analytical Chemistry	1999	71	5	911-918	Figure 1
Analytical Chemistry	2006	78	16	5853-5863	Figure 5

From ACS books: include ACS book title, series name and number, year, page(s), book editor=s name(s), chapter author's name(s), and material to be used, such as Figs. 2 & 3, full text, etc.*

* If you use more than three figures/tables from any article and/or chapter, the author's permission will also be required.

Questions? Please call Ar

This space is reserved for ACS Copyright Office Use

12/3/99

PERMISSION TO REPRINT IS GRANTED BY THE AMERICAN CHEMICAL SOCIETY

ACS CREDIT LINE REQUIRED. Please follow this sample: Reprinted with permission from (reference citation). Copyright (year) American Chemical Society.

APPROVED BY: *C. Arleen Courtney* 6/11/08
ACS Copyright Office

☐ **If box is checked, author permission is also required. See original article for address.**

RECEIVED
JUN - 4 2008
ACS COPYRIGHT OFFICE

PERMISSION REQUEST FORM

Date: 6/3/8

From: To: Copyright Office
Publications Division
American Chemical Society
1155 Sixteenth Street, N.W.
Washington, DC 20036

FAX: 202-776-8112

To / ~~From~~: André A. Adams
LSU Chemistry
202 Choppin Hall
Baton Rouge LA 70803

Your Phone No. 225-578-7709
Your Fax No. 225-578-3458

I am preparing a paper entitled:
Novel Devices and Protocols Enabling Isolation and Enumeration...

to appear in a **(circle one)** book, magazine, journal, proceedings, other Dissertation
entitled: Novel Devices and Protocols Enabling Isolation and Enumeration...

to be published by: Louisiana State University Library System

I would appreciate your permission to use the following ACS material in print and other formats with the understanding that the required ACS copyright credit line will appear with each item and that this permission is for only the requested work listed above:

From ACS journals or magazines (for ACS magazines, also include issue no.):

ACS Publication Title	Issue Date	Vol.	No.	Page(s)	Material to be used*
Analytical Chemistry	2005	77	3	933-937	Figure 3

From ACS books: include ACS book title, series name and number, year, page(s), book editor=s name(s), chapter author's name(s), and material to be used, such as Figs. 2 & 3, full text, etc.*

* If you use more than three figures/tables from any article and/or chapter, the author's permission will also be required.

Questions? Please call Arleen Cou

This space is reserved for ACS Copyright Office Use

12/3/99

PERMISSION TO REPRINT IS GRANTED BY THE AMERICAN CHEMICAL SOCIETY

ACS CREDIT LINE REQUIRED. Please follow this sample: Reprinted with permission from (reference citation). Copyright (year) American Chemical Society.

APPROVED BY: *C. Arleen Courtney* 6/11/04
ACS Copyright Office

☐ **If box is checked, author permission is also required. See original article for address.**

John Wiley & Sons, Inc.
Publishers Since 1807

WILEY

GLOBAL RIGHTS DEPARTMENT
111 River Street, 4-02
Hoboken, NJ 07030-5774

June 20, 2008

Andre Adams
Louisiana State University
202 Choppin Hall
Baton Rouge, LA 70803
aadam14@lsu.edu

VIA FACSIMILE: 225.578.3458

Dear Andre Adams:

RE: Your June 06, 2008 request for permission to republish figure 4, pg. 28 from Cytometry 2005; 68B(1). This material will appear in your forthcoming thesis in print and/or the website <http://etd.lsu.edu> to be published by Louisiana State University.

1. Permission is granted for this use, except that if the material appears in our work with credit to another source, you must also obtain permission from the original source cited in our work.

2. Permitted use is limited to your edition described above, and does not include the right to grant others permission to photocopy or otherwise reproduce this material except for versions made for use by visually or physically handicapped persons. Up to five copies of the published thesis may be photocopied by a microfilm company.

3. Appropriate credit to our publication must appear on every copy of your thesis, either on the first page of the quoted text, in a separate acknowledgment page, or figure legend. The following components must be included: Title, author(s) and /or editor(s), journal title (if applicable), Copyright © (year and owner). Reprinted with permission of Wiley-Liss, Inc. a subsidiary of John Wiley & Sons Inc.

4. This license is non-transferable. This license is for non-exclusive English print rights and microfilm storage rights by Louisiana State University only, throughout the world. This license does not extend to selling our content in any format. *For translation rights, please reapply for a license when you have plans to translate your work into a specific language.*

5. Posting of the Material shall in no way render the Material in the public domain or in any way compromise our copyright in the Material. You agree to take reasonable steps to protect our copyright not limited to, providing credit to the Material as specified in Paragraph 3 above. You agree that access to the Material will be deleted from the web page no later than June 20, 2011

Sincerely,

Brad Johnson
Permissions Assistant
201.748.6786
201.748.6008 (fax)
bjohns@wiley.com

Adams062008.doc

André A. Adams

From: VCH-RIGHTS-and-LICENCES [RIGHTS-and-LICENCES@wiley-vch.de]
Sent: Thursday, June 05, 2008 1:37 AM
To: aadam14@lsu.edu
Subject: WG: Fw: Republication/Electronic Request Form

Dear Customer,

Thank you for your email.

We hereby grant permission for the requested use expected that due credit is given to the original source.
For material published before 2006 additionally: Please note that the author's permission is also required.

If material appears within our work with credit to another source, authorisation from that source must be obtained.

Credit must include the following components:
- Books: Author(s)/ Editor(s) Name(s): Title of the Book. Page(s).
Publication year. Copyright Wiley-VCH Verlag GmbH & Co. KGaA. Reproduced with permission.

- Journals: Author(s) Name(s): Title of the Article. Name of the Journal.
Publication year. Volume. Page(s). Copyright Wiley-VCH Verlag GmbH & Co.
KGaA. Reproduced with permission.

With kind regards

Heike Weller
****

Heike Weller
Copyright & Licensing Department
Wiley-VCH Verlag GmbH & Co. KGaA
Boschstr. 12
69469 Weinheim
Germany

Phone: +49 (0) 62 01- 606 - 585
Fax: +49 (0) 62 01 - 606 - 332
Email: rights@wiley-vch.de

----- Weitergeleitet von VCH-RIGHTS-and-LICENCES/VCH/Wiley am 05.06.2008

08:36 -----

----- Forwarded by Bradley Johnson/P&T/Hoboken/Wiley on 06/04/2008 11:04 AM -----

republication <republication@wiley.com> 06/03/2008 02:50 PM

To <republication@wiley.com>

cc

Subject Republication/Electronic Request Form

Please respond to republication <republication@wiley.com>

A01_First_Name: Andre
A02_Last_Name: Adams
A03_Company_Name: Louisiana State University
A04_Address: 202 Choppin Hall
A05_City: Baton Rouge
A06_State: LA
A07_Zip: 70803
A08_Country: USA
A09_Contact_Phone_Number: 225-578-7709
A10_Fax: 225-578-3458
A11_Emails: aadam14@lsu.edu
A12_Reference:
A13_Book_Title: Electrophoresis
A40_Book_or_Journal: Journal
A14_Book_Author:
A15_Book_ISBN:
A16_Journal_Month: January
A17_Journal_Year: 2001
A18_Journal_Volume: 22
A19_Journal_Issue_Number: 2
A20_Copy_Pages: 284, Figure 1
A21_Maximum_Copies: 5
A22_Your_Publisher: Electronic Thesis Dissertation
A23_Your_Title: Novel Devices and Protocols Enabling Isolation and Enumeration of Low Abundant Biological Cells from Complex Matrices
A24_Publication_Date: 8/8/8

A25_Format: print,Intranet
A31_Print_Run_Size:
A41_Ebook_Reader_Type:
A26_If_WWW_URL:
A27_If_WWW_From_Adopted_Book:
A28_If_WWW_Password_Access: No
A45_WWW_Users:
A29_If_WWW_Material_Posted_From:
A30_If_WWW_Material_Posted_To:
A42_If_Intranet_URL: etd.lsu.edu
A32_If_Intranet_From_Adopted_Book:
A33_If_Intranet_Password_Access: No
A48_Intranet_Users: 28000
A34_If_Intranet_Material_Posted_From: 8/8/8
A35_If_Intranet_Material_Posted_To: 8/8/9
A50_If_Software_Print_Type:
A36_If_Software_Print_Run:
A37_Comments_For_Request: This request if for a dissertation.

ELSEVIER LIMITED LICENSE
TERMS AND CONDITIONS

Jun 03, 2008

This is a License Agreement between Andre A. Adams ("You") and Elsevier Limited ("Elsevier Limited"). The license consists of your order details, the terms and conditions provided by Elsevier Limited, and the payment terms and conditions.

Supplier	Elsevier Limited The Boulevard,Langford Lane Kidlington,Oxford,OX5 1GB,UK
Registered Company Number	1982084
Customer name	Andre A. Adams
Customer address	9919 Mint Dr. Baton Rouge, LA 70809
License Number	1961471300641
License date	Jun 03, 2008
Licensed content publisher	Elsevier Limited
Licensed content publication	Biosensors and Bioelectronics
Licensed content title	Modular concept of a laboratory on a chip for chemical and biochemical analysis
Licensed content author	Gert Blankenstein and Ulrik Darling Larsen
Licensed content date	1 March 1998
Volume number	13
Issue number	3-4
Pages	12
Type of Use	Thesis / Dissertation
Portion	Figures/table/illustration /abstracts
Portion Quantity	1
Format	Both print and electronic
You are an author of the Elsevier article	No
Are you translating?	No
Purchase order number	
Expected publication date	Aug 2008
Elsevier VAT number	GB 494 6272 12

Permissions price	0.00 USD
Value added tax 0.0%	0.00 USD
Total	0.00 USD

Terms and Conditions

INTRODUCTION

1. The publisher for this copyrighted material is Elsevier. By clicking "accept" in connection with completing this licensing transaction, you agree that the following terms and conditions apply to this transaction (along with the Billing and Payment terms and conditions established by Copyright Clearance Center, Inc. ("CCC"), at the time that you opened your Rightslink account and that are available at any time at <http://myaccount.copyright.com>).

GENERAL TERMS

2. Elsevier hereby grants you permission to reproduce the aforementioned material subject to the terms and conditions indicated.

3. Acknowledgement: If any part of the material to be used (for example, figures) has appeared in our publication with credit or acknowledgement to another source, permission must also be sought from that source. If such permission is not obtained then that material may not be included in your publication/copies. Suitable acknowledgement to the source must be made, either as a footnote or in a reference list at the end of your publication, as follows:

"Reprinted from Publication title, Vol /edition number, Author(s), Title of article / title of chapter, Pages No., Copyright (Year), with permission from Elsevier [OR APPLICABLE SOCIETY COPYRIGHT OWNER]." Also Lancet special credit - "Reprinted from The Lancet, Vol. number, Author(s), Title of article, Pages No., Copyright (Year), with permission from Elsevier."

4. Reproduction of this material is confined to the purpose and/or media for which permission is hereby given.

5. Altering/Modifying Material: Not Permitted. However figures and illustrations may be altered/adapted minimally to serve your work. Any other abbreviations, additions, deletions and/or any other alterations shall be made only with prior written authorization of Elsevier Ltd. (Please contact Elsevier at permissions@elsevier.com)

6. If the permission fee for the requested use of our material is waived in this instance, please be advised that your future requests for Elsevier materials may attract a fee.

7. Reservation of Rights: Publisher reserves all rights not specifically granted in the combination of (i) the license details provided by you and accepted in the course of this licensing transaction, (ii) these terms and conditions and (iii) CCC's Billing and Payment terms and conditions.

8. License Contingent Upon Payment: While you may exercise the rights licensed immediately upon issuance of the license at the end of the licensing process for the transaction, provided that you have disclosed complete and accurate details of your proposed use, no license is finally effective unless and until full payment is received from you (either by publisher or by CCC) as provided in CCC's Billing and Payment terms and conditions. If full payment is not received on a timely basis, then any license preliminarily granted shall be deemed automatically revoked and shall be void as if never granted. Further, in the event that you breach any of these terms and conditions or any of CCC's Billing and Payment terms and conditions, the license is automatically revoked and shall be void as if never granted. Use of materials as described in a revoked license, as well as any use of the materials beyond the scope of an unrevoked license, may constitute copyright infringement and publisher reserves the right to take any and all action to protect its copyright in the materials.

9. Warranties: Publisher makes no representations or warranties with respect to the licensed material.

10. Indemnity: You hereby indemnify and agree to hold harmless publisher and CCC, and their respective officers, directors, employees and agents, from and against any and all claims arising out of your use of the licensed material other than as specifically authorized pursuant to this license.

11. No Transfer of License: This license is personal to you and may not be sublicensed, assigned, or transferred by you to any other person without publisher's written permission.

12. No Amendment Except in Writing: This license may not be amended except in a writing signed by both parties (or, in the case of publisher, by CCC on publisher's behalf).

13. Objection to Contrary Terms: Publisher hereby objects to any terms contained in any purchase order, acknowledgment, check endorsement or other writing prepared by you, which terms are inconsistent with these terms and conditions or CCC's Billing and Payment terms and conditions. These terms and conditions, together with CCC's Billing and Payment terms and conditions (which are incorporated herein), comprise the entire agreement between you and publisher (and CCC) concerning this licensing transaction. In the event of any conflict between your obligations established by these terms and conditions and those established by CCC's Billing and Payment terms and conditions, these terms and conditions shall control.

14. Revocation: Elsevier or Copyright Clearance Center may deny the permissions described in this License at their sole discretion, for any reason or no reason, with a full refund payable to you. Notice of such denial will be made using the contact information provided by you. Failure to receive such notice will not alter or invalidate the denial. In no event will Elsevier or Copyright Clearance Center be responsible or liable for any costs, expenses or damage incurred by you as a result of a denial of your permission request, other than a refund of the amount(s) paid by you to Elsevier and/or Copyright Clearance Center for denied permissions.

LIMITED LICENSE

The following terms and conditions apply to specific license types:

15. **Translation**: This permission is granted for non-exclusive world **English** rights only unless your license was granted for translation rights. If you licensed translation rights you may only translate this content into the languages you requested. A professional translator must perform all translations and reproduce the content word for word preserving the integrity of the article. If this license is to re-use 1 or 2 figures then permission is granted for non-exclusive world rights in all languages.

16. **Website**: The following terms and conditions apply to electronic reserve and author websites:
Electronic reserve: If licensed material is to be posted to website, the web site is to be password-protected and made available only to bona fide students registered on a relevant course if:
This license was made in connection with a course,
This permission is granted for 1 year only. You may obtain a license for future website posting,
All content posted to the web site must maintain the copyright information line on the bottom of each image,
A hyper-text must be included to the Homepage of the journal from which you are licensing at http://www.sciencedirect.com/science/journal/xxxxx or the Elsevier homepage for books at http://www.elsevier.com , and
Central Storage: This license does not include permission for a scanned version of the material to be stored in a central repository such as that provided by Heron/XanEdu.

17. **Author website** for journals with the following additional clauses:
This permission is granted for 1 year only. You may obtain a license for future website posting,
All content posted to the web site must maintain the copyright information line on the bottom of each image, and
The permission granted is limited to the personal version of your paper. You are not allowed to download and post the published electronic version of your article (whether PDF or HTML, proof or final version), nor may you scan the printed edition to create an electronic version,
A hyper-text must be included to the Homepage of the journal from which you are licensing at http://www.sciencedirect.com/science/journal/xxxxx , or the Elsevier homepage for books at http://www.elsevier.com and
Central Storage: This license does not include permission for a scanned version of the material to be stored in a central repository such as that provided by Heron/XanEdu.

18. **Author website** for books with the following additional clauses:
Authors are permitted to place a brief summary of their work online only.
A hyper-text must be included to the Elsevier homepage at http://www.elsevier.com
This permission is granted for 1 year only. You may obtain a license for future website posting,
All content posted to the web site must maintain the copyright information line on the bottom of each image, and
The permission granted is limited to the personal version of your paper. You are not allowed

to download and post the published electronic version of your article (whether PDF or HTML, proof or final version), nor may you scan the printed edition to create an electronic version,
A hyper-text must be included to the Homepage of the journal from which you are licensing at http://www.sciencedirect.com/science/journal/xxxxx , or the Elsevier homepage for books at http://www.elsevier.com and
Central Storage: This license does not include permission for a scanned version of the material to be stored in a central repository such as that provided by Heron/XanEdu.

19. **Website** (regular and for author): "A hyper-text must be included to the Homepage of the journal from which you are licensing at http://www.sciencedirect.com/science/journal /xxxxx."

20. **Thesis/Dissertation**: If your license is for use in a thesis/dissertation your thesis may be submitted to your institution in either print or electronic form. Should your thesis be published commercially, please reapply for permission. These requirements include permission for the Library and Archives of Canada to supply single copies, on demand, of the complete thesis and include permission for UMI to supply single copies, on demand, of the complete thesis. Should your thesis be published commercially, please reapply for permission.

v1.2

21. **Other conditions:**

None

NATURE PUBLISHING GROUP LICENSE
TERMS AND CONDITIONS

Jun 03, 2008

This is a License Agreement between Andre A. Adams ("You") and Nature Publishing Group ("Nature Publishing Group"). The license consists of your order details, the terms and conditions provided by Nature Publishing Group, and the payment terms and conditions.

License Number	1961500059969
License date	Jun 03, 2008
Licensed content publisher	Nature Publishing Group
Licensed content publication	Nature Biotechnology
Licensed content title	A microfabricated fluorescence-activated cell sorter
Licensed content author	Anne Y. Fu, Charles Spence, Axel Scherer, Frances H. Arnold, Stephen R. Quake
Volume number	
Issue number	
Pages	
Year of publication	1999
Portion used	Figures / tables
Requestor type	Student
Type of Use	Thesis / Dissertation
Total	0.00 USD
Terms and Conditions	

Terms and Conditions for Permissions

Nature Publishing Group hereby grants you a non-exclusive license to reproduce this material for this purpose, and for no other use, subject to the conditions below:

1. NPG warrants that it has, to the best of its knowledge, the rights to license reuse of this material. However, you should ensure that the material you are requesting is original to Nature Publishing Group and does not carry the copyright of another entity (as credited in the published version). If the credit line on any part of the material you have requested indicates that it was reprinted or adapted by NPG with permission from another source, then you should also seek permission from that source to reuse the material.

2. Permission granted free of charge for material in print is also usually granted for any electronic version of that work, provided that the material is incidental to the work as a whole and that the electronic version is essentially equivalent to, or substitutes for, the print version. Where print permission has been granted for a fee, separate permission must be obtained for any additional, electronic re-use (unless, as in the case of a full paper, this has already been accounted for during your initial request in the

calculation of a print run). NB: In all cases, web-based use of full-text articles must be authorized separately through the 'Use on a Web Site' option when requesting permission.

3. Permission granted for a first edition does not apply to second and subsequent editions and for editions in other languages (except for signatories to the STM Permissions Guidelines, or where the first edition permission was granted for free).

4. Nature Publishing Group's permission must be acknowledged next to the figure, table or abstract in print. In electronic form, this acknowledgement must be visible at the same time as the figure/table/abstract, and must be hyperlinked to the journal's homepage.
5. The credit line should read:

   Reprinted by permission from Macmillan Publishers Ltd: [JOURNAL NAME] (reference citation), copyright (year of publication)

   For AOP papers, the credit line should read:

   Reprinted by permission from Macmillan Publishers Ltd: [JOURNAL NAME], advance online publication, day month year (doi: 10.1038/sj.[JOURNAL ACRONYM].XXXXX)

6. Adaptations of single figures do not require NPG approval. However, the adaptation should be credited as follows:

   Adapted by permission from Macmillan Publishers Ltd: [JOURNAL NAME] (reference citation), copyright (year of publication)

7. Translations of 401 words up to a whole article require NPG approval. Please visit http://www.macmillanmedicalcommunications.com for more information. Translations of up to a 400 words do not require NPG approval. The translation should be credited as follows:

   Translated by permission from Macmillan Publishers Ltd: [JOURNAL NAME] (reference citation), copyright (year of publication).

We are certain that all parties will benefit from this agreement and wish you the best in the use of this material. Thank you.

v1.1

American Chemical Society's Policy on Theses and Dissertations

If your university requires a signed copy of this letter see contact information below.

Thank you for your request for permission to include **your** paper(s) or portions of text from **your** paper(s) in your thesis. Permission is now automatically granted; please pay special attention to the implications paragraph below. The Copyright Subcommittee of the Joint Board/Council Committees on Publications approved the following:

> Copyright permission for published and submitted material from theses and dissertations
> ACS extends blanket permission to students to include in their theses and dissertations their own articles, or portions thereof, that have been published in ACS journals or submitted to ACS journals for publication, provided that the ACS copyright credit line is noted on the appropriate page(s).
>
> Publishing implications of electronic publication of theses and dissertation material
> Students and their mentors should be aware that posting of theses and dissertation material on the Web prior to submission of material from that thesis or dissertation to an ACS journal may affect publication in that journal. Whether Web posting is considered prior publication may be evaluated on a case-by-case basis by the journal's editor. If an ACS journal editor considers Web posting to be "prior publication", the paper will not be accepted for publication in that journal. If you intend to submit your unpublished paper to ACS for publication, check with the appropriate editor prior to posting your manuscript electronically.

If your paper has **not** yet been published by ACS, we have no objection to your including the text or portions of the text in your thesis/dissertation in **print and microfilm formats**; please note, however, that electronic distribution or Web posting of the unpublished paper as part of your thesis in electronic formats might jeopardize publication of your paper by ACS. Please print the following credit line on the first page of your article: "Reproduced (or 'Reproduced in part') with permission from [JOURNAL NAME], in press (or 'submitted for publication'). Unpublished work copyright [CURRENT YEAR] American Chemical Society." Include appropriate information.

If your paper has already been published by ACS and you want to include the text or portions of the text in your thesis/dissertation in **print or microfilm formats**, please print the ACS copyright credit line on the first page of your article: "Reproduced (or 'Reproduced in part') with permission from [FULL REFERENCE CITATION.] Copyright [YEAR] American Chemical Society." Include appropriate information.

Submission to a Dissertation Distributor: If you plan to submit your thesis to UMI or to another dissertation distributor, you should not include the unpublished ACS paper in your thesis if the thesis will be disseminated electronically, until ACS has published your paper. After publication of the paper by ACS, you may release the entire thesis (**not the individual ACS article by itself**) for electronic dissemination through the distributor; ACS's copyright credit line should be printed on the first page of the ACS paper.

Use on an Intranet: The inclusion of your ACS unpublished or published manuscript is permitted in your thesis in print and microfilm formats. If ACS has published your paper you may include the manuscript in your thesis on an intranet that is not publicly available. Your ACS article cannot be posted electronically on a publicly available medium (i.e. one that is not password protected), such as but not limited to, electronic archives, Internet, library server, etc. The only material from your paper that can be posted on a public electronic medium is the article abstract, figures, and tables, and you may link to the article's DOI or post the article's author-directed URL link provided by ACS. This paragraph does not pertain to the dissertation distributor paragraph above.

Questions? Call +1 202/872-4368/4367. Send e-mail to copyright@acs.org or fax to +1 202-776-8112. 10/10/03, 01/15/04, 06/07/06

André A. Adams

From: j.hansson@ieee.org
Sent: Wednesday, June 04, 2008 8:56 AM
To: aadam14@lsu.edu; aadadams@gmail.com
Subject: Re: Fw: Permission to Reuse Published Material

Dear André A. Adams:

This is in response to your letter below, in which you have requested permission to reprint, in your upcoming thesis/dissertation, one IEEE copyrighted figure. We are happy to grant this permission.

Our only requirements are that you credit the original source (author, paper, and publication), and that the IEEE copyright line (© 2004 IEEE) appears prominently with the reprinted figure.

Please be advised that wherever a copyright notice from another organization is displayed beneath a figure or photo, you must get permission from that organization, as IEEE would not be the copyright holder.

Sincerely,

Jacqueline Hansson
IEEE Intellectual Property Rights Coordinator IEEE Intellectual Property Rights Office
445 Hoes Lane
Piscataway, NJ 08855-1331 USA
+1 732 562 3828 (phone)
+1 732 562 1746(fax)
e-mail: j.hansson@ieee.org

IEEE Fostering technological innovation
and excellence for the benefit of humanity.

----- Forwarded by William Hagen/PUBS/STAFF/US/IEEE on 06/04/2008 09:27 AM

"André A. Adams" <aadadams@gmail.com>		To
	<w.hagen@ieee.org>	
		cc
06/03/2008 03:21 PM		Subject
	Permission to Reuse Published Material	

1

I would like to request permission to reuse the Figure 2 from the following document in my dissertation for illustrative purposes. This does not fit into the RightsLink options that are currently available. Please advise me on how to proceed.

Development of a rare cell fractionation device: application for cancer detection Mohamed, H.; McCurdy, L.D.; Szarowski, D.H.; Duva, S.; Turner, J.N.; Caggana, M.; NanoBioscience, IEEE Transactions on Volume 3, Issue 4, Dec. 2004 Page(s):251 - 256 Digital Object Identifier 10.1109/TNB.2004.837903
Summary: Isolating rare cells from biological fluids including whole blood or bone marrow is an interesting biological problem. Characterization of a few metastatic cells from cancer patients for further study is desirable for prognosis/diagnosis. Traditional.....

Sincerely,

André
André A. Adams
Louisiana State University
Department of Chemistry
202 Choppin Hall
Baton Rouge, LA 70803
Off: (225) 578-7709
Fax: (225) 578-3458
Mob: (225) 938-7528
AOL IM: andre11
Yahoo IM: aadadams
aadam14@lsu.edu
aadadams@yahoo.com
aadadams@gmail.com
Homepage: http://members.cox.net/aadadams

To: André A Adams

No: 001 225 578 3458

113

RSC | Advancing the Chemical Sciences

Permission Request Form for RSC Material

To request permission to use material from a publication published by The Royal Society of Chemistry (RSC), please complete and return this form.

To:	Contracts & Copyright Department The Royal Society of Chemistry Thomas Graham House Science Park Milton Road Cambridge CB4 0WF UK	From:	Name	André A. Adams
			Address	LSU Chemistry 202 Choppin Hall Baton Rouge LA 70803
	Tel +44 (0)1223 432134		Tel	225-578-7709
	Fax +44 (0)1223 423623		Fax	225-578-3458
	Email contracts-copyright@rsc.org		Email	aadam14@lsu.edu

I am preparing the following work for publication:

Article/Chapter Title	Novel Devices and Protocols Enabling Isolation and Enumeration...
Journal/Book Title	
Editor/Author(s)	André A. Adams
Publisher	Electronic Dissertation at Louisiana State University Library

I would very much appreciate your permission to use the following material:

Journal/Book Title	Lab on a Chip
Editor/Author(s)	Witek, M. A. Wei, S. Y. Vaidya, B. Adams, A. A. Zhu, L. Stryjewski, W. McCarley, R. L. Soper, S. A.
Volume Number	4
Year of Publication	2004
Description of Material	Complete
Page(s)	464-472

I will acknowledge the original source as follows *(to be supplied by the RSC on signature)* and in each electronic version of my publication I will include a hyperlink to the article on the Royal Society of Chemistry website:

The RSC recommends the following style for acknowledgements:

[original citation] — Reproduced by permission of The Royal Society of Chemistry

Signed: _____ Date: _____

The Royal Society of Chemistry hereby grants permission for the use of the material specified above in the work described and in all subsequent editions of the work for distribution throughout the world, in all ~~media including electronic~~ and microfilm. You may use the material in conjunction with computer-based electronic and information retrieval systems, grant permissions for photocopying, reproductions and reprints, translate the material and to publish the translation, and authorise document delivery and abstracting and indexing services. Please note that if the material specified above or any part of it appears with credit or acknowledgement to a third party then you must also secure permission from that third party before reproducing that material. The Royal Society of Chemistry is a signatory to the STM Guidelines on Permissions (available on request).

print

You may also include the pdf of the paper in the electronic version of your website, however you may not include it in your online repository on its own.

Signed: _____ Date: 5 June 2008

PRF-B

RSC | Advancing the Chemical Sciences

Permission Request Form for RSC Material

To request permission to use material from a publication published by The Royal Society of Chemistry (RSC), please complete and return this form.

To: Contracts & Copyright Department
The Royal Society of Chemistry
Thomas Graham House
Science Park
Milton Road
Cambridge CB4 0WF
UK

Tel +44 (0)1223 432134
Fax +44 (0)1223 423623
Email contracts-copyright@rsc.org

From: Name André A. Adams
Address LSU Chemistry
202 Choppin Hall
Baton Rouge LA 70803

Tel 225-578-7709
Fax 225-578-3458
Email aadam14@lsu.edu

I am preparing the following work for publication:

Article/Chapter Title: Novel Devices and Protocols Enabling Isolation and Enumeration...
Journal/Book Title:
Editor/Author(s): André A. Adams
Publisher: Electronic Dissertation at Louisiana State University Library

I would very much appreciate your permission to use the following material:

Journal/Book Title: Lab on a Chip
Editor/Author(s): Irimia, D.
Volume Number: 6
Year of Publication: 2006
Description of Material: Figure 3
Page(s): 349

I will acknowledge the original source as follows *(to be supplied by the RSC on signature)* and in each electronic version of my publication I will include a hyperlink to the article on the Royal Society of Chemistry website:

The RSC recommends the following style for acknowledgements:

[original citation] — Reproduced by permission of The Royal Society of Chemistry

Signed: _____ Date: _____

The Royal Society of Chemistry hereby grants permission for the use of the material specified above in the work described and in all subsequent editions of the work for distribution throughout the world, in all media including electronic and microfilm. You may use the material in conjunction with computer-based electronic and information retrieval systems, grant permissions for photocopying, reproductions and reprints, translate the material and to publish the translation, and authorise document delivery and abstracting and indexing services. Please note that if the material specified above or any part of it appears with credit or acknowledgement to a third party then you must also secure permission from that third party before reproducing that material. The Royal Society of Chemistry is a signatory to the STM Guidelines on Permissions (available on request).

Signed: Gill Cockhead Date: 5 June 2008

PRF-B

Registered Charity Number 207890

RSC | Advancing the Chemical Sciences

Permission Request Form for RSC Material

To request permission to use material from a publication published by The Royal Society of Chemistry (RSC), please complete and return this form.

To: Contracts & Copyright Department
The Royal Society of Chemistry
Thomas Graham House
Science Park
Milton Road
Cambridge CB4 0WF
UK

Tel +44 (0)1223 432134
Fax +44 (0)1223 423623
Email contracts-copyright@rsc.org

From: Name André A. Adams
Address LSU Chemistry
202 Choppin Hall
Baton Rouge LA 70803

Tel 225-578-7709
Fax 225-578-3458
Email aadam14@lsu.edu

I am preparing the following work for publication:

Article/Chapter Title	Novel Devices and Protocols Enabling Isolation and Enumeration...
Journal/Book Title	
Editor/Author(s)	André A. Adams
Publisher	Electronic Dissertation at Louisiana State University Library

I would very much appreciate your permission to use the following material:

Journal/Book Title	Lab on a Chip
Editor/Author(s)	Furdui, V. I., Harrison, D. J.
Volume Number	4
Year of Publication	2004
Description of Material	Figure 3
Page(s)	615

I will acknowledge the original source as follows *(to be supplied by the RSC on signature)* and in each electronic version of my publication I will include a hyperlink to the article on the Royal Society of Chemistry website:

The RSC recommends the following style for acknowledgements:

[original citation] — **Reproduced by** permission of **The Royal Society of** Chemistry

Signed: _____ Date: _____

The Royal Society of Chemistry hereby grants permission for the use of the material specified above in the work described and in all subsequent editions of the work for distribution throughout the world, in all media including electronic and microfilm. You may use the material in conjunction with computer-based electronic and information retrieval systems, grant permissions for photocopying, reproductions and reprints, translate the material and to publish the translation, and authorise document delivery and abstracting and indexing services. Please note that if the material specified above or any part of it appears with credit or acknowledgement to a third party then you must also secure permission from that third party before reproducing that material. The Royal Society of Chemistry is a signatory to the STM Guidelines on Permissions (available on request).

Signed: Gale Cochran Date: 5 June 2008

PRF-B

Registered Charity Number 207890

Creative Commons License Deed

Attribution 3.0 Unported

You are free:

to **Share** — to copy, distribute and transmit the work

to **Remix** — to adapt the work

-

Under the following conditions:

Attribution. You must attribute the work in the manner specified by the author or licensor (but not in any way that suggests that they endorse you or your use of the work).

- For any reuse or distribution, you must make clear to others the license terms of this work. The best way to do this is with a link to this web page.
- Any of the above conditions can be waived if you get permission from the copyright holder.
- Nothing in this license impairs or restricts the author's moral rights.

Your fair dealing and other rights are in no way affected by the above.

This is a human-readable summary of the Legal Code (the full license).

NATURE PUBLISHING GROUP LICENSE TERMS AND CONDITIONS

Jul 09, 2008

This is a License Agreement between Andre A. Adams ("You") and Nature Publishing Group ("Nature Publishing Group"). The license consists of your order details, the terms and conditions provided by Nature Publishing Group, and the payment terms and conditions.

License Number	1984941324579
License date	Jul 09, 2008
Licensed content publisher	Nature Publishing Group
Licensed content publication	Nature
Licensed content title	Isolation of rare circulating tumour cells in cancer patients by microchip technology
Licensed content author	Sunitha Nagrath ,Lecia V. Sequist ,Shyamala Maheswaran ,Daphne W. Bell ,Daniel Irimia et al.
Volume number	450
Issue number	7173
Pages	pp1235-1239
Year of publication	2007
Portion used	Figures / tables
Requestor type	Student
Type of Use	Thesis / Dissertation
High-res requested	No
Total	0.00 USD
Terms and Conditions	

Terms and Conditions for Permissions

Nature Publishing Group hereby grants you a non-exclusive license to reproduce this material for this purpose, and for no other use, subject to the conditions below:

1. NPG warrants that it has, to the best of its knowledge, the rights to license reuse of this material. However, you should ensure that the material you are requesting is original to Nature Publishing Group and does not carry the copyright of another entity (as credited in the published version). If the credit line on any part of the material you have requested indicates that it was reprinted or adapted by NPG with permission from another source, then you should also seek permission from that source to reuse the material.

2. Permission granted free of charge for material in print is also usually granted for any electronic version of that work, provided that the material is incidental to the work as a whole and that the electronic version is essentially equivalent to, or substitutes for, the print version. Where print permission has been granted for a fee, separate permission must be obtained for any additional, electronic re-use (unless, as in the case

of a full paper, this has already been accounted for during your initial request in the calculation of a print run). NB: In all cases, web-based use of full-text articles must be authorized separately through the 'Use on a Web Site' option when requesting permission.

3. Permission granted for a first edition does not apply to second and subsequent editions and for editions in other languages (except for signatories to the STM Permissions Guidelines, or where the first edition permission was granted for free).

4. Nature Publishing Group's permission must be acknowledged next to the figure, table or abstract in print. In electronic form, this acknowledgement must be visible at the same time as the figure/table/abstract, and must be hyperlinked to the journal's homepage.
5. The credit line should read:

   Reprinted by permission from Macmillan Publishers Ltd: [JOURNAL NAME] (reference citation), copyright (year of publication)

   For AOP papers, the credit line should read:

   Reprinted by permission from Macmillan Publishers Ltd: [JOURNAL NAME], advance online publication, day month year (doi: 10.1038/sj.[JOURNAL ACRONYM].XXXXX)

6. Adaptations of single figures do not require NPG approval. However, the adaptation should be credited as follows:

   Adapted by permission from Macmillan Publishers Ltd: [JOURNAL NAME] (reference citation), copyright (year of publication)

7. Translations of 401 words up to a whole article require NPG approval. Please visit http://www.macmillanmedicalcommunications.com for more information. Translations of up to a 400 words do not require NPG approval. The translation should be credited as follows:

   Translated by permission from Macmillan Publishers Ltd: [JOURNAL NAME] (reference citation), copyright (year of publication).

We are certain that all parties will benefit from this agreement and wish you the best in the use of this material. Thank you.

v1.1

VITA

André Antonio DeAngelo Adams was born to Mr. Robert T. Adams and Mrs. Charlotte A. Adams in September of 1971, in Shreveport, Louisiana. He has two younger siblings, one brother and one sister. He attended Captain Shreve High School in Shreveport, Louisiana, from 1985 – 1989. Shortly after graduation André enrolled at Grambling State University, Grambling, Louisiana. He obtained his Bachelor of Science in chemistry in May of 2000.

Upon receiving his Bachelor of Science he immediately went to work for Dow Chemical Company in Plaquemine, Louisiana, as an analytical chemist. In January 2001, André entered the graduate school at Louisiana State University in the Department of Chemistry, Baton Rouge, Louisiana, where he focused on bioanalytical chemistry. As recently as 2008 he received the Excellence in Teaching Analytical Chemistry Award. Prior to that he won several 1st place awards for presenting his research; one of which was awarded internationally while he attended the 2004 Miniaturized Total Analysis Systems Conference in Malmo, Sweden. He is a member in good standing of the American Chemical Society (ACS), the American Academy for the Advancement of Science (AAAS), and the National Organization for Professional Advancement of Black Chemists and Chemical Engineers (NOBCChE). He is a also a member of three national honor societies: Pi Mu Epsilon (Mathematics), Beta Kappa Chi (Scientific), and Golden Key (Scholarly). While at LSU, André presided over the Chemistry Graduate Student Council and the local student affiliate of NOBCChE. André Antonio DeAngelo Adams is currently a candidate for the Doctor of Philosophy in bioanalytical chemistry, which will be awarded at the August 2008 commencement.